

Recent Trends in Charged Particle Optics and Surface Physics Instrumentation

Proceedings

of the 6th International Seminar,
held in Skalský dvůr near Brno, Czech Republic,
from June 29 to July 3, 1998,
organised by
the Institute of Scientific Instruments AS CR and
the Czechoslovak Society for Electron Microscopy

Edited by Ilona Müllerová and Luděk Frank

ISBN 80-238-2333-7

Proceedings have been printed from the camera-ready manuscripts supplied by the authors
Published and distributed by the Czechoslovak Society for Electron Microscopy,
printed in Czech Republic by Artiq Brno

Czechoslovak Society for Electron Microscopy (CSEM), Královopolská 147, 612 64 Brno, Czech Republic:
fax +420 5 41514 402, e-mail csem@isibrno.cz, <http://www.isibrno.cz/csem>

© CSEM Brno 1998

All rights reserved. No part of this publication may be reproduced without the prior written permission of the publisher.

PREFACE

Two years have quickly elapsed and the seminar on the Recent Trends in Charged Particle Optics and Surface Physics Instrumentation is again here, already the sixth one. The history of the meeting was described in the preface to the previous seminar's proceedings. Let us now summarise briefly the main points. The germ was the traditional summer seminar held nearly regularly in the Institute of Scientific Instruments in Brno on the occasion of visits of Professor Tom Mulvey from University of Aston in Birmingham, UK. In the seventies and eighties, this was valuable enough for us and offered us the opportunity to make the seminar English spoken. In the summer of 1989 we started to extend the participation, and the 1989 seminar was numbered the first. In 1990, there were as many as 30 participants from 5 countries. The third seminar in 1992 was moved to hotel Skalský dvůr in Highlands and the next three seminars organised there, each with around forty participants, had a similar schedule, at least from the point of view of non-scientific aspects of organisation. The fifth seminar was the first one to which the proceedings were published.

It seems there have been no important events since the previous seminar that are worth adding to the seminar history. This may be simply the consequence of that the seminar has established a fully defined regularly repeating meeting and nothing is new about it except that its serial number increases by one and the year by two and that the registered participation is so numerous and high-quality one as it was expected. This could be a sign of stability and tradition and we do hope that this is the explanation.

It was claimed many times at various occasions during the seminars that their prevailing orientation to charged particle optics was and remains desirable owing to the lack of meetings of that kind. This argument is generally correct but this time much less than usually: in 1998 the seminar coincided with the CPO conference held in Europe, in April in Delft. We are really happy that this circumstance has not caused any reduction in the participation in Recent Trends. (To be exact, the "collision" appeared already earlier, in 1990, when the CPO3 was held in Toulouse but our second seminar was then still smaller and less ambitious.)

Our traditional and a bit unusual style of the meeting, based on a not too large circle of personalities, knowing one another quite well, more and more seems to be something that will become usual in the future. Large congresses, aiming at gathering hundreds or even thousands of anonymous professional colleagues to one place to present their contributions to the crowd, are mainly organised because of tradition. But in fact they are also already split into symposia of a moderate size, attended by groups similar to ours. One surely cannot consider quite unrealistic a vision that presentation of scientific contributions will be fully replaced by electronic conferences. But this will never be (as we hope) the case for personal face to face meetings and discussions.

The surface physics has apparently disappeared to a significant extent from our program of a meeting of people connected in different ways with electron microscopy. No wonder, the newest surface analytical methods, various scanning probe microscopies but not only them, exhibit surface sensitivities unachievable by electron beams. A few of us, operating the low energy electron microscopes that have those capabilities, are the only

exceptions. Nevertheless, further development and extended application of the scanning very low energy microscopy, with its high surface sensitivity and broad family of contrasts, can restore relevance of combination of both of our topics, created in times when, e.g., the Auger electron detection in an electron microscope attracted a greater interest than now.

We hope that this book, being of an improved graphical and technical quality compared to the previous one, will open a series of seminar proceedings, which will not only archive the seminar course but also reflect the progress in one important consistent branch of the instrumentation science.

As proceedings editors and seminar organisers, we would like to thank in advance the participants for all aspects of their contribution to the seminar success.

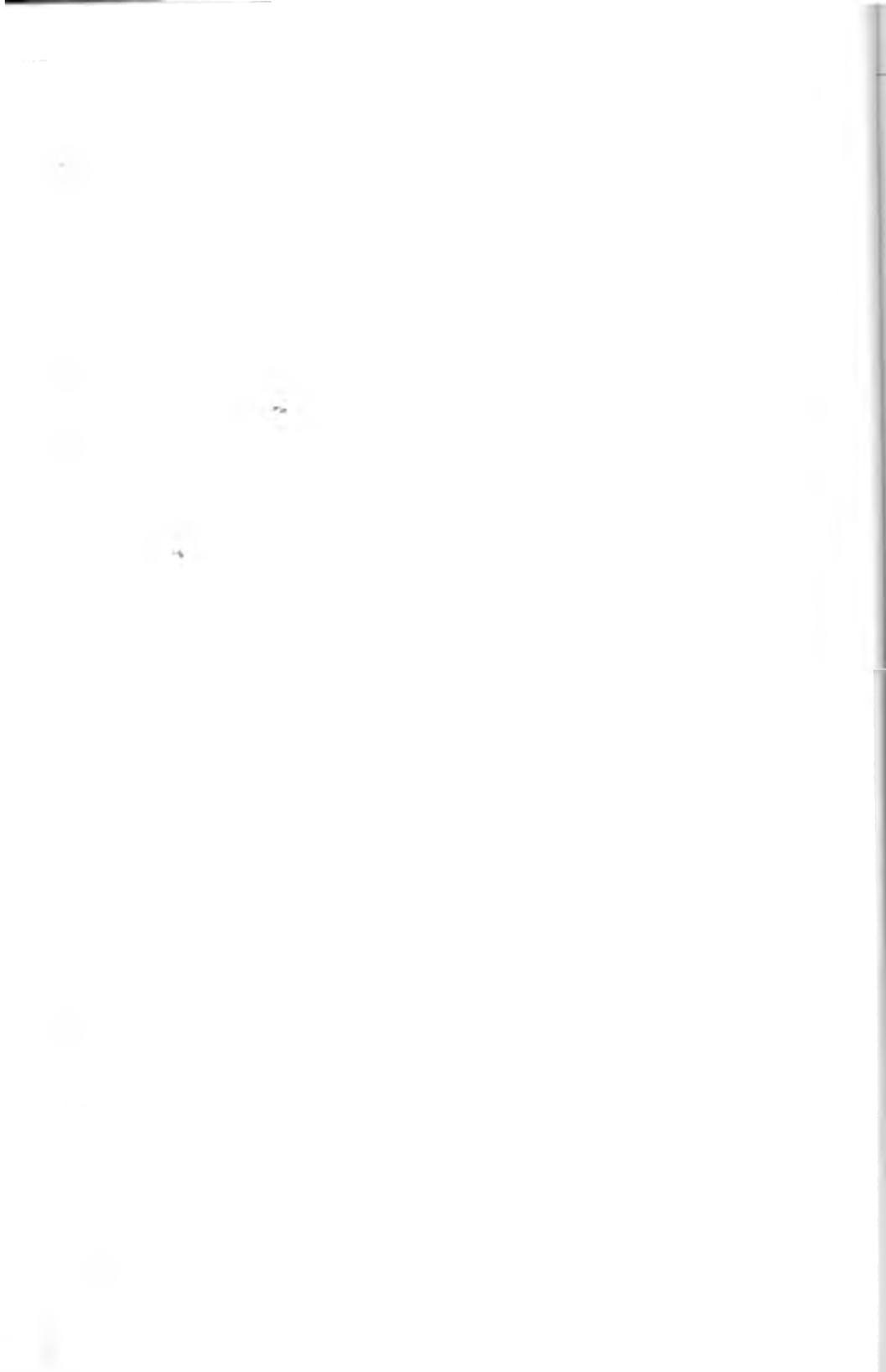
Hlona Müllerova
Luděk Frank

CONTENTS

<i>Autrata R., J. Jirák, M. Klvač, V. Romanovský</i> Detection of backscattered electrons in environmental SEM	9
<i>Autrata R., V. Romanovský, J. Jirák, M. Klvač,</i> Ionisation detector for the environmental SEM	11
<i>Autrata R., J. Jirák, M. Michálek, J. Špínka</i> Amplification of signal electrons in gas environment	13
<i>Autrata R., J. Jirák, M. Michálek, J. Špínka</i> Conditions for specimen observation in environmental SEM	15
<i>Barth J.E., M.D. Nykerk, M.J. Fransen</i> Application of a two parameter bell distribution in charged particle optics	17
<i>DeLong A., V. Kolařík, D.C. Martin</i> Low voltage transmission electron microscope LVEM-5	18
<i>El-Gomati M.M.</i> Quantitative surface analysis at high spatial resolution	20
<i>Gerheim V., H. Rose</i> Quadrupole projector system with variable magnification for energy-filtering transmission electron microscopes	22
<i>Hartel P., D. Preikszas, R. Spehr, H. Rose</i> Test of a beam separator for a corrected PEEM / LEEM	24
<i>Hasselbach F., H. Kiesel, U. Maier</i> Recent advances in ion- and electron-biprism interferometry	26
<i>Hejna J.</i> Optimisation of an immersion lens design in the BSE detector for the low voltage SEM	30
<i>Hutař O.</i> Noncharging microscopy of semiconductor structures	32
<i>Hutař O., R. Auotrata</i> The separation of secondary electrons in annular and planar detectors	34
<i>Janzen R., E. Weimer</i> Study of detection properties of a MEDOL / GEMINI objective lens for secondary electrons	36
<i>Kahl F., H. Rose</i> Outline of an electron monochromator with small Boersch effect	37

<i>Kolařík R., M. Lenc</i> Different ways of adding the aberrations	39
<i>Lencová B.</i> New trends in software for electron optics	40
<i>Lilienkamp G., Th. Schmidt, S. Satchenko, K. Prince, E. Bauer</i> Spectroscopic imaging with the low energy electron microscope	44
<i>Martínez G., A.D. Dymnikov, A.H. Azbaid</i> Optimal synthesis of charged beam focusing systems	45
<i>Merkel M., M. Escher, O. Schmidt, Ch. Ziethen, G. Schönhense</i> The microanalytic prospects of a high resolution PEEM	47
<i>Müller H., H. Rose</i> A coherence function approach to multislice theory	49
<i>Müllerová I., L. Frank, E. Weimer</i> Variable mode retarding field element for low energy SEM	51
<i>Müllerová I., L. Frank</i> Short note on Low-Energy SEM configurations	53
<i>Munro E., X. Zhu, J. Rouse, H. Liu</i> A study of ways of improving the speed and accuracy of computing fields, trajectories and aberrations in electron optics	55
<i>Preikszas D., P. Hartel, R. Spehr, H. Rose</i> Construction of an electron-optical bench for testing a mirror corrector	58
<i>Rose H.</i> Ultimate resolution: what are the needs for future microscopes?	59
<i>Schauer P., R. Ausrata</i> Cathodoluminescent properties of single crystals for S(T)EM detectors	60
<i>Schmid P., H. Rose</i> Outline of a variable-axis lens with arbitrary shift of the axis in one direction	64
<i>Schönhense G.</i> Spectroscopic X-PEEM with emphasis on magnetic contrast	65
<i>Słówko W.</i> Three dimensional scanning electron microscopy	67
<i>Sommentag P., H. Kiesel, F. Hasselbach</i> On the theoretical understanding of the Wien filter in an electron biprism interferometer	71

<i>Spehr R.</i> Variable axis lens with an extremely large scanning area in one direction	75
<i>Steklý R., L. Frank, I. Müllerová</i> Distributed Monte Carlo: smart way for computing complex problems	77
<i>Tsuno K., N. Handa, S. Matsumoto</i> An E+B+E beam separator for detecting secondary electrons in low voltage SEM	79
<i>Tyc T.</i> Antibunching of electrons as a consequence of the indistinguishableness of fermions	81
<i>Zadrazil M., M. El-Gomati</i> Measurements of the secondary and backscattered electron coefficients in the very low energy range	82
<i>Zadrazil M., L. Frank, J. Norris</i> Imaging of non-conducting specimens by noncharging scanning electron microscopy with method for automatically adjusted critical energies	83



DETECTION OF BACKSCATTERED ELECTRONS IN ENVIRONMENTAL SEM

R. Autrata, J. Jiráček*, M. Klvač, V. Romanovský

Institute of Scientific Instruments of ASCR, Královopolská 147, CZ-612 64 Brno, Czech Republic

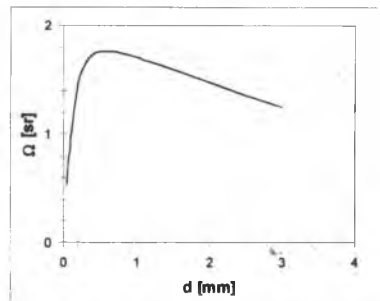
**Department of Electrotechnology, Faculty of Electrical Engineering and Computer Science, Technical University Brno, Antonínská 1, CZ-612 64 Brno, Czech Republic*

Scanning electron microscopy working with pressure in the specimen chamber that are higher than 100 Pa enables investigation of in-situ specimens and certain dynamic effects, which is not possible in conventional SEM.

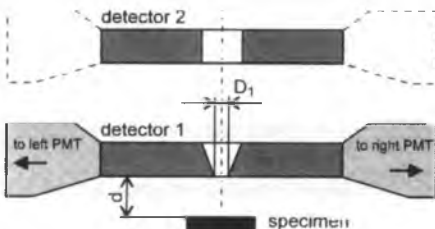
In our case for the detection of backscattered electrons (BSE) in environmental scanning electron microscope we use a paired scintillation detector YAG (yttrium aluminium garnet) doped with Ce^{3+} , provided with a central hole of 300 to 500 μm in diameter. The detector acts simultaneously as a pressure limiting aperture, which allows to achieving different pressures in the specimen and differential chamber. The configuration of the detector ensures a large collection angle for the BSE signal and allows the use of the small working distance of the specimen from detector to ensure a sufficient signal even in high pressures in the specimen chamber when an increase number of collisions of electrons with the gaseous medium occurs. Theoretical calculations and practical measuring showed that a considerable portion of the BSE signal escapes through the hole of the scintillator and is not detected by the detector. Figure 1 shows a decrease in the detection efficiency of the detector in relation to the working distance. This effect is appreciable above all for very small working distances of the specimen from the detector. For this reason a double paired scintillation detector was designed and constructed.

The principle of the double paired detector is evident from Figure 2. For small working distances d of the specimen from detector 1 which are comparable with the diameter of the hole D_1 , the collection angle of the detector 1 decreases rapidly and a considerable portion of BSEs escapes through the hole into the differential chamber. The detector 2 is positioned here and it ensures the detection of those BSEs. The single crystals of both detection stages are symmetrically divided into the right and the left half. The interface between them is provided with an optical reflecting layer. Then both the halves are mechanically associated. Both detection stages thus provide two paired signals with the possibility of further processing signals.

The properties of the detectors 1 and 2 were investigated by measuring the signal and noise levels in relation to the pressure in the specimen chamber and the specimen distance d from detector 1. The signal levels were measured in the signal path behind the photomultiplier and preamplifier. As the measuring specimen a carbon cylinder with a central hole coated with an Au - layer was

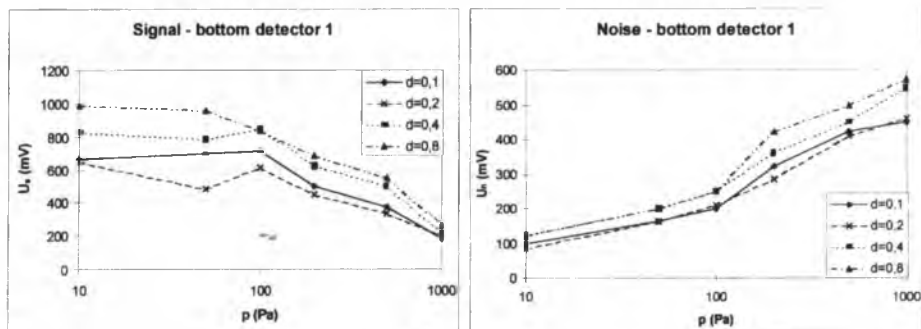


Obr. 1

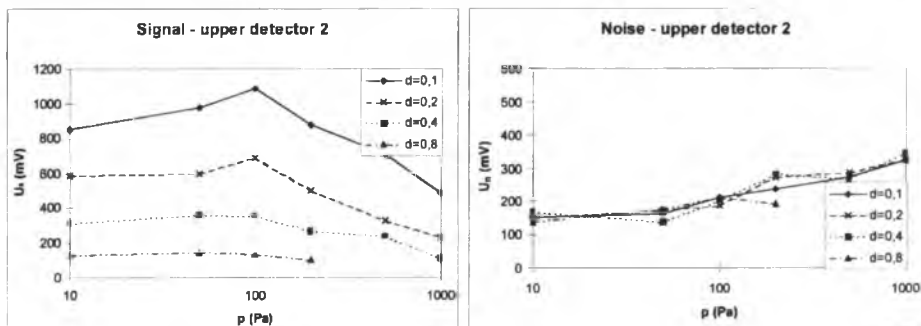


Obr. 2

used. During the scanning signals from the left half of the bottom stage and the right half of the upper detection stage were given. All measurements were carried out at the constant value of the primary beam current in the vacuum.



Obr.3 Dependence of the signal U_s and noise U_n of the bottom detector 1 on the pressure p in the specimen chamber for specimen distances d from the bottom detector ($d = 0.1$ mm, $d = 0.2$ mm, $d = 0.4$ mm, $d = 0.8$ mm). Photomultiplier dynodes voltage $U_d = 400$ V.



Obr.4 Dependence of the signal U_s and noise U_n of the upper detector 2 on the pressure p in the specimen chamber for specimen distances d from the bottom detector ($d = 0.1$ mm, $d = 0.2$ mm, $d = 0.4$ mm, $d = 0.8$ mm). Photomultiplier dynodes voltage $U_d = 600$ V.

From the Figures 3 and 4 it is evident that the upper detector 2 is more suitable for working distances d in the range from 0.1 mm to 0.4 mm because provides a higher signal level than the detector 1. It is possible to use the double paired scintillation detector BSE for the detection BSE for ESEM, for pressures lower than 1000 Pa and for very small working distances d . Equally it is possible to make use of the sum of the signals from both detection stages.

References:

- [1] Atrata R., Jiráček J., Špinko J. (1994) In: Detection of Backscattered Electrons in Environmental SEM. ICEM 13, Paris, pp 127-128.
- [2] Atrata R., Jiráček J., Špinko J.: Backscattered electron detector for environmental scanning electron microscopes. Bedo 26, 1993, p. 13.
- [3] Reimer L.: Scanning Electron Microscopy, Springer - Verlag, 1 ed. Berlin, 1995, p.128.

IONISATION DETECTOR FOR THE ENVIRONMENTAL SEM

R. Autrata, V. Romanovský, J. Jiráček, M. Klvač

Institute of Scientific Instruments of ASCR, Královopolská 147, CZ-612 64 Brno, Czech Republic

**Department of Electrotechnology, Faculty of Electrical Engineering and Computer Science, Technical University Brno, Antonínská 1, CZ-612 64 Brno, Czech Republic*

One of the relatively new trends in the field of scanning electron microscopy focuses on observing specimens placed in the specimen chamber under higher pressures. The group of these microscopes is usually called ESEM (environmental scanning electron microscopy). The value of the working pressure in the specimen chamber 609 Pa in 0 °C is fixed as the limit for the groups of microscopes SEM and ESEM.

The ESEM microscopes have wide application in observing biological specimens and various types of specimen of insulation character. The observation biological specimens does not require any special preparation technology. No charging phenomena occur due to the presence of a gaseous medium. Consequently, the complicated and long coating of the specimen is no longer needed. The coating usually causes the loss of information on the material consistence of the specimen surface.

Nowadays scintillation detectors are usually used for the ESEM field. However, their principle does not enable full application of these microscopes for observing biological specimens, i.e. specimens containing a larger amount of water and especially in the field of topography contrast, which is important, above all, for the already mentioned field of biological specimens.

The configuration of this detector described and used is already fully functional and enables the detection of the low energy electrons, thanks to which we have approached to the possibility of the better detection of the topography contrast which we have lacked when observing certain specimens. In our case, a gaseous medium surrounding the specimen is used as an amplifier. In this medium an avalanche of electrons occurs, produced by collision of signal particles with a gaseous medium.

The aim of the project was a design and construction of the ionisation detector for the ESEM microscopes, containing besides the reached functional configuration also optimisation of the working condition of the detector. In Figure 1 there is a design of a combined detector, which we used and which makes use of the features of the scintillation and ionisation detectors. With this configuration a large collection angle is reached. When designing the detector we tried to find primarily the optimal working distance D and the pressure in the specimen chamber p as you can see in Figure 2. Keeping these optimal conditions, it is possible to reach the maximum possibilities offered by this detector.

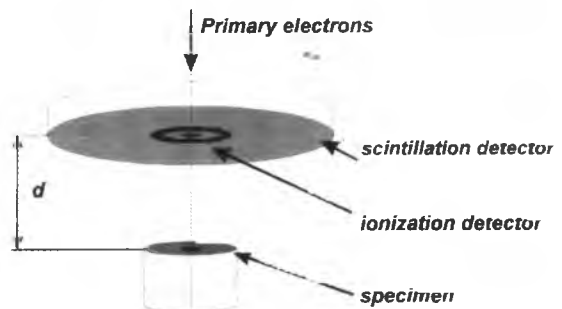


Fig.1 Geometrical configuration of specimen and detector

This type of detector should open new possibilities of the application of the ESEM microscopes in all the fields of microscopy and first of all in biology and the semiconductor industry.

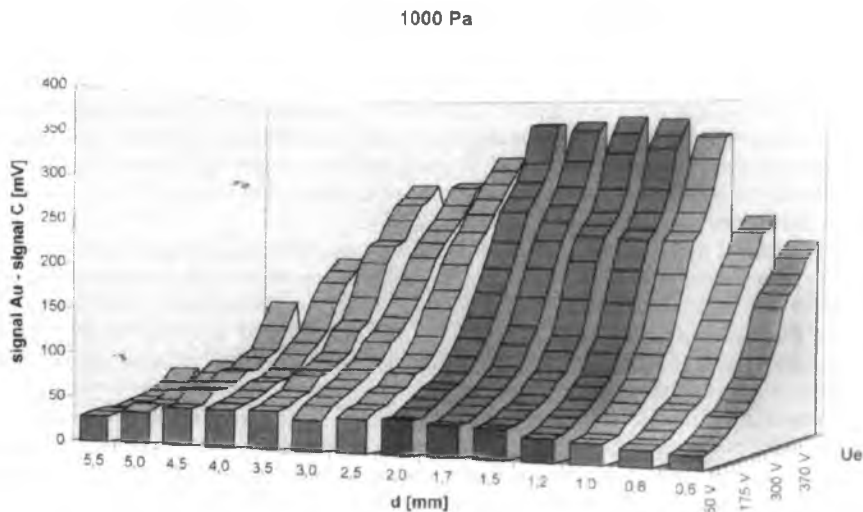


Fig.2 Signal Au – signal C, 1000 Pa

References:

- [1] Meredith P., Donald A.M., Thiel B.: Electron-gas interactions in the environmental scanning electron microscopes. Gaseous detector. *Scanning* 18, 1996 p. 467.
- [2] Schnarr H., Futing W.: Some aspects of optimizing contrast for the investigation of joint materials in the Environmental scanning electrons microscopes. *Scanning* 19, 1997, p. 79

AMPLIFICATION OF SIGNAL ELECTRONS IN GAS ENVIRONMENT

R. Atrata*, J. Jiráček, M. Michálek, J. Špinko

*Institute of Scientific Instruments of ASCR, Královopolská 147, CZ-612 64 Brno, Czech Republic

Department of Electrotechnology, Faculty of Electrical Engineering and Computer Science, Technical University Brno, Antonínská 1, CZ-612 64 Brno, Czech Republic

Environmental scanning electron microscopes (ESEM) enable the observation of specimens at higher pressures than in ordinary SEM. The pressure in the specimen chamber can be between 10^2 - $5 \cdot 10^3$ Pa. Working at higher pressures, it is advantageous to use the ionization of gas for detection of signal electrons. To amplify the signal, ionization detectors take advantage of ionization that occurs in the space between the specimen and the detector.

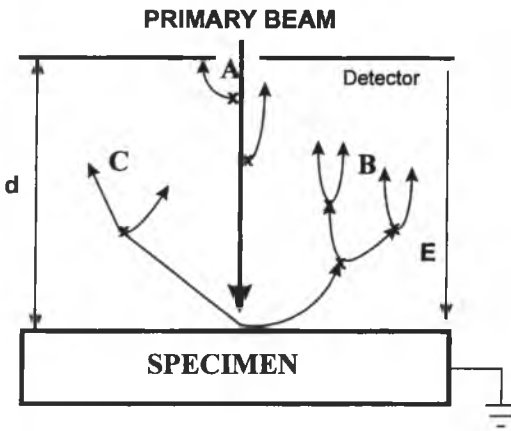


Fig.1. A schematic diagram of the parallel plate electrode system.

A - contribution of primary electrons, B - contribution of secondary electrons (SE), C - contribution of backscattered electrons (BSE) to the total detected current.

d is the sample-to-detector distance, E is the electric field intensity. Electrons are multiplied through ionizing collisions in the gas (indicated by x).

The detected current is proportional to the number of electrons emitted from the specimen. We assume that the total detected current can be found by summing the following contributions:

$$I_{\text{det}} = I_{PE}^a + I_{SE}^a + I_{BSE}^a \quad (1)$$

where I_{PE}^a , I_{SE}^a , I_{BSE}^a are the contributions of the primary electrons, the SEs, and the BSEs to the total detected current, respectively.

According to [1] the total amplification is given by:

$$I_{\text{det}} = I_p' \cdot p \cdot \frac{\exp(\alpha \cdot d) - 1}{\alpha \cdot [1 - \gamma \cdot \{\exp(\alpha \cdot d) - 1\}]} \left(s_{pe} + \frac{\delta \alpha}{p} + \eta \cdot s_{bse} \cdot \frac{d'}{d} \right) \quad (2)$$

where I_p' is the part of the primary beam current impacting the specimen without any collisions with the gas environment, p is the pressure, α and γ are the Townsend first and second ionization coefficients, respectively, s_{pe} and s_{bse} are the field-independent ionization efficiencies of the primary electrons and the BSEs, respectively, and δ and η are the SE and BSE coefficients, respectively.

The calculation of the amplification can only be done for a particular type of the electrode system. In the following part, we consider the parallel plate electrode system as shown in Fig. 1. For the calculation it is also necessary to know the surface emissive properties and the ionization properties of the used gas. Usually, we consider that the environment which surrounds the specimen is air, and that ionization takes place in this gas. However it is also

possible to use other gases as well as mixtures of gases [2]. Changing the gas would influence the coefficients s_{pe} , α , s_{bse} in equation (2). The complete calculation shows that the contribution of SEs to the total detected current is the highest. This contribution is characterized by the first Townsend coefficient α :

$$\alpha = A \cdot \exp\left(\frac{-B}{E}\right) \quad (3)$$

where A and B are constants which express the ability of the gas to be ionized. For this calculation, we used the values A, B, s_{pe} and s_{bse} taken from [3] and values η and δ from [4]. The calculation values of the detected current and their dependence on the pressure in the specimen chamber with the constant working distance $d = 1.3$ mm, are shown in Fig. 2 together with the experimentally measured values.

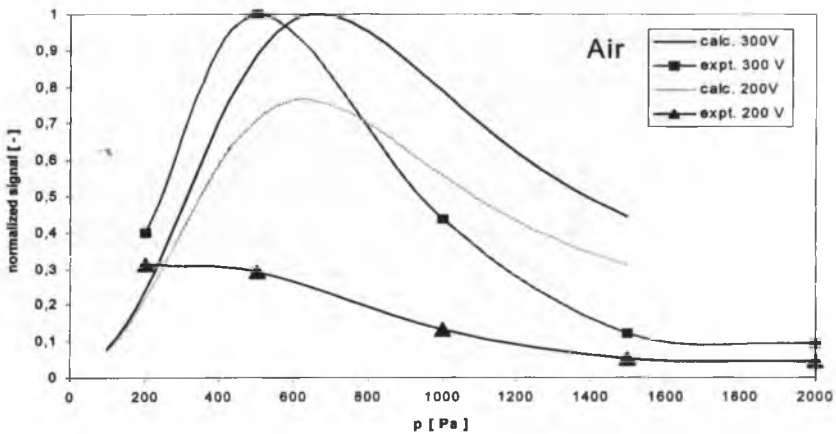


Fig. 2. The dependence of measured and calculated normalized amplification for an ionization detector in air, with the potentials 200 and 300 V on the collection electrode.

The experimental measurement of the signal and its dependence on the pressure for a given working distance was performed for an Au sample in the line-scan mode. An ionization detector with ring electrodes deposited on a YAG:Ce³⁺ crystal was used for the detection of electrons. The potentials on the collection electrode were 200 and 300 V.

The computations confirm that we can theoretically predict the dependence of the amplification signal on pressure. Comparing the measured pressure dependence with the computed pressure dependence of the signal, for a constant sample-to-detector distance, we can see that the maximum signal occurs at lower pressures than those of the computed dependencies. The aim of further work will be to explain these discrepancies.

References:

- [1] P. Meredith, A. M. Donald, B. Thiel: Electron-gas interaction in the environmental scanning electron microscopes gaseous detector, *Scanning*, 18, 1996, p. 467 – 473.
- [2] A. L. Fletcher, B. L. Thiel, A. M. Donald: Amplification measurements of alternative imaging gases in environmental SEM, *J. Phys. D: Appl. Phys.* 30, 1997, p. 2249 – 2257.
- [3] A. von Engel: Ionized gases, Oxford University Press, 2 ed., Oxford 1965, 319 p.
- [4] L. Reimer.: Scanning electron microscopy, Springer – Verlag, 1 ed. Berlin 1985, 457 p.

CONDITIONS FOR SPECIMEN OBSERVATION IN ENVIRONMENTAL SEM

R. Autrata*, J. Jirák, M. Michálek, J. Špinka

* *Institute of Scientific Instruments of ASCR, Královopolská 147, CZ-612 64 Brno, Czech Republic*

Department of Electrotechnology, Faculty of Electrical Engineering and Computer Science, Technical University Brno, Antonínská 1, CZ-612 64 Brno, Czech Republic

Classical scanning electron microscopes (SEM) possess extraordinary properties (resolution, image sharpness, possibility of element analysis of specimens, etc.) but they have certain limitations as regards vacuum that is necessary for their operation.

The examined specimens should be:

- vacuum resistant: On exposing a specimen in vacuum conditions, its properties should not be affected.
- vacuum inert: The specimens may not emit gases or vapours or particles into vacuum. This could endanger successful operation.
- and electrically conducting.

In practice, not all specimens meet these demands. Therefore complex methods, e.g. freezing, fixation, etc., must be used to treat them. Specimens having the character of insulators must be coated with metal mostly.

In the environmental SEM, where we work with pressures around 1000 Pa in the specimen chamber, we can fill the chamber with suitable gases and vapours. From this it follows that it is possible to examine hydrated specimens, to watch the interaction of specimens with the gaseous or liquid atmosphere, and to observe dynamic processes, such as crystal growth, wetting, corrosion processes, cementing process. Charging effects are eliminated, owing to the presence of ionized particles of a gas [1].

Conditions for the creation of an optimum environment in the specimen chamber that is necessary for a successful observation of specimens are different for different cases, depending on the kind of processes and specimens to be examined. Sometimes, some "preparation" of specimens for ESEM is needed.

Let us focus on the most frequent case of observation of specimens containing water that is

carried out in the presence of

water vapour. For the

environmental SEM, the most

suitable range of working

pressures and temperatures

follows from the curves of

relative humidity [2].

To cool specimens, it is

advantageous to use the Peltier

cell which makes it possible to

achieve a temperature difference

as high as 40 K,

compared with the temperature

of the warm end. The setting

and control of temperature of

the cell by a change in the

flowing current are advantageous,

and when needed, the

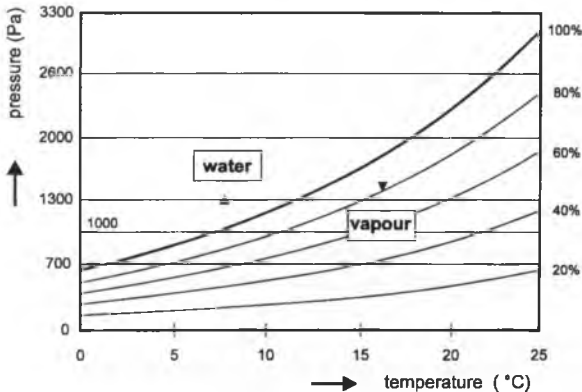


Fig. 1 Relative humidity versus pressure and temperature in the specimen chamber

cell can be used for specimen heating by changing the polarity of the flowing current.

For wet and damp specimens, conditions for observation are set so that the gaseous atmosphere in the specimen chamber is saturated with water vapours. In this way, specimen drying can be avoided. On the contrary, when condensation of water takes place, conditions for specimen wetting can be created

The following facts are important: On evacuating the microscope, the pressure in the chamber of the environmental SEM is higher than that in the chamber of the classical SEM but it is still rather low. Therefore it is necessary for the relatively dry air of the outer atmosphere, which is present in the surrounding of the specimen at the beginning of evacuation, to be replaced in a defined way during the evacuation process by a necessary volume of water vapour.

To determine optimum conditions of evacuation, two criteria must be taken in to account [3]:

1. The whole process of evacuation must be ended in equilibrium state at which air in the surroundings of the specimen is saturated with water vapours.
2. The course of evacuation should ensure that in the system this state is achieved when evaporation of water from the specimen and condensation of water vapours are as low as possible.

All the process of evacuation of the specimen chamber has the following steps:

1. Evacuation by the main rotary pump connected to the specimen chamber using a valve that can be closed and continuous evacuation through a small opening in the so called pressure limiting aperture (PLA) by using a pump which pumps the differential chamber.
2. Filling of air saturated with water vapours.
3. Setting of the equilibrium state at which the in-flow of air enriched with water vapours and the flux of gases pumped through the PLA become balanced.

The following facts must be considered to optimize the process:

- The overall pressure above the specimen should not decrease below the level of the saturated water vapours in the specimen to avoid boiling. The liquid phase should evaporate as little as possible, no bubbles may be produced.

- Most of the dry air must be removed from the specimen chamber so that at the end of the pumping of the microscope the pressure of water vapours approaches the pressure of saturated water vapours for the given temperature (humidity 95% and more).

Specimen temperature also plays a role. It should be as low as possible. However we must consider also the danger of water freezing. An important factor is the temperature of water in the water vapour source.

At our laboratory, we equipped the microscope of environmental type - AQUASEM - with the Peltier cell and a developer of water vapours source. Experimental results will be presented on the poster. Experimental results show that it is possible to stabilize temperature of the specimen in the range 1 to 10 °C and to keep an optimal relative humidity between 200 and 1 200 Pa pressure in the specimen chamber.

References:

- [1] Autrata, R. - Jiráček, J. - Špinko, J.: New possibilities of observation of insulators in scanning electron microscopy. In: Diagnostika 95, FEL ZUČ Plzeň 1995, p. 199-202 (in Czech).
- [2] Technical literature of the firm Philips. An introduction to ESEM, p. 55.
- [3] Cameron, R. E. - Donald, A. M.: Minimizing evaporation in environmental scanning electron microscope. Journal of Microscopy, 173, 1994, p. 227-237.

APPLICATION OF A TWO PARAMETER BELL DISTRIBUTION IN CHARGED PARTICLE OPTICS

J.E. Barth, M.D. Nykerk and M.J. Fransen

Delft University of Technology, Department of Applied Physics, Lorentzweg 1, 2628 C/J Delft, The Netherlands

For the sake of simplicity, the Gaussian distribution $\exp(-w^2x^2)$ is used whenever the actual distribution has more or less such a form. Real distributions often have tails which fall off more slowly than a Gaussian. A, still simple, bell shaped distribution that can model this is $1/(1 + w^2x^2)^p$. Having two parameters, a width measure w and the power p , it can better fit a variety of real distributions than the Gaussian. For large p it approaches the Gaussian.

A practical measure for the size of the image of a point blurred by chromatic aberration is the diameter of the circle containing 50% of the particles,

$$d_c = K_c C_c (\Delta U/U) \alpha.$$

With ΔU the full width half maximum (FWHM) of the energy distribution the value of K_c depends on the form of the energy distribution. $K_c = 0.34$ for the Gaussian and $K_c = 0.62$ for the Lorentzian distribution (bell with $p = 1$). It was found [1] that if instead of the FWHM the FW50 (50% of the particles within ΔU) is used for the measure of ΔU that the coefficient K_c is very nearly independent of the distribution form; $K_c = 0.61 \pm 0.01$.

A practical definition of source reduced brightness is

$$B = I_\Omega / (V(\pi/4)d_1^2).$$

I_Ω is the angular current density, V the energy and d_1 the FW50 diameter of the source image. Fransen has measured [2] the brightness of an ultra sharp tungsten field emitter by analyzing Fresnel fringes occurring at sample edges in the point projection microscope. The fringe intensity profile calculated when a point, Gaussian or Lorentzian distribution is assumed for the source, will be shown.

When making numerical Monte Carlo simulations of the Coulomb interaction deterioration of beam quality in a charged particle optics column it is necessary to make assumptions as to the properties of the source as viewed from the extractor. Inclusion of more realistic distributions for the initial energy spread and source profile should allow better analysis of the effects of adjusting the beam configuration in the column.

[1] J.E. Barth, M.D. Nykerk: Dependence of the chromatic aberration spot size on the form of the energy distribution of the charged particles. In: Proc. of the Fifth Int. Conf. on Charged Particle Optics, to be published in Nucl. Inst. and Methods A

[2] M.J. Fransen: Electron emitters for electron microscopes, PhD. thesis, Delft University of Technology, to be published.

Low voltage transmission electron microscope LVEM-5

Armin Delong*, Vladimír Kolářik*, and David C. Martin**

*Delong Instruments s.r.o., Bulharská 48, 612 00 Brno, Czech Republic

**The University of Michigan, College of Engineering, Dpt. of Materials Science and Engineering,
2022 H.H. Dow Building, Ann Arbor, MI, U.S.A. 48109-2136

1. Introduction

One of the most important problems in transmission electron microscopy of organic and biological materials is the low image contrast typical for samples composed of low atomic number elements. Contrast can be improved by staining with higher atomic number elements such as ruthenium or osmium. It can also be enhanced by certain changes to the electron optics of the instrument such as reduction of the objective aperture angle, or by electron energy filtering. Another approach of considerable potential but which is not possible to pursue in conventional instruments is the use of low energy electron beams.

Given this situation we have designed and constructed a 5 kV Low Voltage Transmission Electron Microscope (LVTEM-5) using a completely unconventional approach [1]. The goal of this effort was to create an instrument which could conveniently provide enhanced imaging contrast for low atomic number specimens without a substantial loss of resolution. Here, we outline the design of this instrument and demonstrate the successful imaging of thin lamellar single crystals of polyethylene deposited onto an amorphous carbon substrate. These images demonstrate that the instrument has considerable potential for the TEM imaging of thin organic samples. Samples of immediate interest include biological sections, small organic and polymer crystals and thin films, and nanometer scale particles and filaments.

2. Instrument description

A picture of our instrument and its diagram are shown in Figure 1 and 2. The system consists of two microscopes which are used together. The first is a miniature 5 kV transmission electron microscope which uses a Schottky emitter source, permanent magnetic lenses for image formation, and electrostatic lenses to control magnification. The images and electron diffraction patterns are formed on a fluorescent YAG screen. The second part of the device is a conventional optical microscope which provides a significant improvement in the numerical aperture, and can be directly equipped with a CCD or 35 mm camera for image recording and subsequent analysis. Other advantages include the small footprint, which makes it convenient for use in the laboratory, and the potential for other modes of analysis such as electron diffraction and focused probe techniques [2].

3. Experimental

The samples which were investigated were single crystals of polyethylene having a weight average molecular weight of 120,000 gms/mole and polydispersity index of 1.19 [3]. The crystals were prepared by heating a 0.1 wt percent solution in tetrachloroethylene and allowing the

suspension to crystallize by cooling to room temperature. It is known from previous studies that this method of sample preparation leads to regular lozenge shaped crystals, with a nominal thickness of 10 nm. The crystals were deposited from the suspension onto an amorphous carbon coated sheet of cleaved mica and subsequently floated onto the surface of distilled water, where they were retrieved onto copper finder grids.

The images (Figures 3,4) show the well known, lozenge shaped crystals associated with the PE single crystal morphology. The regularity in the crystal faceting and presence of overgrowths at their edges are similar to previous observations of these same samples by conventional high voltage TEM and scanning tunnelling microscopy [3]. The estimated resolution of these images is on the order of 2 nm. The images show that variations in contrast are perceptible up to three or four layers thick, corresponding to the penetration of the low voltage electron beam through samples with an estimated mass thickness (ρt) of $4 \times 10^{-5} \text{ kg/m}^2$.

References

1. Delong A., Low Voltage TEM, *Electron Microscopy 1992*, Vol.1, 79-82, 1992.
2. Delong A., Hladil K., Kolařík V., A Low Voltage Transmission Electron Microscope, *Microscopy & Analysis*, 27(Europe), January 1994.
3. R. Piner, R. Reifenger, D. C. Martin, E. L. Thomas, and R. Apkarian, *J. Poly. Sci.:C. Poly. Lett.*, 28, 399, (1990)

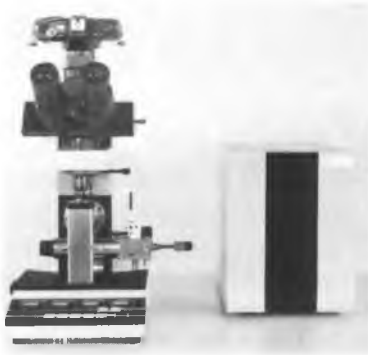


Fig.1: The Low Voltage TEM

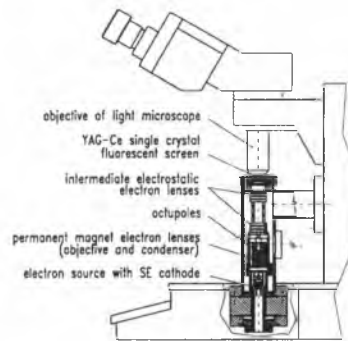


Fig.2: Schematic Device Arrangement

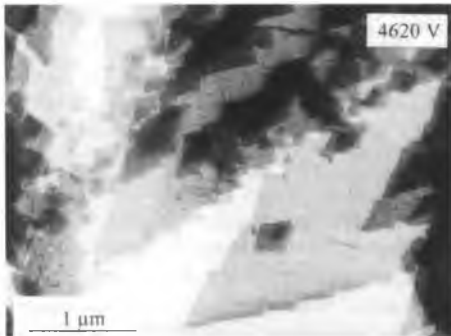


Fig.3: LVTEM Image of PE Single Crystals



Fig.4: LVTEM Image of PE Single Crystals

Quantitative Surface Analysis at High Spatial Resolution.

M M El-Gomati

Department of Electronics, University of York, York YO10 5DD, UK
mmg@ohm.york.ac.uk

Trends in the miniaturisation of integrated circuits leads to the suggestion that in the next 5-10 years, device dimensions on the sub- 0.1 micron will be developed (e.g. 4 Gbit CMOS DRAM/SRAM chips working at clock speeds of 1800 MHz). These in turn will require the fabrication of structures with shallow active interfaces on the scale of 10-20 nm below the surface and of lateral dimensions of at most 100 nm [1]. In material science, there is equally a great deal of emphasis on novel materials made of nano-structures. These are composed of multi-elements where some of which are also radiation sensitive.

The determination of the precise three dimensional distribution of elements both in the surface and near surface regions of a solid is therefore of central interest in a wide variety of areas in electronic devices and material science. For example, this is crucial in the design, fabrication, understanding and modelling of novel sub-micron semiconductor devices; for the control and interpretation of the physics of layer structures in semiconducting, metallic and magnetic multilayer systems; and to the understanding of epitaxial growth processes- particularly of enhancements arising from the presence of surface dopants or imperfections. Quantitative analysis is especially important in semiconductor device technology where the scale of proposed structures is becoming so small that no suitable analytical method is available.

The problems we face today are therefore two folds, quantitative elemental or chemical analysis, and the determination of metrology. Methods for solving both problems need to be fast, accurate and non-destructive. For example, in quality control applications, as is the case in the semiconductor industry, these requirements are further complicated by the need to perform such tests on large sample dimensions and where the sample may be tilted to large angles. Currently, semiconductor plants handle wafers of 200 mm in diameter but plans for the production and testing of 300 mm and 400 mm wafers are being drawn.

The currently available analytical methods comprise one dimensional compositional profiles. These are measured using a surface spectroscopy technique (e.g. Auger electron spectroscopy (AES), x-ray photo-electron spectroscopy (XPS), secondary ion mass spectroscopy (SIMS)) which involves the sequential erosion of the surface by bombarding it with inert gas ions [2]. These techniques are generally time consuming, difficult to execute in such a way as to ensure that all elements that are present are detected and, of course, as well as being non-linear these are destructive and so are not repeatable at the same place. Extending these techniques to 2 and 3 dimensions is still being considered by industry as too slow. In addition, all instrumentations in this field have been designed to handle only small size specimens. These techniques are therefore excluded from routine quality control in on-line inspection. Simulations and electrical measurements are the industry's preferred methods [1]. However, according to El-Kareh, the effects observed in CMOS devices as they are shrunk in size have not been predicted with adequate precision using simulations.

High voltage transmission electron microscopy (STEM), has been used in the past as the prime tool for obtaining dimensional (i.e. metrology) and crystallographic information at high spatial resolution. The technique remains to be so for fundamental research, but is considered less favourable to use in industry and particularly in quality control because of its destructive nature during the course of sample preparation. In addition, in the STEM, the whole sample thickness contributes to the image formation, making the results obtained to be less reliable even with the aid of deconvolution methods. The use of STEMs is therefore considered not to be practical in on-line analysis of large samples.

Metrology techniques currently available primarily involve the use of low voltage electron microscopes (LVSEM). Although there has been a great deal of instrument development in LVSEM over the last decade, and where currently most microscope manufacturers offer SEM operating around the 1 keV and lower, data analysis at these operating voltages is still in its infancy stages. Other probe microscopies, such as the various forms of tunnelling microscopes (STM, AFM etc.) are very slow and are therefore ruled out for the foreseeable future. Energy dispersive x-ray analysis (EDX) at low incident electron energies is an area of research which is seeing some activities. These, however, are again limited to electron energies around the 5 keV region.

The present contribution will attempt to highlight the areas of developments in surface microanalysis and high resolution electron microscopy. In particular the session is to address the recent developments demonstrating the successful use of the cathode lens in scanning electron microscopes (SLEEM) [3] and the measurements of low energy secondary and backscattered electron coefficients from clean solid surfaces for use in both LVSEM and SLEEM [4]. Of importance in this respect is the correlation between the atomic number contrast obtainable in SLEEM and LVSEM as a function of the incident electron energy. Work in combining Auger analysis with low energy imaging as a step in the interpretation of the SLEEM contrast will be covered [5]. Recent developments in parallel data acquisition in AES will also be addressed [6].

References

- [1] El Kereh B, 3rd International Workshop on Measurements and Characterisation of Ultra-Shallow Doping Profiles In Semiconductors. March 1993, N. Carolina, USA.
- [2] See for example Quantitative surface Analysis Seah and Briggs
- [3] Mullerova I and Lenc M, *Ultra microscopy*, 41, (1992) 399, and Mullerova I and Frank L, *Scanning*, 15, (1993) 193.
- [4] El Gomati M and Asaa'd A, *Microchimica Acta*, (1998) In Press.
- [5] El Gomati M, Mullerova I and Frank L, *Proceeding of the International Centennial Symposium on the Electron*, Cambridge, UK, September (1997), In Press.
- [6] Jacka M, Kirk M, Prutton M and El Gomati M, 5th International Conference on Charged particle Optics, Delft, April (1998).

QUADRUPOLE PROJECTOR SYSTEM WITH VARIABLE MAGNIFICATION FOR ENERGY-FILTERING TRANSMISSION ELECTRON MICROSCOPES

V. Gerheim and H. Rose

Institute of Applied Physics, Technical University Darmstadt, Hochschulstraße 6, 64289 Darmstadt.

1 Motivation

The incorporation of a high-resolution energy filter into a transmission electron microscope imposes several conditions on the properties of the projector system [1]. For example, this system must have small chromatic aberrations in order to allow for a sufficiently achromatic imaging in the case of large energy windows. Since the performance of the filter is optimum at a distinct intermediate magnification [2], the magnification of the projector system must be variable by more than one order of magnitude to enable large changes of the total magnification without affecting the image quality. Moreover, this system should alternatively image the energy loss spectrum, which is formed at the dispersion plane behind the filter, without any distortions and loss of energy resolution in the detector plane with variable magnification. This property is necessary for investigating characteristic regions of the energy loss spectrum, such as plasmon excitations, interband and intraband transitions, inner shell excitations and for obtaining an overview over the entire spectrum or over a distinct part of it. To avoid unduly large intensities at the CCD-camera, it is also necessary to convert the stigmatic spectrum at the dispersion plane into a line spectrum at the recording plane such that the lines match the vertical extension of the CCD array. This condition can only be met by an astigmatic imaging system which must necessarily contain non-rotationally symmetric elements.

2 Outline of the projector system

The projector system of conventional electron microscopes consists in general of two magnetic round lenses. A projector system which can alternatively image the achromatic image plane and the dispersion plane in the recording plane with small aberrations requires at least three conventional lenses [3]. To allow for astigmatic imaging of the energy loss spectrum an additional quadrupole is needed. Even in this case the range of magnification of the projector system is strongly limited. To avoid this obstacle we propose a quadrupole projector system consisting of two quadrupole triplets. Quadrupoles are strongly focusing elements enabling a large change of the focal length of the total projector system. Owing to the astigmatic path of rays within the system the third-order distortions can always be compensated by at most four spatially separated octupole fields which can be superimposed onto the quadrupole fields if octupole or twelvepole elements are employed. The quadrupole system can easily yield stigmatic

and astigmatic imaging with any degree of astigmatism (length of the line image). A single quadrupole triplet generally forms either a first order distorted stigmatic image or two line images. These non rotationally symmetric first order deviations are compensated by the second quadrupole triplet. Since the number of the individual quadrupoles is larger than that required for stigmatic and distortion free (first order) imaging, the path of rays within the projector system can be varied even if the magnification is fixed. Owing to this behaviour, it is possible to adjust the quadrupole strengths in such a way that the chromatic aberration of magnification and/or the third order distortion are eliminated or minimized, respectively.

For the recording of the energy loss spectrum, a chromatic aberration perpendicular to the direction of the dispersion can be tolerated, as it only enlarges the extension of the image lines. The component of the axial chromatic aberration in the direction of the dispersion must be eliminated by appropriately readjusting the strength of the hexapoles within the energy filter. For recording the filtered achromatic image of the object or the diffraction plane, respectively, the quadrupoles are excited in such a way that the third order distortion is minimized. Any unduly large remaining component of the distortion can be compensated subsequently by an additional octupole field.

Despite the fact that the quadrupole projector system consists of a few more elements than that composed of rotationally symmetric lenses, its improved performance and variability outweigh this minor disadvantage by far. In addition, the distance between the recording plane and the filter can be shortened due to the strong refraction power of the quadrupole lenses.

References

- [1] Rose, H., Correction of aberrations, a promising means for improving the spatial and energy resolution of energy-filtering electron microscopes. *Ultramicroscopy* **56** (1994) 11-25.
- [2] Uhlemann, S. and Rose, H., The MANDOLINE filter – a new high performance imaging filter for sub-eV EFTEM, *Optik* **96** (1994) 163-178.
- [3] Gerheim, V., Berechnung eines variablen Projektivsystems für ein energiefilterndes Transmissions Elektronenmikroskop, Diplom Thesis, Fachbereich Physik, Institut für Angewandte Physik, Technische Universität Darmstadt (1993).

TEST OF A BEAM SEPARATOR FOR A CORRECTED PEEM/LEEM

P. Hartel, D. Preikszas, R. Spehr and H. Rose

Institute of Applied Physics, Technical University Darmstadt, Hochschulstraße 6, D-64289 Darmstadt, Germany

The beam separator is an essential part of the SMART ("Spectro-Microscope for All Relevant Techniques") [1]. The chromatic and spherical aberration of the electron lenses are eliminated by means of an electrostatic mirror. This correction procedure necessitates the incorporation of an aberration-free beam separator. It consists of a highly symmetric configuration of magnetic dipole fields which provide stigmatic imaging and a 90° -deflection. The dipole fields are realized by four coil triplets which are placed into grooves on the inner surfaces of two plane-parallel quadratic pole plates [2, 3, 4, 5]. Additional inner and outer tuning coils are placed on top of each groove to provide the possibility of electrical adjustment (Fig. 1).

As a test of our electron-optical bench, which is a LEO DSM960 scanning microscope, the beam separator has been centered between the condenser system and the objective lens (Fig. 2a). For reaching the predicted resolution limit (≈ 100 nm) of the lengthened microscope column, it is necessary (a) to demagnetize the pole-plates and (b) to compensate for the magnetic flux between the objective lens and the pole-plates by a coil. The arrangement is also applicable for testing the electrostatic field lens [6] which is placed at the exit face of the deflector. In our setup this lens forms the electron probe of the SEM. The measured resolution limit of $0.8 \mu\text{m}$ is very close to the calculated value.

At present we investigate a single passage of the electron beam through the beam separator with a deflection of 90° (Fig. 2b). In this mode of operation the field lenses are used as additional imaging elements which change the magnification and position of the intermediate image. These changes enable one to measure the performance of the beam separator. The alignment procedure consists of a mechanical preadjustment with an accuracy of a few tens of a millimetre followed by an electrical adjustment by the tuning coils. The best indicator for a correct alignment is the dispersion-free passage of the electrons through the beam separator.

References:

- [1] Fink et al. *J. Electr. Spectr.* **84** (1997) 231–250.
- [2] D. Preikszas and H. Rose, 13th Int. Congr. Electr. Micr. Paris (1994).
- [3] D. Preikszas, H. Müller and H. Rose, 27. Tagung der DGE, Leipzig (1995).
- [4] H. Müller, D. Preikszas and H. Rose, 11th Eur. Congr. Electr. Micr. Dublin (1996).
- [5] D. Preikszas, H. Müller and H. Rose, 5th Int. Sem. on Recent Trends in Charged Particle Optics, Brno (1996).
- [6] S. Planck, D. Preikszas and R. Spehr, Dreiländertagung 1997 für Elektronenmikroskopie, Regensburg (1997).

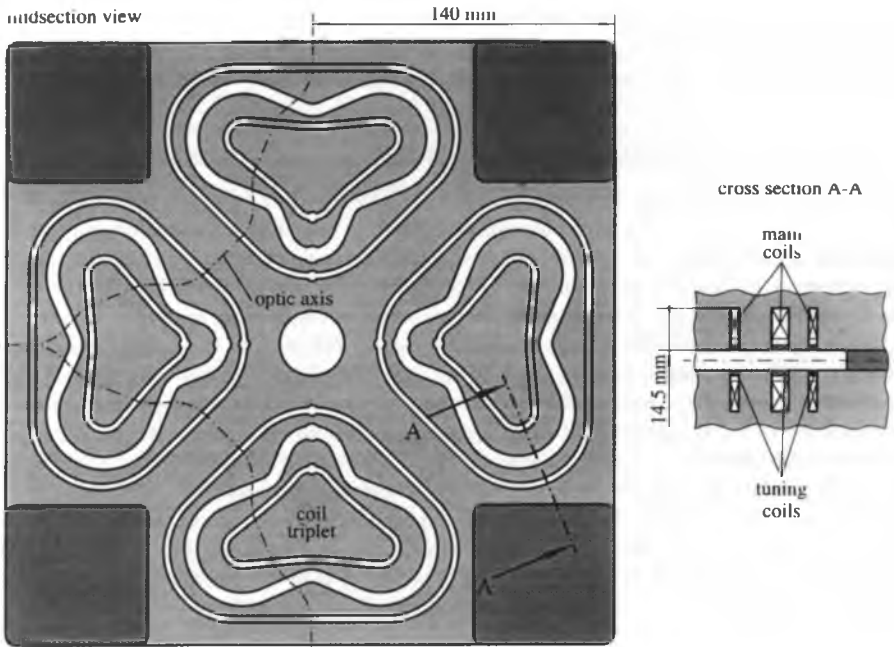


Fig. 1 - Midsection view and vertical cross section of the beam separator

a) Test of the electron-optical bench

b) Test of the beam separator

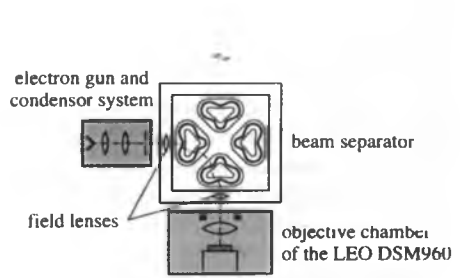
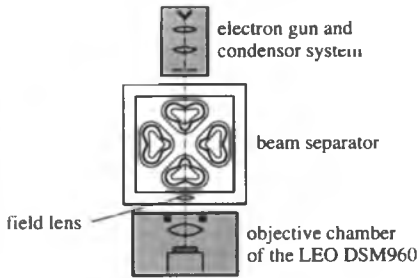


Fig. 2 - Test facilities for the beam separator

RECENT ADVANCES IN ION- AND ELECTRON-BIPRISM INTERFEROMETRY

Franz Hasselbach, Harald Kiesel and Uwe Maier

*Institut für Angewandte Physik der Universität Tübingen
Auf der Morgenstelle 10, D-72076 Tübingen, Germany*

1. Biprism interferometry with He^+ -ions

While diffraction of atoms has been realized [1] shortly after L. de Broglie's discovery of wave particle duality, the first atom interferometers were put in operation only at the beginning of this decade [2]. One cause for this long delay has been the lack of the technology necessary to develop powerful optical components for neutral particles. On the other hand, powerful optics for charged particles (with the corresponding ease of manipulation of these) has been available for more than 50 years. Yet, due to the lack of concept of a highly stable ion interferometer, it has not been developed in spite of the fact that ion interferometers were expected to solve about the same important questions as atom interferometers do: Fundamental tests of quantum mechanics and relativity, multiparticle interferometric effects [3], development of inertial sensors with unprecedented sensitivity [4]. Additionally, *charged atoms* couple to the electromagnetic field. Due to the ions internal structure, with an ionic Aharonov-Bohm experiment, one can conduct the crucial test whether the phase shift caused by electromagnetic vector potentials depends on internal degrees of freedom of the structure-rich ions, or is the same as for structureless 'point' particles as electrons.

In this paper we present the first interferometer for ions (Fig. 1.). It uses wavefront division by an ion optical biprism whereby a true physical separation of the coherent ion wave packets in space is achieved. In essence, it is a modified type of our electron interferometer [5], which has proved to be extraordinarily rugged, insensitive to vibrations, and electronically stable. These features are indispensable for an ion interferometer since, compared to atom interferometers working with thermal beams with wavelengths on the order of Å, the wavelengths of our ions are in the pm range. The field-ion source incorporated in the instrument can be switched between ion and electron emission. All optical components of the interferometer are electrostatic, therefore alignment of the interferometer optics can be performed with electrons. In order to maximize the coherent flux of He^+ -ions emitted by the field ion source, we use a specially treated 'supertip' [6], cooled down during operation to 77 K. The 'supertip', i.e., a protrusion consisting of a small number of tungsten atoms on a (111)-oriented tungsten field emission tip, which has a relatively large radius of curvature of the apex, is prepared in-situ in the interferometer. During preparation, its emission pattern can be controlled on the screen of a channel plate image intensifier, which is inserted temporarily between ion source and interferometer (Fig. 1). After preparation, the source is emitting into a single spot of angular diameter of about 1 degree only. Nevertheless, the very small part of the current of ions which is emitted into the tiny angle where the interference fringes are formed ($\sim 10^{-7}$), leads to exposure times as long as 30 minutes. The primary interference pattern is magnified by an electrostatic quadrupole lens, intensified by two cascaded channel plates and fiberoptically transferred to a cooled slow scan CCD-camera. On-chip integration of single events, and image processing in a personal computer, are provided in order to improve the signal-to-noise ratio.

In summary, Fig. 2a shows diffraction at the edges of the biprism filaments, and Fig. 2b shows biprism interference fringes of He^+ -ions. In order to reduce noise the integrated intensities \bar{I}_n of about 50 successive lines perpendicular to the fringe direction are given in Fig. 2a,b. No additional filtering was applied in the diagrams on top. All but one of the crucial stability requirements for ions with sub-pm wavelengths are met by the interferometer. The only exception is for the ion source whose emission site tends to move uncontrollably in lateral direction during the long exposure time. Lateral coherence is destroyed and, with it, the fringe visibility. Improvement of source stability and brightness are the next important goals on the way to an ion interferometer as a research tool.

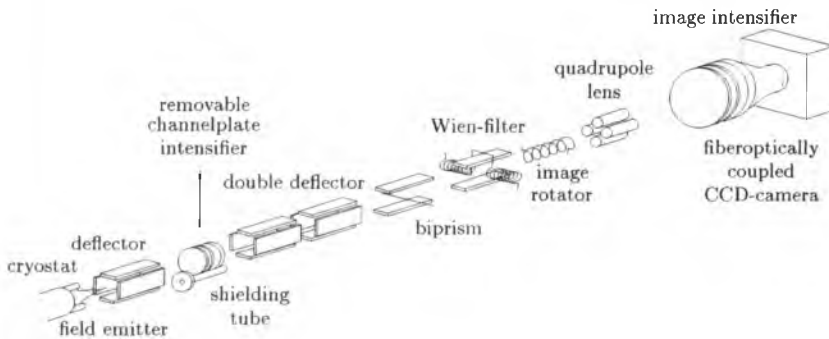


Fig. 1: Schematic set-up of the ion interferometer

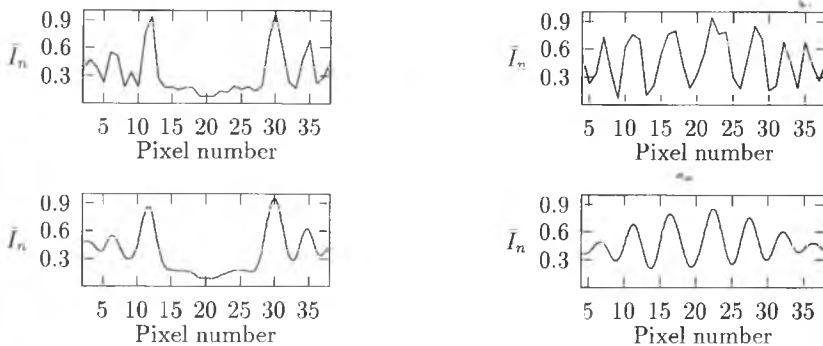


Fig. 2a: Ion-diffraction at both edges of the biprism filament. Top: Original data. Bottom: Smoothed.

2b: Biprism interference fringes of He^+ -ions

2. An electron antibunching experiment

The only candidate to prove fermion antibunching is electrons[12, 13, 14, 15, 16, 17] because for heavier particles the beam degeneracies of the available sources are hopelessly small. The beam degeneracy δ means the ratio of the actual brightness of the emitter (occupation number per cell in phase space) to the theoretical maximum brightness B_{max} (by Pauli's exclusion principle the maximum occupation per cell is two for fermions with opposite spin directions)[7, 8, 9, 10, 11].

$$B_{max} = (4m\epsilon/h^3)E\Delta E = 5.2 \times 10^9 E(\text{eV})\delta E(\text{eV}) (\text{A}\cdot\text{cm}^{-2}\cdot\text{sr}^{-1})$$

The beam degeneracy δ of the electron beam in a standard field emission electron microscope is according to M.P. Silverman[15]:

	standard field emission microscope	diode electron gun
degeneracy	10^{-6}	$5 \cdot 10^{-5}$
energy	10^5eV	10^3eV
ΔE	0.3 eV	0.3 eV
Brightness B	$10^8 \text{ A cm}^{-2} \text{ sr}^{-1}$	$10^8 \text{ A cm}^{-2} \text{ sr}^{-1}$

With our low aberration diode field emission gun a brightness of the same order as for the microscope given above at 1 keV seems realistic. Consequently, the beam degeneracy of about $5 \cdot 10^{-5}$ is nearly two orders of magnitude larger and compares quite favourably with that of 10^{-3} which was available in the classical Hanbury Brown Twiss experiment.

In our experiment, two electron detectors in the interference plane of the interferometer measure coincidences of the arrival times of electrons. The time resolution of the fast coincidence will be of the order of 10^{-10} s[18, 19, 20], which is by 4 orders of magnitude less than the theoretically required resolution given by the coherence time τ_c in order to really see that no two electrons arrive within the coherence time. Having a resolution of 10^{-10} s only, we expect to measure a by $1 \cdot 10^{-4}$ reduced random coincidence rate since within the first 10^{-14} s after the arrival of an electron no second one arrives due to the Pauli principle. This causes the reduction of random coincidences in a coherent electron beam. In conclusion, antibunching of electrons should be observable with our electron interferometer and presently available technology of fast coincidence counting.

Acknowledgement

This work was made possible by support from the Deutsche Forschungsgemeinschaft.

References

- [1] Esterman I., Stern O., *Z. Phys.* **61**(1930), 95.
- [2] Carnal O., Mlynek J., *Phys. Rev. Lett.* **66**(1991), 2689; Keith D.W., Ekstrom Ch.R., Turchette Q.A., Prichard D.E., *Phys. Rev. Lett.* **66**(1991), 2693.
- [3] Shimizu F., in 'Atom Interferometry', P.R. Berman editor, p. 153, Academic Press (1997).
- [4] Clauser J.F., *Physica B* **151**(1988), 262-272; Gustavson T.L., Bouyer P., Kasevich M.A., *Phys. Rev. Lett.* **78**(1997), 2046; Lenef A. et al., *Phys. Rev. Lett.* **78**(1997), 760.
- [5] Hasselbach F., *Z. Phys. B Condensed Matter* **71**(1988), 443-449; Hasselbach F., Nicklaus M., *Phys. Rev. A* **48**(1993), 143-151.

- [6] Hanson G.R., Siegel B.M., *J. Vac. Sci. Technol.* **16**(1979), 1875-1878; Börret R., Böhringer K., Kalbitzer S., *J. Phys.* **D23**(1990), 1271-1277.
- [7] D. Gabor: Light and Information, *Progress in Optics* **1**(1961), 109, Ed. E.Wolf, North Holland, Amsterdam.
- [8] M.L.Goldberger, H.W.Lewis, K.M.Watson: Use of intensity correlation to determine the phase of scattering amplitude, *Phys. Rev.* **132**(1963), 2764.
- [9] E. Zeitler: Coherence in scanning transmission microscopy, *SEM, Chicago* (1975), 671-678.
- [10] E. Zeitler: Zusammenhänge, die mit der Kohärenz zusammenhängen, *Optik* **77**(1987), 13.
- [11] H. Rose, R. Spehr: Energy broadening in high-density electron and ion beams: The Boersch effect, *Adv. in Electronics and Electron Phys. Suppl.* **13C**(1983), 475.
- [12] M.P. Silverman: Fermion ensembles that show statistical bunching, *Phys. Lett. A* **124**(1987), 27.
- [13] M.P. Silverman: Distinctive quantum features of electron intensity correlation interferometry, *Il Nuovo Cimento* **97B**(1987), 200.
- [14] M.P. Silverman: Second order temporal and spatial coherence of thermal electrons, *Il Nuovo Cimento* **99**(1987), 227-245.
- [15] M.P. Silverman: On the feasibility of observing electron antibunching in a field-emission beam, *Phys. Lett. A* **120**(1987), 442.
- [16] M.P. Silverman: Application of photon correlation technique to fermions, *OSA Proceedings on Photon Correlation Techniques and Applications* **1**(1988), 26-34, Eds. J.B.Abbiss, A.E.Smart, OSA Washington DC.
- [17] M.P. Silverman: Quantum interference effects on fermion clustering in a Fermion interferometer, *Physica B* **151**(1988), 291.
- [18] S. Cova, M. Ghioni, F. Zappa: Improving the performance of ultrafast microchannel-plate photomultipliers in time-correlated photon counting by pulse pre-shaping, *Rev. Sci. Instrum.* **61**(1990), 1072.
- [19] S. Cova, M. Ghioni, F. Zappa: Optimum amplification of microchannel-plate photomultiplier pulses for picosecond photon timing, *Rev. Sci. Instrum.* **62**(1991), 2596.
- [20] S. Cova, M. Ghioni, F. Zappa, A. Lacaita: Constant-fraction circuits for picosecond photon timing with microchannel plate photomultipliers, *Rev. Sci. Instrum.* **64**(1993), 118.

OPTIMIZATION OF AN IMMERSION LENS DESIGN IN THE BSE DETECTOR FOR THE LOW VOLTAGE SEM

J. Hejna

Institute of Material Science and Applied Mechanics, Wrocław University of Technology, Smoluchowskiego 25, 50-370 Wrocław, Poland

A brightness of a thermionic electron gun decreases when an accelerating voltage is lowered and this effect impairs parameters of the SEM equipped with such a gun at low beam voltages. Observations at low beam energies are mainly conducted in microscopes equipped with much brighter field-emission guns, but efforts are also being made to improve parameters of microscopes equipped with thermionic guns. The improvement can be achieved when the gun is operated at relatively high voltage (≥ 10 kV) and the beam is subsequently decelerated to low energy by an electrostatic field in the microscope column or over the specimen. The latter solution is very simple and can be realised in any SEM. It can be done in two ways: by biasing the specimen with a high negative voltage and forming a cathode lens over the specimen [1,2] or by placing an immersion electrostatic lens below the microscope objective lens and leaving a field-free space over the specimen [3,4]. The latter solution does not change of initial directions of backscattered electrons and gives a possibility to detect BSE at high and low takeoff angles and to obtain topographic and material contrast. In the present study an influence of a shape of electrodes of an immersion lens on aberration coefficients of the lens was investigated.

Figure 1 shows shapes of electrodes of an immersion lens - electrodes have a rotational symmetry and only halves of them are shown. Two flat electrodes (a), two conical (b), one flat and the second conical (c) and one flat and the second tapered conical (d) were studied. Primary electrons move from the left side to the right through apertures in electrodes. They reach the left electrode as a convergent beam, preliminary focused by a magnetic lens of the SEM, next they move along parabolic trajectories in the retarding field between electrodes and finally are focused on the specimen traced at a distance z_1 from the right electrode. Calculations of parameters of lenses were performed by numerical modelling. The ELD (Electrostatic Lens Design) program obtained from the Delft Particle Optics Foundation was used. It is based on the finite element method for computing a distribution of potentials [5]. The program was used for an evaluation of a distribution of an axial potential and an axial field and for computations of the chromatic and spherical aberration coefficients of lenses. Results are shown in Figs. 2 and 3. We can see that the spherical aberration coefficient drops with increasing aperture diameter (Fig. 2a) and that an increasing cone angle in versions (c) and (d) influences very little aberration coefficients (especially in the case of the tapered cone electrode). Electrodes were implemented in the BSE detector and tested in the SEM [6,7], and it was confirmed that the design from Fig. 1d gives the best results.

1. Yau YW, Pease RFW, Iranmanesh AA, Polasko KJ, *J. Vac. Sci. Technol.* **19**(1981), 1048
2. Müllerova I and Frank L, *Microch. Acta* **114/115**(1994), 389
3. Zach J and Rose H, *EUREM 88*, IOP Publishing Ltd., Bristol 1988, 81
4. Aihara R, Kasahara H, Sawaragi H, Shearer MH, Thompson WB, *J. Vac. Sci. Technol.* **B7**(1989), 79
5. Lencova B and Wisselink G, *Nucl. Instr. Meth. Phys. Res.* **A298**(1990), 56
6. Hejna J, *EMAG97*, Inst. Phys. Conf. Ser. No. 153, IOP Publishing Ltd. Bristol 1997, 69.
7. Hejna J, Hoffmelster H and Kohl H, Submitted to ICEM 14 (Cancun, Mexico 1998)

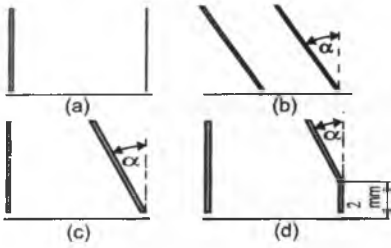


Fig. 1. Shapes of electrodes. Thickness of the second electrode in (a) is 0.1 mm and the aperture diameter changes from 0.1 to 1 mm. Thickness of all other electrodes is 1 mm and the aperture diameter is 1 mm. The distance between electrodes is 5 mm in (b) and 10 mm in (a), (c) and (d). Plots (a) ÷ (d) in Figs. 2 and 3 refer to versions (a) ÷ (d) in this figure.

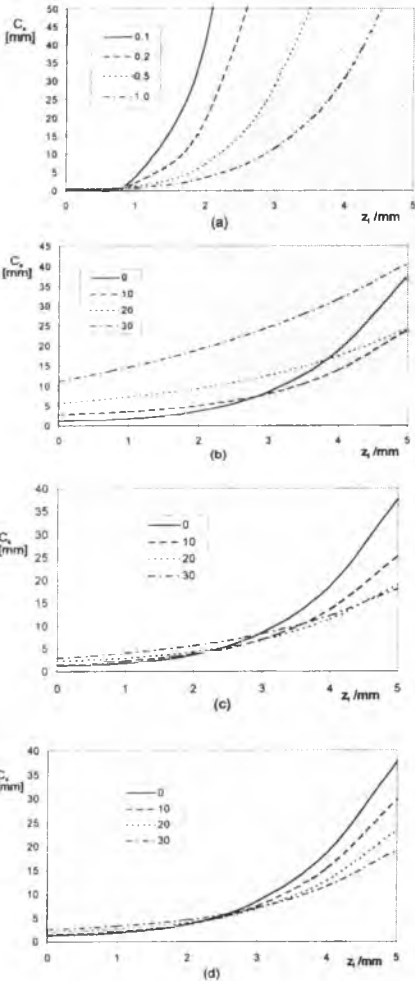


Fig. 2. Dependence of the spherical aberration coefficient on the distance from the right electrode for lenses from Fig. 1. Parameter is the aperture diameter in (a) and the cone angle in (b) to (d)

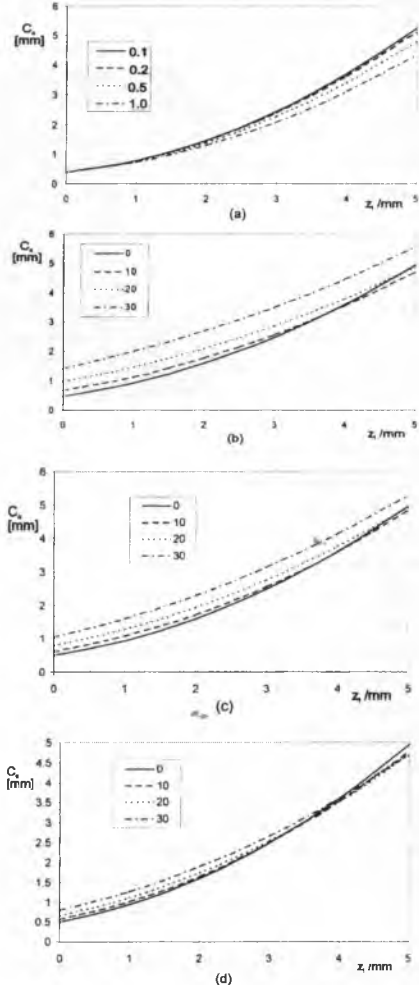


Fig. 3. Dependence of the chromatic aberration coefficient on the distance from the right electrode for lenses from Fig. 1. Parameter is the aperture diameter in (a) and the cone angle in (b) to (d)

NONCHARGING MICROSCOPY OF SEMICONDUCTOR STRUCTURES

Otakar Hutar

*Institute of Scientific Instruments, Academy of Sciences of the Czech Republic,
Kralovopolská 147, CZ - 61264 Brno, Czech Republic*

Introduction

Noncharging scanning electron microscopy is an important tool for the diagnostics of semiconductor devices. For charging suppression, it is necessary to match the PE landing energy in order that the total electron yield of the electron emission from the surface is equal to 1, on each point of the specimen surface. (Energy E_1 or E_2 , in the graph of the total emission yield vs the energy of PE). The E_2 values are practically applicable because of their autostable character - small, local positive or negative charges in the surface cause local increase or decrease of PE landing energy and in this way maintain the noncharging conditions. E_2 values depend on tilt angle [1]. Also, the subsequent technological operation like ion implantation or plasma etching change the E_2 values by one hundred volts or more, for the photoresist layers.

Methods

A commercial SEM was equipped by the cathode lens designed by Mullerova and Frank (Fig. 1), [2]. Samples of positive photoresist and SiO_2 pattern fabricated on different surfaces (Al, Si etc.) served as specimens. The accelerating voltage for PE was 10kV. Programs ELD and TRASYS made by Lencova and Wisselink were used for the simulations of the electrostatic field and trajectories of signal electrons.

Results and conclusions

Fig. 2 shows the positive photoresist pattern on Al surface under noncharging conditions. The landing energy of PE was 620eV. The strong electric field of the cathode lens extracts the signal electrons and helps to set up noncharging conditions more sharply. The PE energy is small, the penetration depth is then greatly reduced, and the image should carry more surface information. But for some materials and layers it is difficult to meet these expectations. The reasons for this are not clear. The image becomes too flat no pattern profile is seen, and the topographic contrast is reduced. It is probable that the surface and bulk conductivity play a certain role. This will be the subject of the further investigations. A cathode lens is intended to be used for the measurements of critical dimensions also. Simulations of the signal electron trajectories demonstrate that the BSEs contribute to the signal creation much more than the SEs (Fig. 3, 4). The fraction of SEs with energies between 2 - 7eV, escape through central bore in the scintillator and do not contribute to the signal. Despite of strong electric field in the cathode lens, trajectories of both BSE and SE are influenced significantly by the take-off angle of the electrons. (The take-off angle is measured with the respect to specimen level). The use of 10kV accelerating voltage for PE and 5mm distance between specimen and grounded electrode is a compromise for the achievement of good optical properties and the prevention of electrical breakdowns.

This project No.A2065703 is supported by the Grant Agency of the of the Academy of Sciences of the Czech Republic.

References

- [1]. Joy, D.C.: Scanning, 1989, 11, pp.1- 4
- [2]. Mullerova, I., Frank, L.: Scanning, 1993, 15, pp.193 - 201

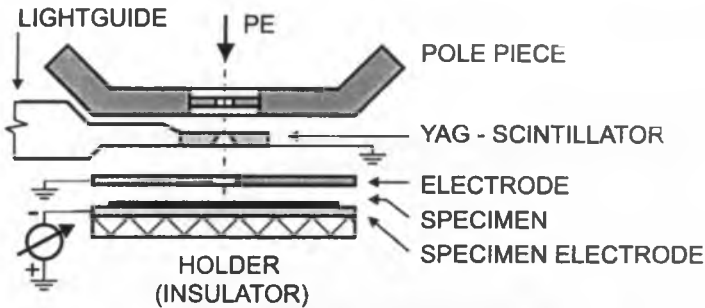


Fig. 1. Design of the cathode lens



Fig. 2. Image of the positive resist pattern on Al surface. PE landing energy 620eV

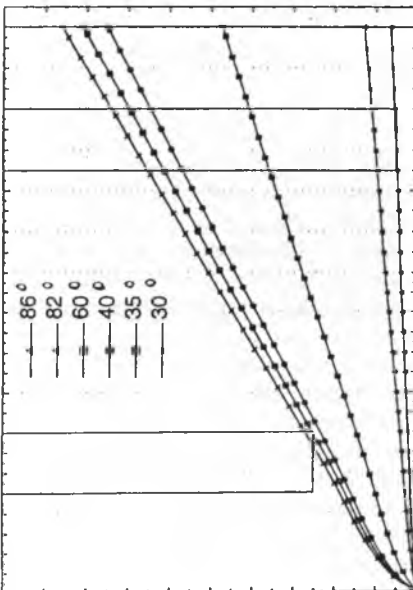


Fig. 3. The BSE trajectories . E = 500eV
Take-off angles 30, 35, 40, 60, 82, 86 degree

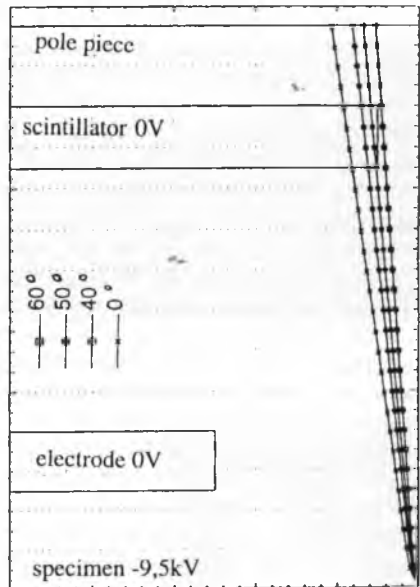


Fig. 4. The SE Trajectories. E = 5eV
Take-off angles 0, 40, 50, 60 degree

THE SEPARATION OF SECONDARY ELECTRONS IN ANNULAR AND PLANAR DETECTORS

Otakar Hutár, Rudolf Aufrata

*Institute of Scientific Instruments, Academy of Sciences of the Czech Republic,
Kralovopolska 147, CZ - 61264 Brno, Czech Republic*

Introduction

Annular and planar detectors are the scintillation LVSEM detectors proposed by Aufrata et. al. [1,2]. The principles of their function are demonstrated in Fig.1. The grids in both detector systems have two functions: First, to prevent the penetration of high intensity accelerating electric field from the scintillator and to influence the PE and the signal electrons, second, to separate the SEs from the signal electrons impinging scintillator - if the grid is negatively biased sufficiently (cca -100V). In this case the image is created by the BSEs only. The models of these two detectors were used for the study of the imaging mechanisms and imaging properties in the low energy range of the PE, up to 1keV.

Methods

Experiments were performed on a commercial SEM, equipped by the continual setting of the cathode accelerating voltage up to cca -800V. The structures of semiconductor devices were used as test specimens. A special specimen for the evaluation of the material contrast was made from plates of copper ($Z = 29$) and zinc ($Z = 30$), with the backscatter coefficients 0,311 and 0,318 respectively, and they are almost independent of the PE energy. The calculated material contrast value is 0,023. We investigated the dependence of the image and signal characteristics on the work conditions such as grid and scintillator voltages, energy of PE, grid density and the diameter of their wires. These results were correlated with the results of simulations of the electrostatic field and the trajectories of signal electrons computed using the programs EKVIPOT and TRACER developed by Chmelik et. al. in our institute.

Results and conclusions

Annular and planar detectors are the low voltage detectors which can be operated as either BSE or BSE + SE detectors, in dependence on grid voltage. The grid voltage which is essential for the separation of the SEs varies typically from -100 V to -200V, and depends mainly on the grid density (Fig. 2). Both material and topographic contrast can be obtained by means of these detectors in BSE mode. By the higher working distance, the high loss BSEs are collected and they carry a material contrast. By the low working distance, from 10mm for annular detector to 1 or 2mm for planar detector, the low loss BSEs hit the scintillator and the topographic contrast is obtained (Fig. 3). For the planar detector, the signal is weaker compare to annular detector because the small working distance causes the useless escape of BSEs to the central tube. The material contrast for the Cu/Zn system can be distinguished up to $E_0 = 2\text{keV}$. Below $E_0 = 2\text{keV}$, it can be seen in annular detector by means of the "amplification effect" of SE III emitted from the golded pole piece in case when the grid is positively biased. In this case the image can be noisy because of the SE I and SE II coming from the specimen. Both detectors exhibit a good sensitivity to the voltage contrast. It reaches the maximum by slightly negative (cca -8V) grid potential (Fig. 4). Positive grid biasing does not enhance the voltage contrast.

This project No.A2065703 is supported by the Grant Agency of the Academy of Sciences of the Czech Republic

References:

- [1]. Austrata, R.: Scanning Microscopy, 1989,3, pp.739-763
 [2]. Austrata, R., Hejna, J.: Scanning ,1991, 13, pp.275-287

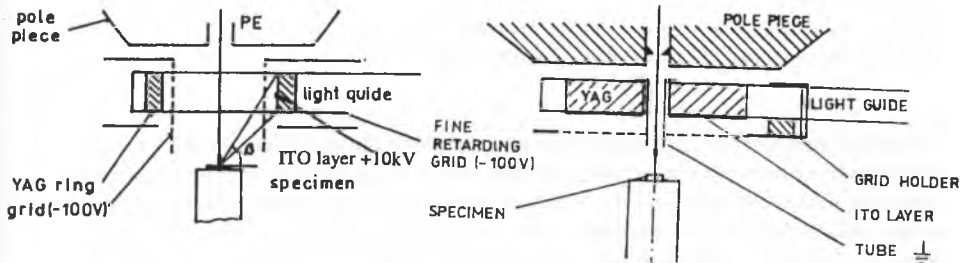


Fig. 1. The annular (left) and planar (right) detector for low voltage operation

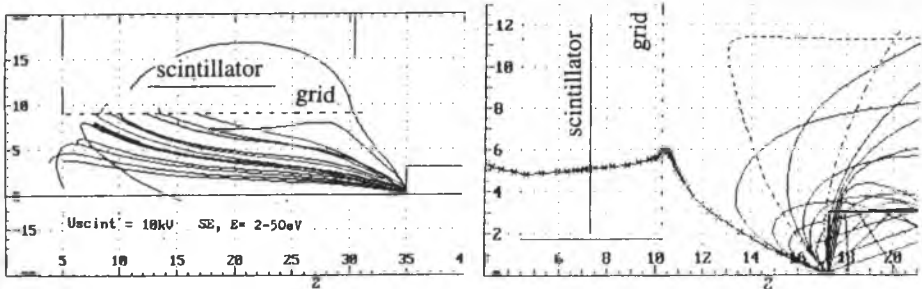


Fig. 2. SE trajectories in annular and planar detector with a negatively biased grid (-100V).

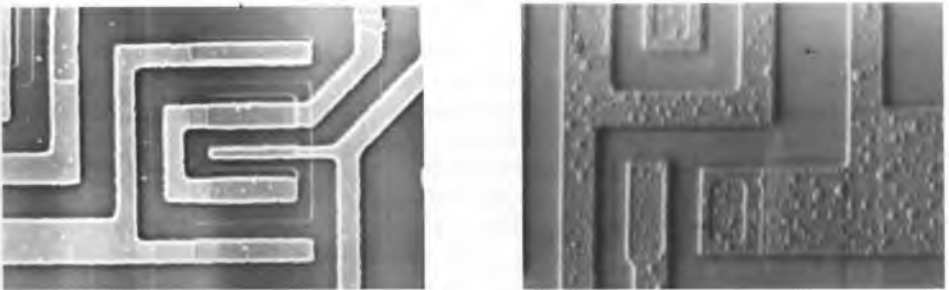
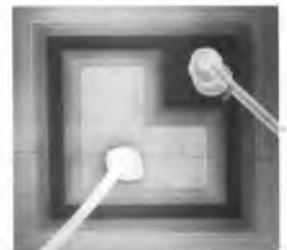


Fig. 3. Topographic contrast in BSE mode. Annular detector (left), planar detector (right).
 IC surface covered with the passivating SiO_2 APCVD layer. $E_0 = 2,2\text{keV}$.

Fig. 4. Voltage contrast in BSE + SE mode. Annular detector.
 Transistor KFY 18. Without passivation.
 $U_{BE} = +5\text{V}$ applied. The rest of the circuit is grounded.
 Voltage contrast is visible below 1V .



STUDY OF DETECTION PROPERTIES OF A MEDOL/GEMINI OBJECTIVE LENS FOR SECONDARY ELECTRONS

R. Janzen and E. Weimer*

Janzen Consulting, Ludwigstr. 3, 64653 Lorsch, Germany

**LEO Elektronenmikroskopie GmbH, 73446 Oberkochen, Germany*

Compared with an Everhart Thornley detector the MEDOL/GEMINI objective lens not just collects secondary electrons but it images them onto an in-lens detector. We used a ray tracing computer simulation to analyse the transfer properties of such a system. It is shown that by a proper selection of the column potential and the position of the magnetic pole piece a fourier transform like transfer of secondary electrons can be achieved. In this case the axial distance of secondary electrons in the detection plane strongly depends on their angle of emergence at the specimen surface and the topographic image contrast is improved.

OUTLINE OF AN ELECTRON MONOCHROMATOR WITH SMALL BOERSCH EFFECT

F. Kahl and H. Rose

*Institute of Applied Physics, Technical University Darmstadt,
Hochschulstr. 6, D-64289 Darmstadt, Germany.*

The attainable information in electron microscopy and holography is ultimately limited by the chromatic aberration. For round lenses this defect can only be reduced by decreasing the energy width of the incident electron beam [1]. To push the information limit below 1 Å at voltages higher than about 200 kV, the energy width must not exceed 0.2 eV. Unfortunately, the energy width of field-emission guns lies in the range between 0.6 eV and 0.8 eV for beam currents required in TEM. As shown by experiments, about 30 % of the electrons have an energy deviation from the mean value smaller than 0.1 eV for an emitted beam current of a few μA . If the remaining 70 % of the electrons could be filtered out by a monochromator, one would obtain a nearly monochromatic source with sufficient beam current. The acceleration voltage at the location of the monochromator should not exceed 3–5 kV to achieve a dispersion which is sufficiently large for filtering. Hence the monochromator must be placed immediately behind the source. Due to the high voltage to ground (a few hundred kV) in a TEM, a purely electrostatic design is mandatory. Such an electrostatic monochromator was first proposed by Plies [2]. Unfortunately, his design consists of a large number of elements and requires a large extension of the height of the microscope. The electrostatic Ω -shaped monochromator proposed by Rose [3] is significantly shorter. However, a common disadvantage of both designs is the formation of several stigmatic intermediate images of the source within the system. The high current density in the surrounding of these images produces a large Boersch effect [4,5] which significantly increases the energy width of the beam.

To minimize the Boersch effect, we recently analyzed the feasibility of Ω -shaped monochromators with astigmatic and virtual stigmatic intermediate images of the source. The line-shaped astigmatic images produce a much lower current density than stigmatic images. The schematic construction of this type of monochromator is sketched in figure 1. To avoid a loss of lateral coherence and brightness, the monochromator must be free of dispersion at the exit plane. Hence it is useful to maximize the dispersion at the symmetry plane z_s and select the energy there. The line image in the energy selection plane is perpendicular to the direction of the dispersion. The dispersion shifts this image away from the axis by a distance which is proportional to the energy deviation. By properly adjusting the width of the selection slit, all electrons with too large energy deviations can be filtered out. To allow for an accurate filtering, the second-order aberrations, especially the aberrations caused by misalignment of the source, must be kept small in the direction of the dispersion. To preserve the diameter of the source, the second-order aberrations at the final image plane z_i must also be negligibly small. Owing to the symmetry of the monochromator, the aperture aberrations and the distortions vanish at this plane.

The dipole field of each deflector curves the optic axis, focuses the electron beam in the xz -section and defocuses it in the yz -section. In order to focus the beam also in this section an additional quadrupole field must be excited within each deflector which overcompensates the defocusing refraction of the dipole field in the yz -section and reduces the focusing effect in the other section. The required quadrupole field can be obtained by an appropriate curvature of

the electrode surfaces. A line image of the source perpendicular to the dispersion is formed at the selection plane if the axial ray x_α , yet not the corresponding ray y_β , vanishes at this plane. Owing to the symmetry condition, x_α must be point symmetric and y_β mirror symmetric with respect to the selection plane. Since the dispersion should be large at this plane and vanish at the exit plane, the path of the dispersion ray must be mirror symmetric. The fourth condition is the roundness of the illumination at the object plane. Here roundness means the preservation of the round emission characteristic of the source. The fundamental rays of a feasible design are plotted in figure 2. For the computation of this design we used the Sharp Cut-Off Fringe Field approximation (SCOFF) which allows an analytical evaluation of the fundamental rays and of the second-order aberrations. The path of the fundamental axial rays x_α and y_β reveals that both the entrance image z_o and the exit image z_e of the source are virtual. Thus, stigmatic crossovers are completely avoided.

To find a realistic design, we start from a suitable solution of the SCOFF approximation and take into account the finite extension of the fringe fields of the deflectors. The fields are calculated by approximating the surfaces of the electrodes by meshes of triangles. For each triangle a linearly distributed charge density over the surface is assumed. In this case the corresponding potential can be expressed analytically. This procedure enables a calculation of the partial derivatives of the potential with sufficiently high accuracy for computing the aberrations up to the third order inclusively. In addition, we implement a Monte-Carlo simulation to estimate the influence of the Boersch Effect.

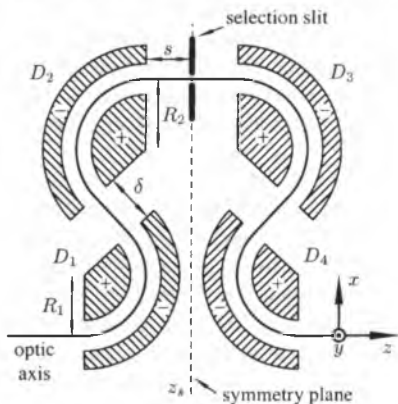


FIG. 1 - Cross-section of the monochromator containing the optic axis

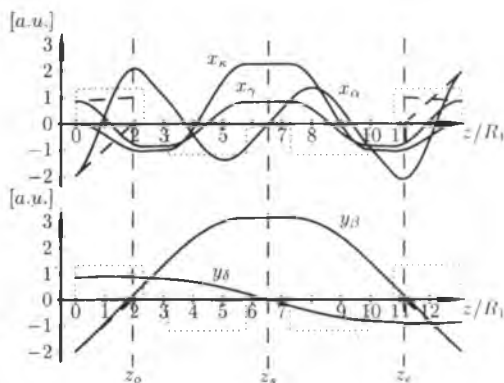


FIG. 2 - Paths of the fundamental rays along the optic axis straightened along the xz -section (top) and the yz -section (bottom).

References

1. Scherzer O., *Optik*, 2 (1947) 114.
2. Plies E., *Proc. Int. Conf. Electr. Micr.* Toronto Vol. 1, p. 50. (1978).
3. Rose H., *Optik*, 86 (1990) 95.
4. Rose H., Spehr R., In: *Advances in Electronics and Electron Physics Suppl. 13C*. (edited by Hawkes P.), p. 475. Acad. Press (1983).
5. Boersch H., *Z Phys.*, 139 (1954) 115.

DIFFERENT WAYS OF ADDING THE ABERRATIONS

Robert Kolařík and Michal Lenc

Dept. of Theor. Physics and Astrophys.

Kotlářská 2, 611 37 Brno

Czech Republic

In our paper [1] the main idea was to get a general expression for the resolution σ_r (when considering unavoidable axial aberrations - spherical and chromatic - and the finite source size) in terms of wave optics. The resulting expression enables to choose an arbitrary criterion for the resolving power and to seek for the maximum resolution (optimization is being performed with respect to defocus and image aperture angle) in an analytical way. Our predictions for the resolution were compared with the results of Mory [2] and Barth [3]. Hammel and Rose studied similar problems in [4].

The discussion in [1] did not concentrate on another result - a form of the intensity distribution function $I(\sigma)$ (σ being the radial coordinate in the observation plane). This function depicts the probe profile in the observation plane. The main effort of our present work has been directed to study the possibility of verifying the validity of $I(\sigma)$ experimentally. Basic idea was to design an appropriate optical alignment, whose optical parameters would enable us to measure the probe profile on the screen (the CCD camera is supposed as a detector). In order to get a sufficient magnification within the optical distance, where disturbing effects can be neglected, we have to work with a multi-lens system. We have considered a column with three lenses working in different modes. Using the computation program ELD [5], we were trying to design lenses suffering from very large spherical and chromatic aberration coefficients for given focal distances and magnifications. In such case we should obtain measurably wide probe spot close to the diffraction-limited situation, where our $I(\sigma)$ form is exact as a consequence of used approximation.

We assume that it is possible to derive similar formulae for the other experimental configurations, where only one aberration term becomes dominant.

- [1] R. Kolařík, M. Lenc: An expression for the resolving power of a simple optical system. *Optik* **106** (1997) 135-139.
- [2] C. Mory, M. Tence, C. Colliex: Theoretical study of the characteristics of the probe for a STEM with a field emission gun. *J. Microsc. Spectrosc. Electron.* **10** (1985) 381-387.
- [3] J. E. Barth, P. Kruit: Addition of different contributions to the charged particle probe size. *Optik* **101** (1996) 101-109.
- [4] M. Hammel, H. Rose: Resolution and optimum conditions for dark-field STEM and CTEM imaging. *Ultramicroscopy* **49** (1993) 81-86.
- [5] B. Lencová: Computation of electrostatic lenses and multipoles by the first order finite element method. *Nucl. Instr. Meth.* **A363** (1995) 190-197.

NEW TRENDS IN SOFTWARE FOR ELECTRON OPTICS

Bohumila Lencová

Institute of Scientific Instruments, Academy of Sciences of the Czech Republic
Královopolská 147, 612 64 Brno, Czech Republic

Introduction

This paper represents a set of notes for the 6th seminar on Recent Trends in Charged Particle Optics and Surface Physics Instrumentation, organized by the Institute of Scientific Instruments in 1998. The discussion below concentrates on the computations of potentials and fields. The text is intentionally unpolished, hoping to serve the purpose of provoking discussion. It is also not intended to influence any author, user or potential buyer of any software.

Sources of information

The newest book on electron optics published by CRC Press [1] should provide the most recent overview of software trends. Its Chapter 1 on *Computational Techniques for Design of Charged Particle Optical Systems* by E. Munro does; unfortunately it hardly mentions any programs that were not written by the author or his group.

An opportunity to observe the current trends in software for electron optics is given at the international *Charged Particle Optics* conferences, held in 4 year intervals [2]. The last one, CPO5, took place in April 1998 in Delft. Most people involved in this subject show up, and the size of the meeting is small enough to listen to all lectures or to talk to other people (unless, as this time, parallel sessions are introduced). Computer programs should be at the center of attention this year, and almost 20 were demonstrated at the conference. Some of the subjects discussed there will be mentioned. Under similar or even the same name *Charged Particle Optics* SPIE organized other conferences [3]. This year's CPO of SPIE was canceled.

An important workshop [4] bringing together people from all of Europe involved in particle optics computation was held in Delft in 1994; it was sponsored by European Union. (Its Proceedings is not widely available, equally as those of the current seminar). As a consequence the most complete list of programs for particle optics was set up [5]. Most links to other relevant sites on Internet can be traced from [6].

Finite element method

FOFEM, the first order FEM, is my favorite subject, and naturally I must claim that it has had some development. First let us consider the **short computation time**. If the solution of 100000 equations in a topologically regular mesh lasts only 60 seconds on a 200 MHz PC, one could expect that the idea of using large meshes will be generally accepted. Let us just remind, that the computation back in 1988 in meshes with the maximum possible number of points of 8000 on then the fastest (8 MHz) AT computers needed about 20 minutes! The mesh with 8000 points needs just 8 s on (now obsolete) 486/66 MHz PC, meshes with 16 thousand points need 30 s, and 100 thousand 10 minutes (the program then needs only around 12 MB RAM).

Surprisingly, it is still possible to find references to problems with the use and accuracy of the FOFEM with small meshes (e.g. Tsuno in his chapter on magnetic lenses in [1] or Khursheed in 1997 in [3] or at CPO5). The same arguments hold for the use of graded meshes: if most users see that the axial field behaves strangely at the places where the mesh step change abruptly, the most natural solution is the use of smoothly graded meshes. Another fact that nobody uses the value of the integral of magnetic field along the axis and/or around the lens as a check of correctness of the magnetic lens computation is really difficult to understand.

Next question is that of **computation accuracy**. The accuracy of any 'mesh' method depends on the type of mesh and the number of mesh points used. I will in this respect briefly mention an important but overlooked aspect of checking the accuracy of FEM computations, the extrapolation to 'infinite number of points'; the first example of that for magnetic lenses we published already in 1994 [4], and I have discussed this in detail at CPO5.

In the practical application of any program, the aspect of **user friendliness** and **user interface** becomes important. We have devoted to this aspect a lot of attention in Brno as well as in Delft in our software packages, that use a unified approach to magnetic and electrostatic lenses and multipoles. The computation times are reasonably short, and cheap and available personal computers are used for the computations. In the user interface graphical editing is used, the generation of graded fine mesh is done automatically, and all results are shown or exported graphically. The program packages thus meet most requirements from a user point of view, in spite of leaving some space for improvements, because the interfaces were written in a pre-Windows time. The numerically obtained results are accurate enough to allow not only computation of paraxial properties and aberrations from axial potentials or fields but also ray tracing.

SOFEM by Munro group was introduced 10 years ago, and it is often put as a competitor to FOFEM. This seems to be the case of their program **SOURCE** for calculating guns and space charge limited beams. In spite of the considerable span of time since the introduction of SOFEM, hardly any attention is given to accuracy (an exception being the discussion of the computation accuracy of axial potential in a two-cylinder lens by Munro in [4] and later by me at CPO4 where it could be shown that the FOFEM produces competitive results). Electrostatic lens computations seem to work, although the mirror results in [1] are surprisingly inaccurate (as discussed in 1996 at this seminar). In **magnetic lens computations with SOFEM** no limit of maximum number of points is ever mentioned (but it is known that it is impossible to calculate on large meshes). No integral along the axis is computed, so the very basic check, if the result is correct, is missing. Some of the SOFEM results on saturated lenses look strange [7]. What is published by Munro on the **computation of multipole components with SOFEM** is even ridiculous, and the same error since [4] is in [1]. The FOFEM implemented by Munro does not work properly for the computation of hexapole field component in deflectors, in particular with small number of points and with large mesh step change at the place where the field is still strong and varying (the computations in meshes where the problem is stated last less than 1 s on obsolete 486 PC), and their program does not work for 5th harmonic component at all. It does not mean that this is a problem that cannot be handled by FOFEM accurately [8]. As a summary I do not see SOFEM as the 'competition' of FOFEM, and I would like to see more accuracy tests of the method.

Finite difference method

The FDM is used in particle optics for a long time, as the use of rectangular mesh makes programming easy, although material properties (dielectrics or magnetic saturation) are more difficult to implement. In **two dimensions** Kasper at CPO3 [2] (see also 1997 paper in [3]) described the advantages of 9 point FDM (since then it was also implemented by Becker [5]).

The FDM is the way to go into **three dimensions**, in particular in electrostatic systems or magnetostatic systems without saturation. In the MEBS 3D FDM programs [1] Rouse successfully resolved the problem of mesh lines cut by boundaries and electrodes. Our 3D FDM program written at TU Brno [9] (see also 1996 seminar) has implemented the same approach. Since then it was not much developed, and recent strict accuracy tests against SIMION and 3D BEM program of Read showed slight problems in interpolation and ray tracing. This fortunately does not prevent its application in ion beam simulations of space charge limited beams.

A popular program based on FDM is **SIMION** [5]; it is since 1996 also in 3D, although the objects have to be approximated by steps. It started in ion (mass spectroscopy) applications, and as it has a colorful graphical Windows interface, its use grows in popularity. Unfortunately, nobody from its authors was ever at international CPO conferences. Attempts to check its accuracy against 3D BEM methods were presented at CPO5 (see below).

Boundary Element Method

Field computation in BEM is based on calculating the source distribution, and so it is used mostly in electrostatics (thus it is often called **charge density method**). 2D and 3D computations with the inclusion of space charge are handled by CPO programs of Read [5]. If the singularities in the field sources are hidden inside electrodes, we talk about '**charge simulation**', a method used also by Preikszas (see the last seminar), and the latest status of similar programs of Kasper were demonstrated at CPO5. At the same conference Tiunov presented his program based on rather an interesting approach: use AutoCAD as an interface. Many problems were, as usual with Russian authors, left hidden or unexplained. Let me leave most of the responsibility for this subject rather to Prof. Martinez at this meeting.

In the past BEM was also used for magnet computations [10]. At CPO5 a hybrid method combining BEM with FDM in the magnetic material [11] was discussed.

Comparison with other methods

It is my impression that often people are addicted to a given method of computing potential, mostly to the one they developed themselves, and thus they do not try to compare it with the performance of other programs and methods. There are some program aspects that are actually difficult to compare, like how easy they are to (learn to) use, their documentation, on which computers they run, how easy it is to get given specific results, and how fast the results can be obtained. The last argument is losing on importance, because the speed of computers grows very fast. Another question is what problems to use for comparison: even programs written for particle optics may have difficulties with a given specific test. We have tried to make such a comparison recently [12] for electrostatic 2D programs (FEM, BEM and SIMION as the FDM

program) for three problems where analytical solutions are known: spherical analyzer, thin aperture between two regions of constant field, and a two-cylinder lens, where computation accuracy was given against computation time. The results in 3D computation were added for the presentation at CPO5. One test was actually left out, which can be used as an ultimate test of any electrostatic program: the dipole mirror of Preikszas and Rose (see the notes for 1996 seminar).

Conclusions

Even the best software for electron optics cannot solve all problems. A 'dedicated' user can produce ANY result - including often the biggest nonsense. Sometimes this is a consequence of the usual 'human' approach to computers and programs: some people tend to trust any result produced by a computer if it keeps them from thinking. Are there any ways how to prevent this?

Another fact is that in the places where the actual research is done into computational methods and extreme applications of programs, nobody is actually interested in having a nice program as an output. Should the universities do more to finish the software into a commercial product? Everyone implicitly requires a full range of services (Windows interfaces, on-line help, full documentation, many options implemented in a program), but is there somebody really willing to pay for all these features? What should be in a good software for electron optics?

Acknowledgment

Supported by a grant of Acad. Sci. of the Czech Republic No. A1065804. Software for FEM is distributed by Delft Particle Optics foundation [5] - cooperation with G. Wisselink, M. Lenc, J. Chmelík (and recently with J. Zlámal) acknowledged. F. H. Read and D. Cubric from U. Manchester were involved in the comparison of electrostatic programs; the project was supported by a grant of Royal Society. Let me also mention recent fruitful discussions started with R. Becker, U. Frankfurt, and G. Martinez, U. Complutense, Madrid.

References

- [1] **Handbook of Charged Particle Optics**, ed. Jon Orloff, CRC Press, 1997.
- [2] Proc. of CPO3 published in Nucl. Instr. Meth. **A298**(1990), CPO4 in NIM **A363**(1995).
- [3] Proceedings of SPIE 2014 (1993), 2522 (1995), 2858(1996) and 3135(1997), respectively.
- [4] Workshop on Computer Assisted Design of Particle Optics Instrumentation, Delft, June 1994.
- [5] <http://cpo.tn.tudelft.nl/bbs/cposis.htm>.
- [6] <http://chaos.fullerton.edu/mhslinks.html>.
- [7] K. Tsuno, Ultramicroscopy **72**(1998), 31-39.
- [8] M. Lenc and B. Lencová, Rev. Sci. Instrum. **68**(1997), 4409-4413.
- [9] J. Zlámal, MSc. Thesis, TU Brno 1996 (see also 1996 seminar).
- [10] K. J. Binns, P. J. Lawrenson and C. W. Trowbridge, **The analytical and numerical solution of electric and magnetic fields** (J. Wiley & Sons, 1992).
- [11] A. von der Weth, Dissertation FB Physik, U. Frankfurt/Main (1997).
- [12] D. Cubric, B. Lencová and F. H. Read, Proc. EMAG97. Inst. Phys. Conf. Ser. 153, 91-94.

SPECTROSCOPIC IMAGING WITH THE LOW ENERGY ELECTRON MICROSCOPE

G. Lilienkamp¹, Th. Schmidt¹, S. Satchenko², K. Prince³ and E. Bauer¹

¹ *Physikalisches Institut der TU Clausthal, Leibnizstr. 4, D 38678 Clausthal-Zellerfeld Germany*

² *Institute for Analytical Instrumentation, 198103 St. Petersburg, Russia*

³ *ELETTRA, Sincrotrone Trieste, SS14 km 163.5, Basovizza, 34012 Trieste, Italy*

The capabilities of a Low Energy Electron Microscope (LEEM) have been described e.g. in [1]. An electrostatic energy filter opens up spectroscopic contrast for instance by imaging of photoelectrons, Auger-electrons or inelastically scattered electrons. First results with a simple 90° electrostatic version of the filter have been published in [2,3]. Recently an improved filter with 180° deflection angle has been installed and first results have been achieved under illumination with VUV-light at the gas phase beamline of ELETTRA.

The benefits from the new filter are: improved energy dispersion of about 40 μm/eV, optimised transmission at a fixed energy resolution, the possibility of selecting an area of interest on the sample (field of view aperture), and the possibility of imaging the dispersive plane.

Besides the known modes of operation: imaging of elastically scattered electrons, photoemission microscopy near threshold, mirror-microscopy, energy filtered imaging, and imaging of the diffraction pattern further modes are now possible:

- parallel acquisition of an energy spectrum of a selected area of interest
- acquisition of diffraction patterns (e.g. photoelectron diffraction patterns) from objects as small as 1 μm.

The resolution obtained so far is:

- 25 nm spatial resolution in the secondary emission mode (excitation with VUV-light)
- about 400meV energy resolution,
- better than 8 meV line resolution in the LEEM mode.

[1] E. Bauer, Rep. Prog. Physics **57** (1994) 895

[2] E. Bauer, C. Koziol, G. Lilienkamp and Th. Schmidt, J. Electron Spectrosc. Rel. Phen. **84** (1997) 201

[3] G. Lilienkamp, C. Koziol, Th. Schmidt, and E. Bauer to be published in: X-ray Microscopy and Spectromicroscopy, eds.: J. Thieme, G. Schmahl, E. Umbach. D. Rudolph, Springer Verlag, Heidelberg

OPTIMAL SYNTHESIS OF CHARGED BEAM FOCUSING SYSTEMS

G. Martínez^(a), A. D. Dymnikov^(b) and A. H. Azbaïd^(a)

^(a)*Dept. Física Aplicada III, Fac. de Física, Universidad Complutens, E-28040 Madrid, Spain*

^(b)*C.I.E.M.A.T., Avda. Complutense 22, E28040 Madrid, Spain*

One of the main characteristics of contemporary Science is a quick creation of knowledge that is frequently associated to the appearance of new or more refined measurements. There has been a continuous improvement of the existent instrumentation and a development of sophisticated new devices that has made possible this outstanding progress.

To go on this tendency we need to prepare appropriate tools: mathematical and physical models to simulate the behaviour of a system and the way in which this behaviour can be optimized. In this talk I will present a scheme of work that we are applying to the optimal design of electrostatic lenses. Even if this is a small area in Charged Particle Optics the scheme could be extended to other beam guide systems.

The direct method for finding the optimal design would be to compute simultaneously the field and trajectories of the particles through the quadruplet, but these trial and error tests demand a huge amount of computing time that is not possible to do in practise. To overcome this problem we use two models: an analytical model and a numerical field model. The first one utilises analytical functions for the axial electrostatic potential and its partial derivatives. With these functions it is possible to obtain the analytical solution in matrix form up to the desired order approximation, in our case up to third order. In the analytical model the initial approximate differential equations are replaced by the linear equations in the space of the phase moments with the same approximation accuracy. Thus we can use all the advantages of linear differential equations over non-linear ones, including the independence of the matrix of the choice of the initial point of the phase space [1].

An interesting finding is that placing two slits at the appropriate place before entering the lens allows to shape optimally the initial beam and to obtain the minimum spot size at the target. By this way it is possible to find the optimal parameters of the system with minimum computing time.

At the second stage we apply an accurate version of the boundary element method which simulates the geometry of the real system and performs a very precise calculation of the field. In fixing the initial conditions for ray tracing, we use the information provided by the analytical model. Thus, the combination of both techniques allows the synthesis of the best lens in a straightforward way.

As a first example let us consider the optimization of electrostatic axisymmetric lenses consisting of multiple coaxial cylinders [2]. A new analytical model of the axial potential distribution is applied which corresponds to realistic multiple cylinder systems. Using the version of BEM described in reference [3] to solve Laplace's equation we obtain the parameters of the physical model that has the same axial potential distribution as the analytical model. The parameters of the physical model are lengths and radii of the cylinders, the gaps between them, and the applied potentials. Figure 1 shows the computed axial potential for a 3-cylinder lens and the corresponding analytical function. The coincidence between the two profiles allows matching the focal distance and the demagnification within at least three digits.

To analyse the beam spot size we find the matrix (or transfer matrix function) for the linear and nonlinear equations of motion using the effective recursive computational method

proposed by one of the authors of this paper [1]. Applying this method the phase volume of the beam can be strictly conserved at each step of the numerical integration. For the optimiza-

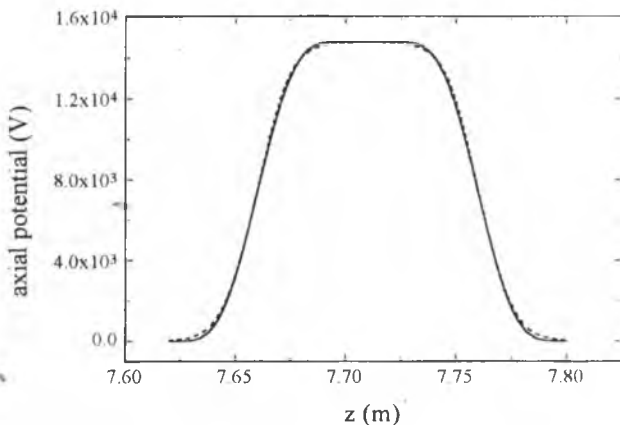


Figure 1. Axial potential as calculated for a 3-cylinder lens. Continuous line is for the mathematical model, dashed line is for the numerical potential. (Taken from reference [2])

tion we determine the average radius of the beam using the matrix of the moments of the distribution function over the whole totality of the phase coordinates

As a second example we consider a microprobe consisting of four electrostatic quadrupoles forming a separated Russian quadruplet [4]. Electrodes providing quadrupole fields can have different geometries. Rods or sections of rods are the most commonly used. In the analytical modelling we used a step-like function for the axial electrostatic field gradient and its second derivative. For the numerical solution we applied an accurate BEM version [5]. We have found the optimal construction for different emittances and investigated the influence of the rods, for a given aperture of the quadrupoles, on the final beam spot. Our results show that for low emittances the optimum diameter of rods is less than for high emittances.

In conclusion, for the two studied cases, the optimal spot size obtained in the analytical model had a very good coincidence with the best spot size found in the numerical model. Both methods together can be an efficient tool for the optimal synthesis of focusing systems.

REFERENCES

- [1] A. Dymnikov, R. Hellborg, Nucl. Instr. and Meth. A 330 (1993) 323
- [2] A.D. Dymnikov, G. Martínez, A.H. Azbaid, Nucl. Instr. and Meth. A 403 (1998) 195
- [3] G. Martínez, M. Sancho, in: P. Hawkes (Ed.), Adv. Electron and Electron Phys., Vol. 81, Academic Press, New York, 1991, p. 1.
- [4] A.D. Dymnikov and S. Ya. Yavor, Sov. Phys. Tech. Physics (USA) 9 (1965) 1544
- [5] A.H. Azbaid, A.D. Dymnikov, G. Martínez, Proc. SPIE'97, San Diego, USA, 1997

THE MICROANALYTIC PROSPECTS OF A HIGH RESOLUTION PEEM

M.Merkel⁽¹⁾, M.Escher⁽¹⁾, O.Schmidt⁽²⁾, Ch.Ziethen⁽²⁾, G.Schönhense⁽²⁾⁽¹⁾: Focus GmbH, Am Birkhecker Berg 20, D65510 Hünstetten-Görsroth, Germany⁽²⁾: Universität Mainz, Institut für Physik, Staudinger Weg 7, D55099 Mainz, Germany

Using synchrotron radiation at BESSY or a Mercury lamp we perform microspectroscopy experiments with a photoelectron microscope (FOCUS IS-PEEM) equipped with an electron energy analyser (FOCUS MICRO-ESCA). In this arrangement we are able to determine the chemical composition of solid surfaces with a high lateral resolution down to appr. 250 nm.

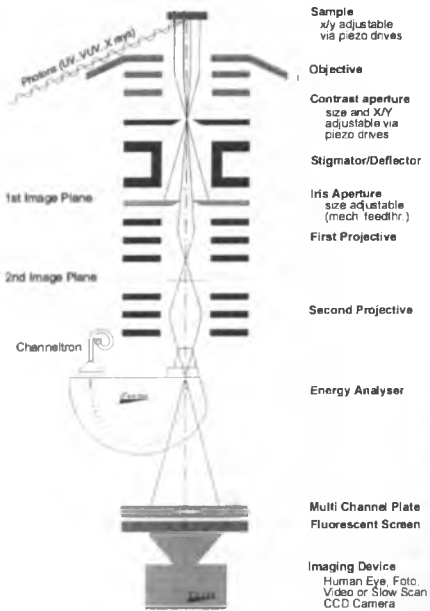
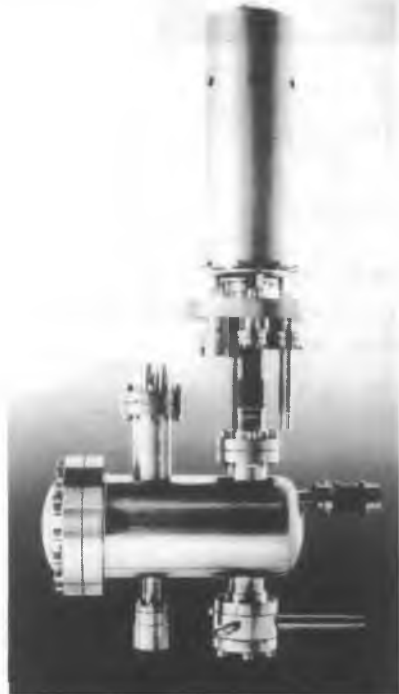


Figure 1: FOCUS IS-PEEM equipped with the μ -ESCA energy analyser



The experimental set-up is shown in Fig.1: The PEEM is used to get a lateral image of the chosen sample region with a resolution of today down to about 20..25nm. To get chemical information of a certain feature this region of interest is centred in respect to the actual field of view by means of the piezo driven x-y sample stage. Now the field of view is to be limited using the iris aperture located at the first image plane of the microscope objective lens. The iris aperture can be closed giving an effective field of view of down to about 250nm depending on the actual total magnification of the PEEM. The deflecting potentials of the analyser have to be switched on and choosing a suitable pass energy the energy spectrum of the selected region can be taken. More detailed information is given elsewhere [1],[2].

For demonstration of the recent performance we show in Fig.2 an example: This PEEM micrograph was taken with a photon energy of 95 eV at BESSY I (Undulator U2 combined to a multilayer optics). The sample consists of 20x20 μ m Pt-Co-Pt multilayer squares deposited onto a silicon substrate. There are plotted three valence band spectra taken at different μ -spot

(appr. $1 \times 1 \mu\text{m}$) positions of the sample. A first comparison shows significant differences in the chemical composition of regions "a" and "b" whereas these areas should consist both of the same deposited multilayer system. The

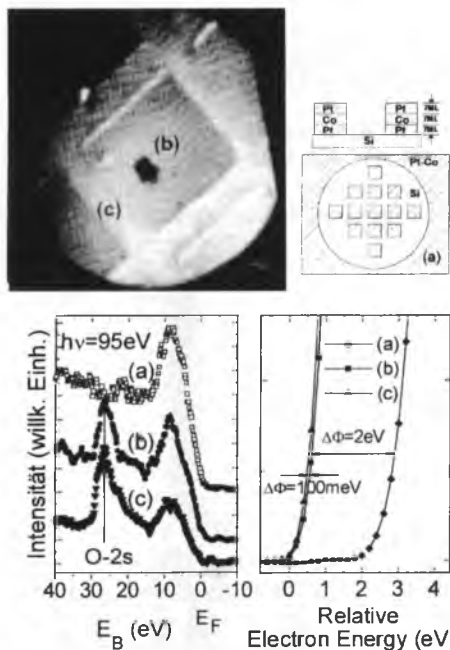


Figure 2: PEEM micrograph of a $20 \times 20 \mu\text{m}$ Pt-Co-Pt square deposited onto silicon together with energy spectra of labelled micro regions

The main difference seems to be the respective concentration of oxygen at these two different positions. A further hint to a qualitative difference is given by the second plot showing the low energy cut off of that three spectra. The huge energy shift between "a" and "b" of about 2eV has to be interpreted by a work function difference of this magnitude. The labelled small energy shift between "b" and "c" demonstrates at least an energy resolution of the system to be well below 100meV.

Some more examples and technical details will be shown.

A second approach to get chemical microanalysis with a PEEM is also shortly reported: By accomplishing the time structure of synchrotron light sources ("bunches") we took advantage of the time-of-flight method to get at one hand similar microanalytic energy spectra of certain sample regions. On the other hand we were already able to get quasi monochromatic PEEM images what offers the field of lateral elemental mapping ("Spectromicroscopy"). Some first results will be shown [3].

A versatile possibility to get chemical information is already a standard technique[4]: Without any additional equipment the PEEM is able to deliver information on the chemical elements and their binding character ("orbital mapping") using the presence of X-ray absorption edges of the elements. The synchrotron beam line monochromator has only to be tuned onto the right photon energy. Also for this approach we will show some examples.

The experiments were funded by BMBF (05644UMA7 and 05621UMA2).

References:

- [1] O.Schmidt, Ch.Ziethen, G.H.Fecher, M.Merkel, M.Eschler, D.Menke, U.Kleineberg, U.Heinzmann, G.Schönhense; *J.El.Spec.Rel.Phen.* **88-91** (1998) ; 1009-1014
- [2] Ch.Ziethen, O.Schmidt, G.H.Fecher, C.M.Schneider, G.Schönhense, R.Frömter, M.Seider, K.Grzelakowski, D.Funnemann, W.Swiech, H.Gundlach, J.Kirschner ; *J.El.Spec.Rel.Phen.* **88-91** (1998) ; 983-989
- [3] H.Spiecker, O.Schmidt, Ch.Ziethen, D.Menke, U.Kleineberg, R.Ahuja, M.Merkel, U.Heinzmann, G.Schönhense; *Nucl.Instr.Meth.*; in press (1998)
- [4] Ch.Ziethen, O.Schmidt, G.Schönhense, R.Frömter, J.Gilles, C.M.Schneider, J.Kirschner ; *BESSY Report* (1997) ; 414-416

A COHERENCE FUNCTION APPROACH TO MULTISLICE THEORY

H. Müller and H. Rose

*Institute of Applied Physics, Technical University Darmstadt,
Hochschulstraße 6, D-64289 Darmstadt, Germany.*

The simulation of high-resolution electron micrographs is a valuable tool for determining the atomic structure of objects by means of electron microscopical techniques. Although a number of different simulation methods have been proven useful, a quantitative correspondence between HREM simulations and experimental images has not yet been reached.

To take the step from qualitative to quantitative HREM image simulation, a theory of image formation which is solely based on the propagation of the stationary wave function of the scattered electron proves to be insufficient. To avoid this shortcoming, we have proposed a theory of image simulation based on the propagation of the stationary mutual coherence function [1]

$$\Gamma_c(\rho, \rho', \tau) = \langle \Psi(\rho, t) \Psi^*(\rho', t - \tau) \rangle_T. \quad (1)$$

Here Ψ is the electron wave function and $\langle \dots \rangle_T$ denotes the time average over the recording time T of the micrograph; ρ, ρ' are 2-dimensional coordinate vectors perpendicular to the optical axis. The recorded intensity in the image plane is given by $I(\rho) = \Gamma_c(\rho, \rho' = \rho, \tau = 0) = \langle |\Psi(\rho, t)|^2 \rangle_T$. The coherence function approach correctly accounts for the partially coherent nature of the electron optical imaging process and the quasi-elastic and inelastic scattering processes within the object. The propagation of the coherence function through the object can be calculated efficiently by a generalized multislice formalism [1,2]. In this formulation the scattering properties of each thin object slice are approximately described by the mutual transmission function

$$M(\rho, \rho', \tau) = \exp \left(i(\mu_1(\rho) - \mu_1(\rho')) - \frac{1}{2}(\mu_2(\rho) + \mu_2(\rho')) + \mu_{11}(\rho, \rho', \tau) \right). \quad (2)$$

This transmission function depends only on the first and second stochastic momenta of the projected slice potential considered as a time-dependent stochastic process. This approach considers the fact that for weak objects the ideal inelastic image represents the variance of the projected potential [3]. The terms in the exponent are explicitly given by

$$\begin{aligned} \mu_1(\rho) &= \langle \chi(\rho, t) \rangle_T, & \mu_2(\rho) &= \mu_{11}(\rho, \rho' = \rho, \tau = 0), \\ \mu_{11}(\rho, \rho', \tau) &= \langle (\chi(\rho, t) - \mu_1(\rho))(\chi(\rho', t - \tau) - \mu_1(\rho')) \rangle_T. \end{aligned} \quad (3)$$

The second relation ensures that our formulation does not violate the optical theorem as it is the case for the conventional multislice theory which uses an absorption potential to account for inelastic scattering. The information about the stochastic measures μ_1 , μ_2 , and μ_{11} can be calculated from simple analytical models describing the elementary quasi-elastic and inelastic scattering processes with a sufficient degree of accuracy. Currently we employ the Einstein model of lattice dynamics for thermal diffuse scattering and a modified Raman-Compton approximation for inelastic electron scattering resulting in electronic excitations [1,2].

To demonstrate the feasibility of our calculation method we have simulated unfiltered diffraction patterns of Si (110) for different crystal thicknesses. The calculation considers the influence of elastic, quasi-elastic, and inelastic scattering processes within the object. The results are compared with experimental diffraction patterns of specimens of comparable thickness. The

experiments have been performed by W.D. Rau and P. Schwander from the Institute of Semiconductor Physics in Frankfurt/Oder, Germany [4].

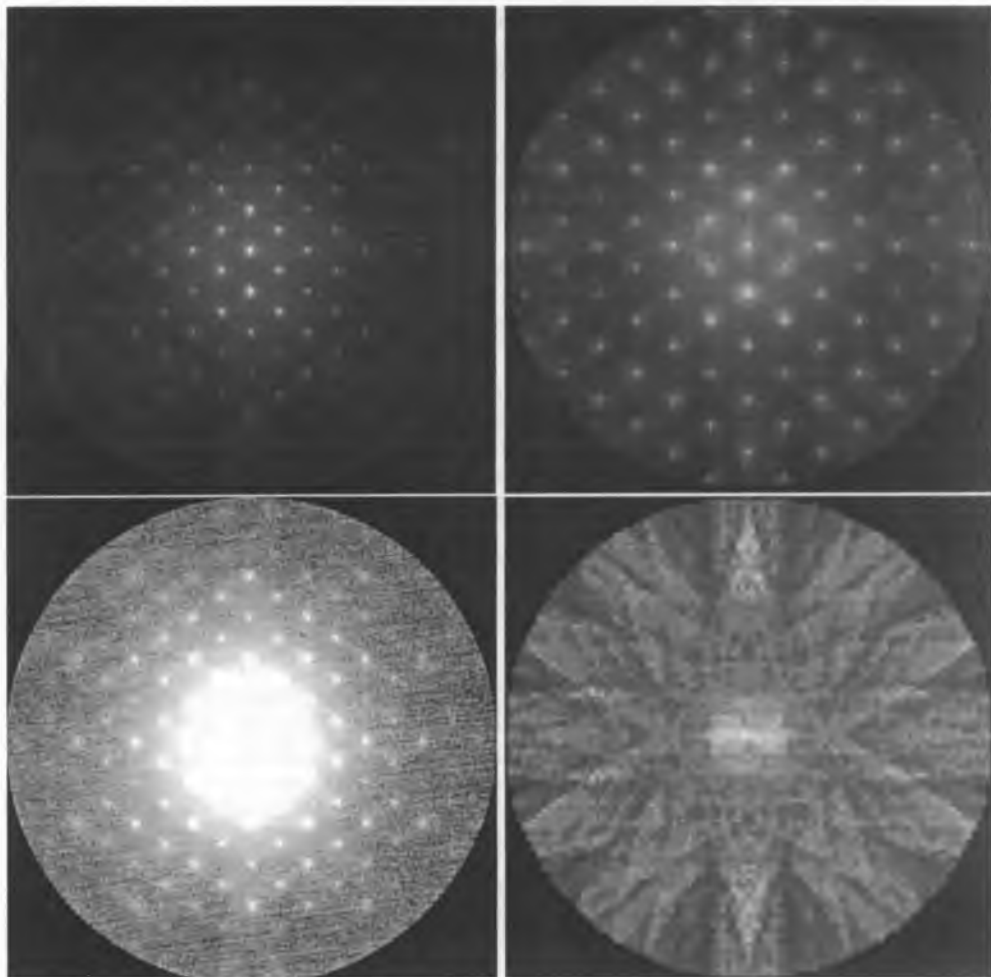


Figure 1: Comparison of experimental and simulated diffraction patterns of Si (110) with thickness between 150 to 300 nm. *Top left:* Unfiltered experimental diffraction pattern, *top right:* Unfiltered simulated diffraction pattern, *bottom left:* rescaled experimental diffraction pattern with phonon background visible, *bottom right:* simulated phonon background.

REFERENCES:

1. H. Müller, H. Rose and P. Schorsch, *Journal of Microscopy* **190**, (1998).
2. A. Berger, C. Dinges and H. Rose, *Ultramicroscopy* **60** (1995).
3. H. Rose, *Ultramicroscopy* **15** (1984).
4. W.D. Rau and P.Schwander, IHP, Frankfurt/Oder, *private communication*.

VARIABLE MODE RETARDING FIELD ELEMENT FOR LOW ENERGY SEM

I. Müllerová, L. Frank and E. Weimer*

Institute of Scientific Instruments AS CR, Královopolská 147, 612 64 Brno, Czech Republic

**LEO Elektronenmikroskopie GmbH, 73446 Oberkochen, Germany*

Today's trend toward low electron energies in a SEM is motivated by reasons connected solely with the specimen itself. At low energy electron impact, the interaction volume diminishes so that the information is better localized, the total electron yield is generally higher and the specimen charging-up can be suppressed, and moreover many new types of contrast appear. Contrary to this, although significant progress has been made in designing low voltage guns and electron optical columns, principal needs for keeping the beam energy at least at few keV throughout the column cannot be avoided. These include suppression of influences of both the external stray fields and the mutual interactions of the beam electrons, and extraction of a sufficient current from the cathode. Using the SEM designs employing variable electron energy along their trajectory between the gun final anode and the specimen can combine both demands.

One important possibility is to use an integrated beam accelerator or booster [1,2] which holds the beam, between the gun extractor and the objective lens, at an energy higher than the landing one, which is given by the cathode potential with respect to the earthed specimen. An immersion electrostatic lens, combined with a normal objective lens, closes the booster. The combination lowers the aberrations and they even decrease with the increasing immersion ratio or decreasing landing energy. Alternative is to apply a high negative bias to the specimen and to lower the beam energy immediately above the specimen surface with the help of a cathode lens [3,4]. This combination is capable of preserving a nearly constant image resolution throughout the energy scale and even commercial SEMs can be adapted to this mode, provided a special detector is fitted [5,6].

The operation of the booster is limited by a maximum reasonable immersion ratio of its closing lens – otherwise it becomes too strong to form the probe [7]. For a two-aperture lens with the aperture distance D and "sharp" field transitions in electrodes, we get, from a simple analytical calculation [8], the lower focal point lying at the distance D below the lower aperture already at an immersion ratio of 7. Computer simulation [9] brings the ratio of 36 for both aperture diameters equal to D while the field strength on the specimen reaches already 5% of the full value. The focusing power is further increased by the magnetic lens so that one can consider this principle viable down to electron landing energies of 200-500 eV only. This energy range brings already most of the advantages mentioned above. Nevertheless, principally new contrasts appear below 50 eV where the electron reflection yield acquires a vector character, dependent on the specimen crystallinity, and wave-optical contrasts become possible. In addition, the probing depth starts to increase again, weakening the vacuum demands. This range can be reached only with a cathode lens with the full field strength on the specimen surface and difficulties connected with the specimen biasing.

A booster equipped SEM column (Fig. 1a) offers a very efficient way of combining both described methods. When insulating even the lower immersion lens electrode from the column body, one can simply switch the retarding field to the cathode lens mode but with the advantage of the specimen earthed (Fig. 1b) – in-lens detector is then available only. Furthermore, an insulated specimen holder enables one to use also a highly efficient (retractable) anode/detector assembly (Fig. 1c).

The variable mode arrangement makes the full energy scale accessible with the possibility to adjust the electric field on the specimen.

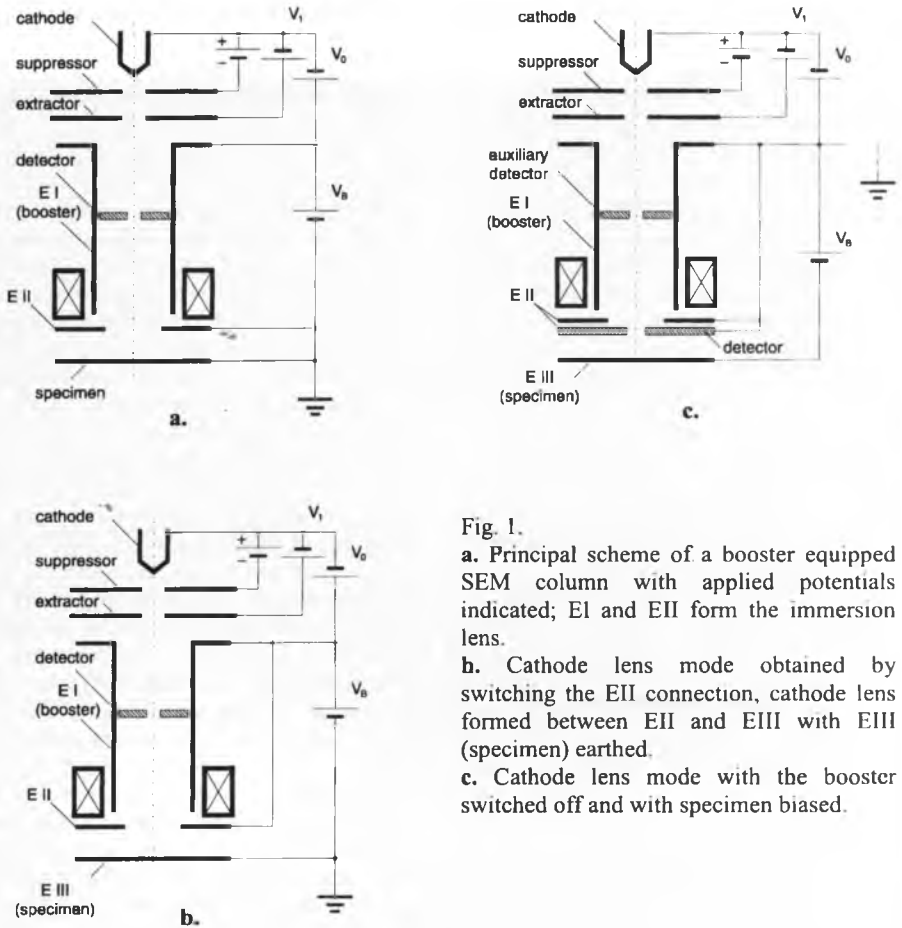


Fig. 1.
a. Principal scheme of a booster equipped SEM column with applied potentials indicated; E I and E II form the immersion lens.
b. Cathode lens mode obtained by switching the E II connection, cathode lens formed between E II and E III with E III (specimen) earthed.
c. Cathode lens mode with the booster switched off and with specimen biased.

[1] J.P.Martin, E.Weimer, J.Frosien, S.Lanio, *Eur. Microscopy and Analysis* (1994) 28, 43
 [2] E.Weimer, J.P.Martin, *Proc. ICEM 13, Paris 1994, Vol. 1*, 67.
 [3] I.Müllerová, M.Lenc, *Mikrochim. Acta* (1992) [Suppl.] 12, 173.
 [4] M.Lenc, I.Müllerová, *Ultramicroscopy* (1992) 45, 159.
 [5] I.Müllerová, L.Frank, *Scanning* (1993) 15, 193.
 [6] I.Müllerová, L.Frank, *Mikrochim. Acta* (1994) 114/115, 389.
 [7] B.Lencová, in *Handbook of Charged Particle Optics* (ed. J.Orloff), **CRC Press** 1997, 210.
 [8] W.Glaser: *Grundlagen der Elektronenoptik*, Springer 1952, §89.
 [9] SIMION 3D Version 6.0; D.A.Dahl, 43rd ASMS Conf. on Mass Spectrometry and Allied Topics, Atlanta 1995, 717.

SHORT NOTE ON LOW-ENERGY SEM CONFIGURATIONS

I. Müllerová and L. Frank

Institute of Scientific Instruments AS CR, Královopolská 147, 612 64 Brno, Czech Republic

There are good acknowledged reasons to lower the landing energy of primary electrons incident onto a specimen in the SEM down to hundreds and even tens and units of eV. But there are equally good reasons to produce the primary electron beam at a high energy of tens of keV. To satisfy both, SEM designs are desirable in which fast primary electrons are decelerated somewhere in front of the specimen surface.

Modifications of this general principle, proved to date, can be divided according to where the deceleration field is applied. It can simply be between two bored electrodes of an electrostatic immersion lens fitted into the magnetic objective lens so that the fields overlap. Another alternative is to replace the final electrode with the specimen, i.e. to use the cathode lens. Both approaches differ mainly in the electric field intensity on the specimen surface. A higher field causes a more effective collimating of the emitted electron toward the axis, which affects the detection conditions. On the other hand, the specimen geometry, tilt and surface quality become more critical. Some specimens can be even intolerant to a high electric field. The main difference is that the aberration coefficients keep proportionally decreasing down to the lowest energies for the cathode lens [1] while for the immersion lens, it falls only down to values similar to its working distance [2,3].

Both versions can be treated in the dependence on the working distance w of the electrostatic immersion lens, so that the cathode lens is for $w=0$; this is similar to the systematic approach in [4]. Fig. 1 shows the electric field on the specimen surface, as a function of w/D , where D is both the diameter and distance of the electrodes. Obviously, the surface field can easily range in tens of per cent of the maximum while the aberration coefficients still remain in tenths of w while for the cathode lens they are roughly equal to D divided by the immersion ratio. This speaks in favor of the cathode lens whenever it is applicable.

A further aspect is that for a compound lens composed of electrostatic and magnetic lenses, both aberration contributions are generally comparable. For a cathode lens, the focusing lens influence diminishes at very low energies and the resolution is mainly governed by the axial electric field (see Fig. 2). Consequently, if a cathode lens can be fitted into an existing SEM, good results can be obtained irrespectively of the original SEM performance. Furthermore, the effect of such an adaptation is enhanced due to the favorable property shown in Fig. 3. If the beam aperture is kept constant at a value aligned for a certain landing energy, the image resolution remains acceptable and moderately offset from the ultimate value throughout the energy scale.

From the practical point of view, the landing energy is defined by a (small) potential difference between the gun cathode and specimen while the (high) column energy can be reached either by biasing both negatively or by biasing positively the whole microscope column. The second case is discussed elsewhere in this book [5], the first [6] can be even applied to commercial SEMs. In a cathode lens, the full electron emission is, in the anode plane, collimated to within a diameter of $4w(k-1)^{-1/2}$ where $k = E_p/E_L$ is the ratio of primary and landing energies. This enables one to employ, for the cathode lens based configurations, both the EDOL-type in-lens detection [7] with electrons passing through the anode opening, and an anode/detector combination with a very small central bore (made e.g. from the YAG crystal). The latter type has a very high efficiency but needs a working distance of 8 mm at least. Doubts have been many times expressed as regards restrictions, put onto the specimen surface properties when the specimen serves as the cathode in a cathode lens. Particularly, the

cases of nonconductive and unsmooth specimens were addressed. Nevertheless, the experience with the noncharging SEM performed in a cathode lens equipped device [8] is fully positive. Recent experiments demonstrated that even surface steps of a depth up to 5 μm are well imaged down to below 10 eV.

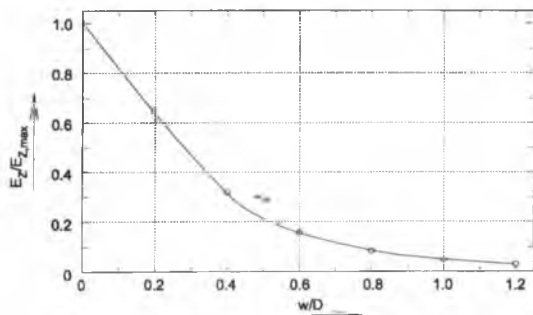


Fig. 1. Intensity of the axial electric field on the specimen surface, expressed relatively to the maximum value between the electrodes, in the dependence on the working distance measured in units of the (mutually equal) electrode diameter and distance.

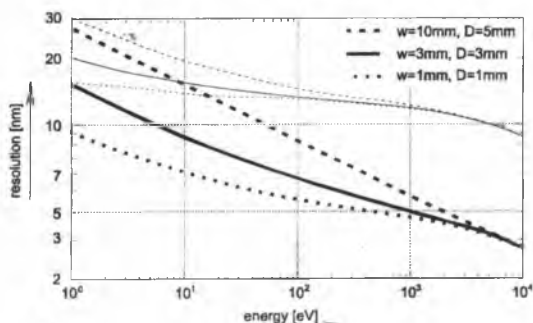


Fig. 2. Resolution of the cathode lens in combination with a focusing lens, for the spherical and chromatic aberration coefficients of the focusing lens equal both to 10 mm (thicker lines) and to 100 mm. Further, curves differ by the cathode/anode distance w and the anode bore diameter D .

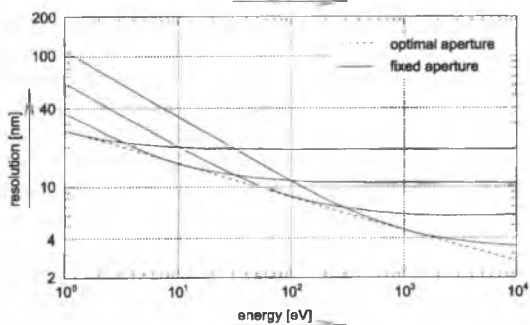


Fig. 3. The resolution as in Fig. 2 (for aberration coefficients 10 mm) when the beam aperture is either the optimum one (as in Fig. 2) or when it is fixed to values optimum for some selected energies.

- [1] M.Lenc, I.Müllerová, *Ultramicroscopy* 45 (1992), 159.
- [2] H.Rose, D.Preikszas, *Optik* 92 (1992), 31.
- [3] B.Lencová, in *Handbook of Charged Particle Optics* (ed. J.Orloff), CRC Press 1997, Chapt.5.
- [4] D.Preikszas, H.Rose, *Optik* 100 (1995), 179.
- [5] I.Müllerová, L.Frank, E.Weimer, these Proceedings.
- [6] I.Müllerová, L.Frank, *Scanning* 15 (1993), 193.
- [7] J.Zach, H.Rose, *Inst. Phys. Conf. Ser. No. 93, 1988, Vol. 1, 81.*
- [8] L.Frank, M.Zadrazil, I.Müllerová, *Mikrochim. Acta [Suppl.]* 13 (1996), 289.

A STUDY OF WAYS OF IMPROVING THE SPEED AND ACCURACY OF COMPUTING FIELDS, TRAJECTORIES AND ABERRATIONS IN ELECTRON OPTIC'S

E. Munro, X. Zhu, J. Rouse and H. Liu

Munro's Electron Beam Software Ltd, 14 Cornwall Gardens, London SW7 4AN, England.

Tel. & Fax: (+44) 171 581 4479 e-mail: mebs@compuserve.com

The main objective in the computer simulation of electron optical systems is usually to predict as accurately as possible the image blurring and distortions of an imaging or probe-forming system. This essentially involves computing fields, trajectories and aberrations. The traditional way of doing this is to compute the electrostatic and/or magnetic field distribution along the system axis and then evaluate the primary aberration coefficients with a set of aberration integrals involving the paraxial rays, axial fields and their axial derivatives.

Although this traditional method has served electron optical designers well, the design of some of the latest instruments is straining the capabilities of the standard simulation methods. Examples that are hard to simulate by traditional methods include LEEM systems, aberration correctors, electron mirrors, curved axis systems for beam separators, Wien filters, etc. In LEEM systems, images are formed with electrons emitted from the sample surface with low energies and large angles. At such low energies and large angles, conventional aberration analysis may become inadequate, the energy spread can dominate the initial energy, and the concept of chromatic aberration coefficients may become almost meaningless. In aberration correctors, analysis of high-order and asymmetry aberrations may be needed, and this is very complicated using conventional aberration analysis methods. In mirror systems, conventional aberration formulations break down near the reversal point, and very involved theoretical treatments are needed unless direct ray-tracing is used. For curved axis systems and Wien filters, the expansion of field functions, paraxial rays and aberrations of various orders about a general curved optical axis involves great complexity and enormous scope for mistakes.

To help address such problems, the aim of this paper is to investigate methods for improving the speed and accuracy of numerical field analysis and direct electron ray-tracing. The aim is to identify areas where improvements can be made in the simulation techniques. In particular, we aim to try to compute field distributions very accurately (off-axis as well as on the axis), and to see how fast and accurately we can directly compute rays through these fields, without resorting to aberration theories. We then compare the results of these simulations with conventional aberration results and try to assess the relative merits of the various approaches.

The most difficult task, by far, in most electron optical simulations, is accurate field analysis, since if the fields are known accurately the trajectories can be computed with negligible truncation errors, using high-order Runge-Kutta or Bulirsch-Stoer methods [1]. For high accuracy field analysis of structures with rotational or multipolar symmetry, second order finite element method (SOFEM) [2] is in principle an attractive candidate. Isoparametric second order finite elements use biquadratic basis functions for both the element geometry and the potential. The biquadratic element geometry allows the elements to be curved, thus allowing accurate geometrical modelling of structures with curved cathodes, electrodes, polepieces, grids, etc. The biquadratic potential functions allow a closer fit to real potential distributions than linear basis functions do, for a given number of grid points.

The main difficulty with SOFEM is that it's much more complicated to program than first order finite element method (FOFEM), and there have been more difficulties in using fast equation solvers such as the ICCG method, which has proved so successful with FOFEM [3,4]. Our second-order ICCG solver works well with rotationally symmetric scalar potential problems (electrostatic lenses and magnetic lens polepiece analysis by magnetic scalar potential), but has encountered some difficulties with magnetic vector potential analysis (for magnetic lens magnetic circuits), where it has sometimes converged slowly or not at all. In such cases, we have still been using Gaussian elimination, which involves high cost in both memory and execution time. In this paper, we discuss some improvements we are trying to make in our second-order ICCG solver to overcome these problems. These include (1) pre-elimination of the internal nodes in each second-order element – this reduces the number of equations by 25%, and reduces the number of terms per equation, and the required number of iterations, which all combine to significantly increase computation speed without loss of accuracy, and (2) treating all the nodes, including all boundary nodes, as possible variables, to enable symmetry planes and various boundary conditions at the axis (e.g. Neumann boundaries for the scalar potential and Dirichlet boundaries for the vector potential) to be handled by the same solver in a unified way. Results obtained with these improvements will be presented. We have used an analytic model for a bipotential lens to check the accuracy of the computed fields, off-axis as well as on the axis. This model can handle exactly both the case where the lens electrodes are terminate at finite distance (using a discrete Fourier-Bessel series) and where they go to infinity in the axial direction (using a Fourier-Bessel integral). This enables us to assess precisely the truncation errors introduced in the finite element method when the field calculation is terminated by boundaries at a finite distance.

For direct ray-tracing, accurate values of the field components at off-axis points are needed. Within a finite element, the field components can be obtained by an interpolation scheme between the potentials at nodes within the finite element and the potential at nodes of four surrounding elements (involving 49 grid points). Comparison with the analytic model results shows this method is accurate – field components can be obtained to 1 part in 10^6 . However, the method is slow. When trajectories are computed by this method, one trajectory can take about 0.3 seconds to compute to an accuracy of 10 nm on a 150 MHz Pentium-based PC. This may be unacceptably slow for the design of LEEM systems, where tens of thousands of trajectories may be needed to obtain accurate aberration information by direct ray-tracing.

To overcome this problem, we have been investigating methods for representing the potential and field components near the optical axis using analytic functions. We first compute the field distribution using SOFEM, with the mesh layout quite rectangular in the (z,r) plane, in a central cylindrical region of radius R around the axis (R being the outermost radius within which we will later wish to compute the trajectories). Then at each plane z , we take the computed potentials at N points in the radial direction (typically $N \approx 6$), spanning the range from $r = 0$ to $r = R$, and we fit a polynomial, in powers of r^2 , through these N points. Only even powers of r are required, because of the rotational symmetry, and thus the highest degree term in the polynomial fit will be of degree $r^{2(N-1)}$. We compute such a polynomial fit in the radial (r) direction, using Lagrange interpolation. We do this at each axial (z) plane. Then we fit together the radial polynomials, in the axial (z) direction, using cubic or quintic spline fits in the z direction. By this means, the potential (and field components) throughout the entire region of interest, are completely fitted by elementary functions to a high accuracy. Tests show that the radial field components throughout the region, computed with the interpolation polynomials, agree to better than 1 part in 10^6 with those computed by numerical differencing of the potentials at the finite element mesh-points. However, the fields can be computed

much faster with the interpolation polynomials. The field computation and the resulting direct ray-tracing are both speeded up by at least a factor of 20, for the same accuracy. A typical trajectory can be computed in about 0.016 seconds with less than 10 nm truncation error. This enables 10,000 trajectories for a LEEM system to be computed, and the results plotted, all in < 3 minutes. Results illustrating the technique will be presented.

In general, using the above method, the potential near the axis of a round lens is expressed in the form:

$$\Phi(r, z) = c_0(z) + c_2(z)r^2 + c_4(z)r^4 + \dots + c_{2(N-1)}(z)r^{2(N-1)}$$

$c_0(z)$ represents the axial potential, $c_2(z)$ is related to the second radial derivative at the axis, $c_4(z)$ to the fourth radial derivative, and so on. These functions have been plotted as functions of z and are very smooth, well-behaved functions. Assuming the potential obeys Laplace's equation, both the radial and axial derivatives of the potential, at the axis, can be directly derived from these functions:

$$\text{Radial derivatives at } r=0: \quad \partial^2\Phi/\partial r^2 = 2c_0 \quad \partial^4\Phi/\partial r^4 = 24c_4 \quad \partial^6\Phi/\partial r^6 = 720c_6 \quad \text{etc.}$$

$$\text{Axial derivatives at } r=0: \quad \partial^2\Phi/\partial z^2 = -4c_0 \quad \partial^4\Phi/\partial z^4 = 64c_4 \quad \partial^6\Phi/\partial z^6 = -2304c_6 \quad \text{etc.}$$

These functions can all be obtained directly from the radial polynomial fits. Since the axial derivatives are exactly the functions needed for computing aberrations by the ordinary integral methods, these functions can be used to evaluate the aberration integrals directly, without any need for integrations by parts, which greatly simplifies the formulae and their programming. The aberration coefficients up to fifth order, or possibly even seventh order, should be able to be computed accurately in this way. We are in the process of comparing the aberration integral results with direct ray-tracing, for ordinary imaging systems, and hope to present results of this at the meeting.

Techniques for improving the speed and accuracy of the direct ray-tracing itself are also being investigated. Instead of using a standard fourth-order Runge-Kutta formula, we are evaluating a fifth-order Runge-Kutta formula due to Cash and Karp [5], which involves six field evaluations per step. This formula is accurate to fifth-order terms in the Taylor series expansion, but simultaneously also allows an estimation of truncation error on each step, using an embedded fourth-order Runge-Kutta formula. This can be incorporated into an adaptive step-size control algorithm, that optimizes the step size to produce a fast ray-trace with the truncation errors contained below a specified threshold. This typically enables < 10 nm cumulative truncation error over an entire trajectory in < 100 steps.

We are also trying to apply the above techniques to the analysis of multipole and curved axis systems and hope to also present some initial results for these cases at the meeting.

References:

- [1] W.H. Press et al., "Numerical Recipes in C", 2nd Ed., Cambridge University Press, 1992, 707-732.
- [2] X. Zhu and E. Munro, *Journal of Microscopy* **179** (1995) 170-180.
- [3] B. Lencová and M. Lenc, *Scanning Electron Microscopy* 86/III (1986) 897.
- [4] B. Lencová, *Nucl. Instr. and Meth. In Phys. Res. A* **363** (1995) 190-197.
- [5] J.R. Cash and A.H. Karp, *ACM Transactions Mathematical Software* **16** (1990) 201-222.

CONSTRUCTION OF AN ELECTRON-OPTICAL BENCH FOR TESTING A MIRROR CORRECTOR

D. Preikszas, P. Hartel, R. Spehr and H. Rose

Institute of Applied Physics, Technical University Darmstadt, Hochschulstraße 6, D-64289 Darmstadt, Germany

An electrostatic mirror has been designed which is capable of compensating simultaneously for the chromatic and the spherical aberration of electron lenses. This corrector is implemented into the column of an electron microscope by means of a beam separator with 90°-deflection. The concept of the correction and the features and calculation procedures [1, 2] of the different elements have already been outlined previously [3, 4, 5, 6]. The mirror corrector is also a fundamental part of the SMART-project ("Spectro-Microscope for All Relevant Techniques") which is concerned with the construction of a corrected spectro-microscope for Röntgen-emitted electrons [7].

Owing to the complexity of the corrected microscope, the individual elements are tested separately. For testing the mirror, we use a LEO DSM960 scanning microscope as an electron-optical bench. The beam separator is placed between the condenser system and the objective lens. Electrostatic field lenses are placed at the entrance and exit faces of this deflector for adjusting a symmetric path of rays. In our test these lenses are used to adapt the scanning microscope to the electron optical requirements of the mirror corrector.

In the first step we investigate a single passage of the electron beam through the beam separator with a deflection of 90°. Since the DSM960 does not decelerate the electrons within the objective lens, as it will be the case in the SMART, the aberrations of the deflector are large compared with the aberrations of the scanning microscope. As a result the properties of the deflector can be determined accurately. Moreover, we are able to develop the alignment procedure and to measure the performance of the beam separator.

In the second step the electron mirror will be added and the additional passage of the reflected beam through the beam separator adjusted. Since in this arrangement the tetrode mirror produces the dominant aberrations, the adjustment of the whole corrector can be optimized. By placing an image of the probe between the deflector and the objective lens, the intermediate magnification can be changed considerably. In this case it should be possible to demonstrate the compensation of the chromatic and the spherical aberration.

References:

- [1] H. Rose and D. Preikszas, *Nucl. Instrum. Methods A* **363** (1995) 301-315.
- [2] D. Preikszas and H. Rose, *J. Electr. Micr.* **1** (1997) 1-9.
- [3] D. Preikszas and H. Rose, 13th Int. Congr. Electr. Micr. Paris (1994).
- [4] D. Preikszas, H. Müller, and H. Rose, 27. Tagung der DGE, Leipzig (1995).
- [5] D. Preikszas, H. Müller, and H. Rose, 11th Eur. Congr. *Electr. Micr.* Dublin (1996).
- [6] D. Preikszas, H. Müller, and H. Rose, 5th Int. Sem. on Recent Trends in Charged Particle Optics, Brno (1996).
- [7] Fink et al. *J. Electr. Spectr.* **84** (1997) 231-250.

ULTIMATE RESOLUTION: WHAT ARE THE NEEDS FOR FUTURE MICROSCOPES?Harald Rose

Institute of Applied Physics, Technical University Darmstadt, D-64289 Darmstadt, Germany

To fully understand the properties of solid objects, a detailed knowledge of the atomic structure, the chemical composition and the local electronic states is necessary. The atomic structure of nonperiodic details can be determined in principle by means of tomography provided that the resolution limit can be lowered to about 0.06nm. In order to achieve quantitative information, a high-performance imaging energy filter with an energy resolution of at least 0.2 eV at a voltage of 200 kV is mandatory. If such a filter is incorporated in a combined STEM-TEM, it will become possible to elucidate the bonding of segregant atoms and the local distribution of electronic states near interfaces or defects.

For achieving sub-ångström and sub-eV resolution, an entirely new generation of electron microscopes must be developed. The ideal future microscope will be a combined STEM-TEM operating at voltages between 150 and 300kV. It will consist of a field emission gun followed by a monochromator yielding an energy width below 0.2 eV. The condenser system must provide genuine Koehler illumination for the TEM mode and a spot size of about .2nm for the STEM mode. This system also enables selected-area diffraction with variable cone angle if the diameter of the illuminated area is large compared to the diffraction-limited spot size. The spherically corrected aplanatic objective lens will consist of coma-free round lens and an integrated hexapole corrector. The formation of a spatially extended energy loss spectrum is performed by the highly dispersive aberration-free MANDOLINE-filter which has by far the highest transmissivity and the best overall performance of all filters proposed so far. The filtered intermediate image or the energy loss spectrum are imaged onto a CCD array by means of an aberration-free projector system consisting of several lenses. For obtaining sub-ångström resolution it is a "conditio sine qua non" that the incoherent defects resulting from parasitic mechanical and electromagnetic instabilities are reduced to such an extent that the information limit is pushed below 0.06 nm. The realization of this ambitious task is by far the most difficult problem encountered on the route towards sub-ångström resolution.

CATHODOLUMINESCENT PROPERTIES OF SINGLE CRYSTALS FOR S(T)EM DETECTORS

P. Schauer and R. Aufrata

Institute of Scientific Instruments, Academy of Sciences of the Czech Republic, Královopolská 147, CZ - 612 64 Brno, Czech Republic (petr@isibrno.cz)

INTRODUCTION

The cathodoluminescent (CL) emission spectrum, CL efficiency (emission intensity), and decay time are three basic scintillator parameters of a scintillation detector for a scanning electron microscope and/or a scanning transmission electron microscope - S(T)EM. They are important not only for the estimation of suitability of the single crystals application in S(T)EM but also for the physical analysis of CL. Besides the scintillator efficiency, the scintillator decay time is the decisive characteristic for a high detective quantum efficiency (DQE), and the emission spectrum is an important characteristic for the spectral matching to the photomultiplier tube (PMT).

INVESTIGATED CRYSTALS AND EXPERIMENTAL ARRANGEMENT

At our laboratory, some tens of different single crystal CL materials were measured. Of these, single crystals of cerium activated yttrium aluminum garnet (YAG:Ce - $Y_3Al_5O_{12}:Ce^{3+}$), cerium activated yttrium aluminum perovskite (YAP:Ce - $YAlO_3:Ce^{3+}$), cerium activated yttrium silicate ($Y_2SiO_5:Ce^{3+}$, which chemically corresponds to the powder phosphor P47), and europium activated calcium fluoride ($CaF_2:Eu^{2+}$) were chosen as the most interesting ones for S(T)EM applications. Cathodoluminescent (CL) properties of the scintillators investigated were measured using a computer assisted CL apparatus [1]. For spectral measurement, the CL signal was spectrally decomposed by a mirror monochromator, picked up by a PMT at the output slit of this monochromator, and measured using a lock-in nanovoltmeter. The individual instruments were connected to the general purpose interface bus (GPIB, IEEE-488), and the measuring apparatus was controlled by a personal computer. The measuring and processing software which contained correction algorithms was written in programming languages Turbo Pascal and Basic.

SURVEY OF SINGLE CRYSTALS PROPERTIES

Emission spectra

The CL emission spectra of YAG:Ce, YAP:Ce, P47 and $CaF_2:Eu$ single crystals are shown in Fig. 1, and the spectral sensitivities of S 11 and S 20 photocathodes used are presented in Fig. 2. The emission spectra are corrected for the spectral sensitivity of the PMT used and each is normalized with regard to its maximum value. This gives better information about the position of the emission bands but at the same time makes the comparison of intensities impossible. For each single crystal, the position of the maximum of the emission band and the value of the full width of the half maximum (FWHM) together with the value of the spectral matching to the S 20 photocathode used, as well as to S 11, are given in Table I. It follows from the results summarized in the table that the $CaF_2:Eu$ and YAP:Ce single crystals show the best and the worse spectral matching, respectively, to the S 20 PMT used. However, the spectral matching of YAP:Ce could be markedly increased by using the PMT with the quartz entrance window. It is not the photocathode itself but the glass entrance window that causes the low spectral sensitivity of PMT in the short wave spectrum region.

The YAG:Ce is the only single crystal that is suitable for CL screens for direct observation. Unlike other investigated single crystals, it emits light in the yellow spectrum region, and this is very favourable for the human eye. On the contrary, this is unfavourable for conventional PMTs

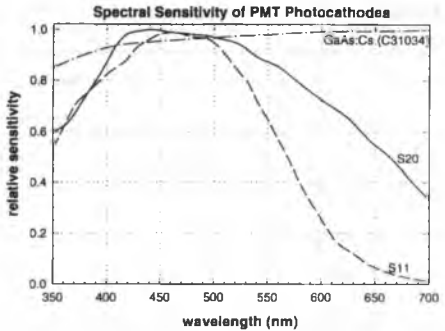
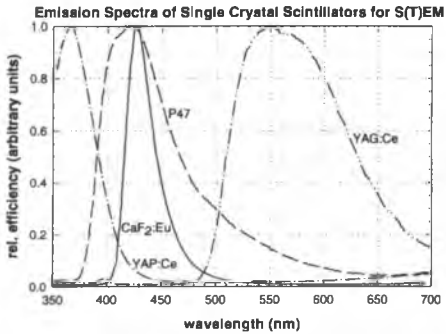


Figure 1 Normalized cathodoluminescent spectra of single crystal scintillators for S(T)EM.

Figure 2 Normalized spectral response of the sensitivity of the photocathodes used.

Table I Spectral properties of single crystals for S(T)EM

single crystal	spectral characteristic			
	maximum [*] (nm)	FWHM ^{**} (nm)	S20 PMT matching ^{***} (%)	S11 PMT matching ^{****} (%)
YAG:Ce	560	122	73	45
YAP:Ce	366	52	60	58
P47	420	77	85	80
CaF ₂ :Eu	426	30	92	88

^{*}position of the maximum of the main emission band.

^{**}full width of the half maximum of the main emission band

^{***}matching to the spectral response of S20 photocathode

^{****}matching to the spectral response of S11 photocathode

with alkali photocathodes. In the case of YAG:Ce, it is necessary to use the S 20 photocathode (its long wave spectrum region differs from that of S 11). All other single crystals investigated can also work with the S 11 photocathode. In addition to the characteristic broad yellow emission band with a maximum at 560 nm, the YAG:Ce shows a very weak emission in the blue, violet and UV spectrum regions. This weak emission which is more marked for specimens with a low activator concentration has a sharp maximum at 400 nm which is superimposed on the broad emission band with a maximum in the UV region, i.e. beyond the capabilities of the measuring device used.

Efficiency

For all applications in S(T)EM, high CL efficiency is required. The relative CL efficiency of the investigated single crystals is shown in Table II. The values of this quantity are always related to the corrected value of the YAG:Ce single crystal. The as measured integral (spectrally non-decomposed) efficiency includes the influence of the PMT photocathode spectral sensitivity. This quantity is interesting from the viewpoint of application in scintillation detectors where the

Table II Efficiency of single crystals for S(T)EM

single crystal	corrected** for PMT	relative efficiency*		forming****
		as measured*** (S20 PMT)	estimated**** (S11 PMT)	after 3 hours (%)
YAG:Ce	100	73	45	2.8
YAP:Ce	142	85	82	1.2
P47	126	107	101	0.8
CaF ₂ :Eu	131	120	115	2.4

* related to the corrected value of YAG:Ce

** corrected for the spectral response of the S20 photocathode used

*** uncorrected for the spectral response of the S20 photocathode used; measured 30 min. after the start of

**** estimated if the S11 photocathode were used

***** efficiency decreasing during given time (related to the initial value).

effects of the PMT photocathode cannot be avoided. In contrast to this, the efficiency corrected for the spectral sensitivity of the S 20 photocathode used is interesting from the physical point of view, and it allows estimation of changes expected in connection with an application of some other photocathode, as shown in column 4 of Table II.

For all single crystal CL materials, the degradation of efficiency was very low. For electrons with an energy of 10 keV and a current density of 4×10^{-8} Acm⁻², the forming of the efficiency of all single crystals measured was observed. During the first three hours, the decrease in efficiency was less than 3% as evident from the last column of Table II. The efficiency decrease was only temporal to a great extent. So, when the measurement was repeated later, similar results, but within a shorter time period, were obtained, and no additional degradation took place.

Decay time

Typical CL decay characteristics for YAG:Ce, YAP:Ce, P47 and CaF₂:Eu single crystals are shown in Fig. 3. The values of the decay time and afterglow are given in Table III. The typical excitation pulse duration was 10 μ s. Both yttrium aluminate single crystals (YAG:Ce and YAP:Ce) have multiexponential decay characteristics. On the other hand, P47 and CaF₂:Eu single crystals have single exponential decay curves, with measured decay times of 41 ns and 1.2 μ s, respectively. The measured decay time of YAG:Ce is 110 ns and the afterglow (measured 5 μ s after the end of excitation) amounts to 2%. For YAP:Ce, the measured decay time is only 45 ns

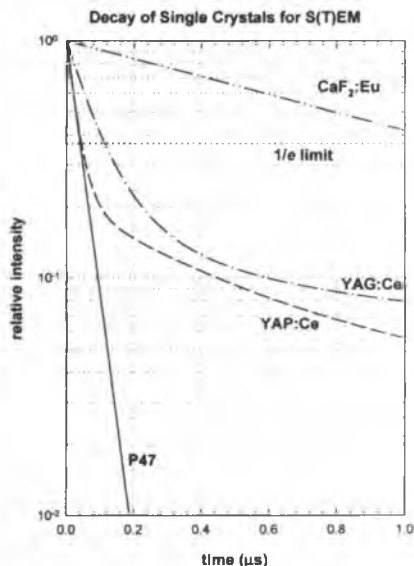


Figure 3 Decay characteristics of single crystals for the S(T)EM. Excitation pulse duration 10 μ s.

Table III Decay properties of single crystals for S(T)EM

single crystal	time characteristic		
	decay time [*] (ns)	corrected decay time ^{**} (ns)	afterglow ^{***} (%)
YAG:Ce	110	103	2
YAP:Ce	45	38	0.5
P47	41	34	unmeasurable
CaF ₂ :Eu	1200	1200	1.3

^{*}uncorrected for the time response of the measuring equipment

^{**}corrected for the time response of the measuring equipment

^{***}intensity measured 5 μ s after the end of excitation

and the afterglow amounts to less than 1 %. In fact, with respect to the fall time of the pulse of the excitation electron beam (5 ns) and the fall time of PMT (2 ns), the short-term decay component must be corrected by subtracting approximately 7 ns of the fall time of the measuring equipment. The short-term component of the CL decay of both yttrium aluminate single crystals depends only negligibly on the duration of excitation. On the contrary, the long-term component of the CL decay depends strongly on the duration of excitation, so that for a very short excitation the afterglow of YAG:Ce and YAP:Ce can be one order and at least two orders lower, respectively. This is advantageous for applications in S(T)EM electron detectors operating at the TV rate, because the images with a rich topographic content can be of higher quality.

CONCLUSION

Unfortunately, all single crystals that have their CL decay time shorter than 100 ns (which is the condition when the TV scan frequency is used) contain oxygen and just this group of single crystals belongs to those with the least efficiency [2, 3]. This means that calcium fluoride, which is the most efficient of the four chosen, has only limited applicability because its decay time constant is 1.2 μ s. The greatest advantage of YAP:Ce single crystals and P47 is that they are the fastest (38 ns and 34 ns, respectively). Especially, they have no such a marked component of long persistent luminescence as the YAG:Ce single crystals have. The only disadvantage of YAG:Ce single crystals is their speed which can be behind the limit for the TV rate in some cases. It is therefore necessary to search for a way to shorten the decay time of YAG:Ce scintillators.

REFERENCES

- [1] Schauer, P.; Atrata, R.: Inquiry of Detector Components for Electron Microscopy., *Fine Mechanics and Optics*, **42** (1997), 340-342.
- [2] Robbins, D.J.: On Predicting the Maximum Efficiency of Phosphor Systems Excited by Ionizing Radiation. *J. Electrochem. Soc.*, **127** (1980), 2694-2702.
- [3] Lempicki, A.; Wojtowicz, A.J.; Berman, E.: Fundamental Limits of Scintillator Performance. *Nucl. Instrum. Meth. Phys. Res. A*, **333** (1993), 304-311.

OUTLINE OF A VARIABLE-AXIS LENS WITH ARBITRARY SHIFT OF THE AXIS IN ONE DIRECTION

P. Schmid and H. Rose

Institute of Applied Physics, Technical University of Darmstadt, Hochschulstraße 6, 64289 Darmstadt

A sophisticated electrostatic "variable-axis lens" is proposed which allows an arbitrary shift of the axis in one direction. For this purpose we employ a periodic arrangement of the electrodes in a direction perpendicular to the initial axis. The excitations of the electrodes is chosen in such a way that stigmatic imaging is conserved when the axis is shifted. The purely electric field components guarantee a fast dynamic shift of the axis and the focusing lens field. Owing to the translational symmetry of the arrangement, the system enables larger displacements of the axis than the conventional "variable-axis lens" which superimposes an appropriately formed dipole field onto the rotationally symmetric field of a round lens.

SPECTROSCOPIC X-PEEM WITH EMPHASIS ON MAGNETIC CONTRAST

G. Schönhense

Institut für Physik, Johannes Gutenberg-Universität, D - 55099 Mainz

Structural tailoring of magnetic films is a rapidly growing field of research and development because it offers additional parameters for the control of magnetic properties. Vertical heterostructures (multilayers) offer a wide range of technical applications e.g. in magnetic sensor technology (read heads, position sensors) because of the giant magnetoresistance (GMR) effect. Horizontal patterning is crucial for novel devices such as magnetic tunnel junctions for spin transistors being the basic units of future non-volatile magnetic storage elements (MRAM). Also high-capacity hard discs require the controlled creation of well-defined magnetic domains with lateral dimensions down to the 100 nm range.

For all these systems there is an increasing demand of powerful microanalytical tools in the sub-micron range. For patterned structures a resolution of several 10 nm is desirable, for multilayers it would be advantageous to view "buried layers", i. e. to look through a non-magnetic coating. Most of the above-mentioned materials are composed of several chemical elements or intermetallic compounds. Since the constituents contribute differently to the magnetic behavior, it is necessary to distinguish the various magnetically active components in a system. Consequently, an appropriate magnetic imaging technique must *combine magnetic sensitivity with element specificity*.

The pioneering work of Stöhr et al. [1] has demonstrated that Synchrotron-based photoelectron emission microscopy in the soft X-ray range (X-PEEM) is a highly promising technique to attack these problems. If the magnetic X-ray circular dichroism (MXCD) as investigated by Schütz et al. [2] is exploited by using circularly polarised Synchrotron radiation, the magnetic contrast of a selected element becomes visible.

This contribution will give an introduction into the technique [3] and illustrate its performance by means of several typical examples. Technical problems like the chromatic aberration due to the energy distribution will be addressed. The base resolution of our instrument (FOCUS IS-PEEM) is less than 20 nm, visible in threshold photoemission at $h\nu = 4.9$ eV [4]. Operation in the soft X-ray regime results in an effective energy distribution of the imaged secondary electrons with a width of 5-10 eV. This width has been confirmed by spectroscopy using the Micro-ESCA analyser [5]. The energy width leads to a significant chromatical aberration yielding a total resolution of 120 nm. Approaches to improve the resolution e.g. means of a novel Time-Of-Flight mode of operation [6] will be discussed.

Typical results [7,8] are shown in Figure 1. Micro-patterned layers of permalloy (left), a Co/Pt multilayer (middle) and an epitaxial Co-film on Cu(100) (right) have been viewed by means of the magnetic circular dichroism contrast at the iron and cobalt L-edges. Despite of their similar dimensions, the three structures exhibit completely different domain patterns. The permalloy squares show a simple flux closure structure with very few exceptions (like the defect-induced distortion near the centre of the left image). This general behavior reflects the small magneto crystalline anisotropy and the tendency to minimize the magnetic stray field. The Co/Pt multilayer of 7 periods (2.1nm Pt / 2.5nm Co) shows a complicated domain pattern ("magnetisation ripple") being indicative of its high intrinsic anisotropy and the polycrystalline

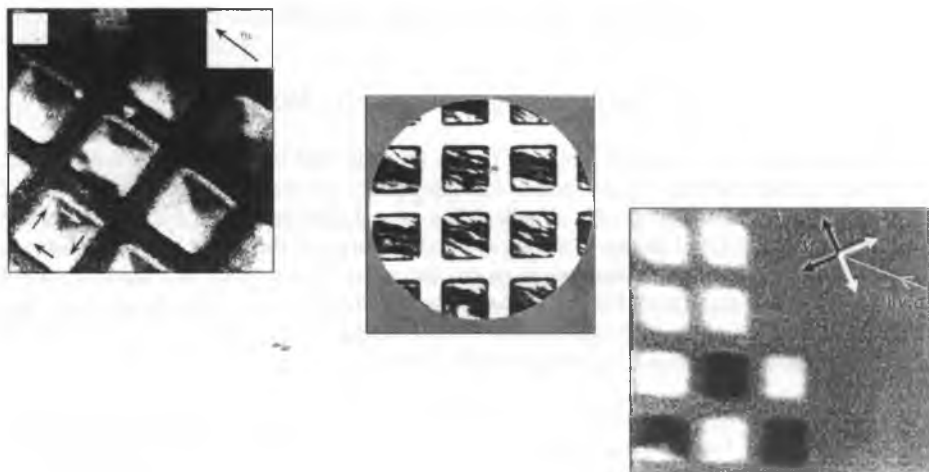


Figure 1: Magnetic domain structure of micro-patterned permalloy, Co/Pt multilayer and Co/Cu(100) (from left to right). Sizes of the squares are $20\ \mu\text{m} \times 20\ \mu\text{m}$ (left and middle) and $8\ \mu\text{m} \times 8\ \mu\text{m}$ (right).

structure. Finally, the epitaxial Co layer on Cu(100), thickness 2.5 nm (actually coated by 1.5 nm Ni) reveals for each square a uniform magnetisation along one of the easy $\langle 110 \rangle$ axes as indicated by the magnetisation arrows. Owing to the symmetry of photon incidence, only two gray levels occur. There is no indication of a magnetic coupling between neighbouring squares.

Acknowledgements: The experiments were funded by BMBF (05 621 UMA 2 and 05 644EFA 5) and carried out at the Synchrotron radiation sources BESSY (Berlin) and ESRF (Grenoble) in a collaboration with the Max-Planck-Institut für Mikrostrukturphysik, Halle. I thank all co-authors of Refs. [7] and [8] for their engagement in the experiments.

References:

- [1] J. Stöhr, Y. Wu, M. G. Samant, B. D. Hermsmeier, G. Harp, S. Koranda, D. Dunham, and B. P. Tonner; *Science* 259, 658 (1993)
- [2] G. Schütz, W. Wagner, W. Wilhelm, P. Kienle, R. Zeller, R. Frahm, and G. Materlik, *Phys. Rev. Lett* 58, 737 (1987)
- [3] W. Swiech, G. H. Fecher, Ch. Ziethen, O. Schmidt, G. Schönhense, K. Grzelakowski, C. M. Schneider, R. Frömter, and J. Kirschner; *J. Electron Spectr. and Rel. Phen* 84, 171 (1997)
- [4] Ch. Ziethen et al.; *J. Electr. Spectr. Rel. Phen.*, in press (1998)
- [5] See M. Merkel et al., Poster contribution on this workshop
- [6] H. Spiecker, O. Schmidt, Ch. Ziethen, D. Menke, U. Kleineberg, R. C. Ahuja, M. Merkel, U. Heinzmann, G. Schönhense; *Nucl. Instr. Meth. A*, in press, May (1998)
- [7] C. M. Schneider, R. Frömter, Ch. Ziethen, W. Swiech, N. B. Brookes, G. Schönhense, J. Kirschner; *Mat. Res. Soc. Sym. Proc.* 475, 381 (1997)
- [8] W. Kuch, R. Frömter, J. Gilles, D. Hartmann, Ch. Ziethen, C. M. Schneider, G. Schönhense, W. Swiech and J. Kirschner (to appear in *Surface Reviews and Letters*)

THREE DIMENSIONAL SCANNING ELECTRON MICROSCOPY

W. Słowko

Institute of Microsystem Technology, Wrocław University of Technology, ul. Janiszewskiego 11, 50-327 Wrocław, Poland

Introduction

Humans and all higher animals are two-eyed so three-dimensional viewing the surface topography should be an expected standard for most electron optical instruments. The subject has also very practical meaning. Quantitative characterisation of surface micro-topography is one of most essential problems in many fields of science and technology, as for instance: microelectronics, micromechanics or tribology of magnetic media. Scanning electron microscopy (SEM) is a very important tool for inspection and measurements of geometrical issues of semiconductor structures (e.g. critical dimensions). Apart from its high lateral resolution, main advantages of SEM are that it imagines the surface topography in the way preferred by human eyes and is very operative to find out some subtle peculiarities in large surface areas. However, it still gives limited information about the third dimension of the surface objects and to measure their elevation and side slopes it is necessary to make cross-sections of the sample. Current investigations on the problem are focused on two groups of methods [1, 2]: those based on principles of stereoscopy or making use of the specific angular distribution of back scattered and secondary electrons (BSE & SE). Unfortunately, each method shows some deficiencies and disadvantages, so three dimensional imaging still is not a very popular technique.

Stereoscopic methods

The utility of a stereoscopic view of the world to communicate depth information resulted in the use of stereo cameras to produce "stereopticon" slides for viewing. The stereoscopic methods of a quantitative characterisation of the surface topography are based on the same rules but they apply strict analysis of the relations between two images registered from two points of view. The idea can be explained on the example showed in Fig. 1, where different images can be obtained by shifting the sample or viewpoint. In this case, the elevation difference H between the two points, A & B, results from the parallax $(d_1 - d_2)$, i.e. from the distance of the two points measured in the horizontal direction:

$$H = W_d (d_1 - d_2) / S \quad (1)$$

where S is the shift distance and W_d is the working distance.

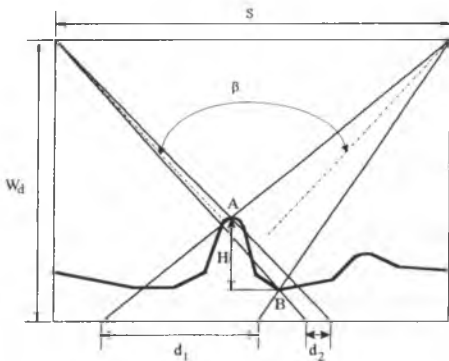


Fig. 1. Characteristic dimensions used to estimate the vertical height of objects when the tilt or shift of the viewpoints is applied

Much greater displacement of the viewpoints can be achieved when it is obtained by changing inclination angles of the view directions rather than by their parallel shift. For instance, the sample stage may be tilted by angle β between the two images to change the view directions (as in Fig. 1). This time, the

height H and the slope angle θ of the object, can be calculated as:

$$H = (d_1 \cos \beta - d_2) / \sin \beta \quad (2)$$

In the two discussed cases, the shift or the tilt of the viewpoints should not be too large to avoid shadowing of some regions adjacent to steep sides of the surface objects.

Generally, the stereoscopic approach to the three-dimensional reconstruction of the surface topography consists in calculating the elevations of particular topographic objects according to the rules described above. The objects should be sharp enough to be identified unambiguously at the both images constituting stereo-pair. The whole rest of the sample surface is usually stretched on the calculated objects like a tent, with use of many possible techniques of data presentation. The stereoscopic methods are in practical use, although an effective and infallible identification of the surface objects is still a problem for the computer systems applied for the task. Anyway, the stereoscopic methods seem most applicable for very rough surfaces, full of edges, rifts and ridges that are good objects for the automatic identification. They may fail at very smooth surfaces where local elevations are monotone changing. In this case, methods called "shape from shading" or better "shape from signal distribution", seem more applicable.

Shape from signal distribution

Primarily, the method was applied in photogrammetry where elevations and side slopes of topographic objects were estimated on the basis of a brightness distribution on photo-grams taken at a side illumination. Later, it was introduced into SEM in a row of varieties [2,3,4]. Generally, the method consists in directional detection of the signal generated from the surface with a known angular distribution, usually realised in multi-detector systems, as it has been shown in Fig. 2.

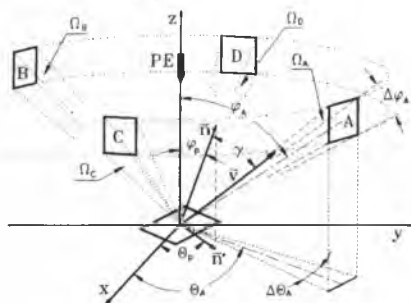


Fig.2. Characteristic angles in a simplified detector system: A,B,C,D - detectors, PE - primary electron beam, \vec{n} - vector normal to the sample surface. φ_p - surface slope angle, γ - electron emission angle, \vec{v} - initial velocity vector. $\Omega_{A,B,C,D}$ - electron detection solid angles, φ_A, θ_A - detector position angles, $\Delta\varphi_A, \Delta\theta_A$ - electron detection angles.

Here, the measure of the side slope is the signal intensity and a profile of the surface can be obtained by integration of the slopes. Apart from light, the directional detection seems easiest for

back scattered electrons that can go along almost straight trajectories thanks to their high energies. However, their angular distribution is rather irregular and it contains diffusion and reflection shares, similarly to the light distribution. According to Murata [5], the distribution can be approximated with the expression:

$$i = \frac{dI}{d\Omega} = A \cos^2 \varphi_p \left[1 - \left(\frac{\cos \varphi_p}{\cos \gamma + \cos \varphi_p} \right)^{\frac{A}{\cos^2 \varphi_p}} \right] \left(1 + \cos \gamma \cos \varphi_p + \sin \gamma \sin \varphi_p \cos \theta \right)^2 \quad (3)$$

Characteristic angles that occur in the formula have been explained in Fig 2. It does not seem easy to solve the equation with respect to the surface slope angle φ_p and to integrate it then. Besides, the back scattered electron signal is generated in relatively large space and can not provide good resolution, which is essential if the 3-d SEM is to fill the gap between scanning

probe microscopy (SPM) and confocal microscopy (SCLM). In this field better results can be expected when the secondary electron signal is applied.

Secondary electrons are generated with Lambert's distribution, so the current collected by one of the detectors shown in Fig.2 can be written in the simple form [6, 7]:

$$I_A = \int_{\Omega_A} i_0 \cos \gamma \sec \varphi_r d\Omega, \quad (4)$$

where: i_0 is a maximum angle density of the secondary current, proportional to the e-beam current and secondary electron yield δ_0 .

After proper operations the expression for the detector A current takes the form:

$$I_A = i_0 \left[d \cdot \text{tg} \varphi_r \cos(\Theta_A - \Theta_r) + c \right], \quad (5)$$

that leads to the following eq. for the relative difference of signals of the detector A and B:

$$a \frac{I_A - I_B}{I_A + I_B} = \frac{dz}{dx}, \quad \text{for } \Theta_A = 0 \text{ and } a = c/d, \quad (6)$$

where c and d are coefficients of material and topographic contrast respectively. They depend on the detector geometry, as it has been shown in Fig.3. Finally, an integral of the expression represents the surface profile along x axis, i.e.:

$$z(x, y_i) = a \int_{x_0}^x \left[\frac{I_A - I_B}{I_A + I_B} \right]_{y=y_i} dx + C_i, \quad (7)$$

where: x_0, x_k - are co-ordinates of the beginning and end of the scan line, C_i - is an integral constant equal with the surface profile height at the beginning of each scan line (numbered i). For the two detector system all lines have to start from the same level. A fully three dimensional image can be obtained when the second pair of detectors (C, D) is used to provide information about surface slopes in yz plane. Then, the final expression defining the surface topography along successive scan lines takes the following shape :

$$z(x, y_i) = a \int_{x_0}^{x_1} \left(\frac{I_A - I_B}{I_A + I_B} \right)_{y=y_i} dx + a \int_{y_{i-1}}^{y_i} \left(\frac{I_C - I_D}{I_C + I_D} \right)_{x=x_0} dy + C_0 \quad (8)$$

The second integral reconstructs the surface profile in the y direction (beginning with the initial altitude C_0) along start points of all lines ($x=x_0$), as it has been shown in Fig. 4.

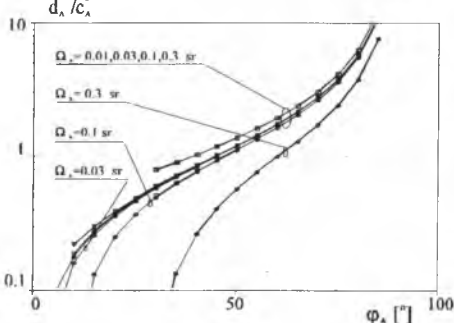


Figure 3. Quotient of the detector geometry coefficients against the detector declination angle (\blacklozenge 0.1rad, \blacktriangledown 0.3rad, \blackboxminus 1rad).

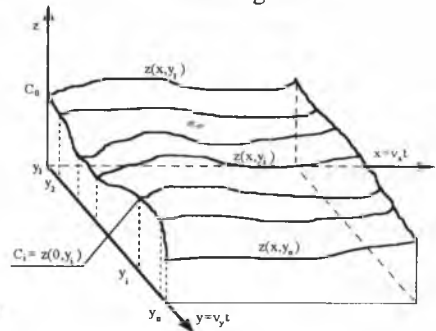


Fig.4. Scheme of the three-dimensional reconstruction of the surface geometry

The formulas for signal processing, (7) and (8), can be realised both in analog and computer systems. Analog systems seem more suitable for the reconstruction of the surface topography in a shape of profiles which is a form of two dimensional representation and can be

displayed on the analog monitor. Besides, relatively simple analog systems provide signal processing in a "real time", which makes all efforts of the operator seen immediately on the screen. A fully three dimensional reconstruction of the surface implies some kind of axonometric imaging, easily accessible on the computer monitor. In this case, the four signals from the quadruple detector, can also be processed in a "real time" when the computer system is equipped with a digital signal processor.

Limitations

The method "shape from signal distribution" (SSD), seems relatively simple and easily applicable. However it still meets numerous limitations that wait for optimum solution. First of all, the integrals (7) and (8) can be realised at continuous surfaces, i.e. relatively smooth, without cracks and leaps, otherwise a new integration constant (a new initial altitude) should be established after each discontinuity. An solution of the problem may be a mixed method where altitudes of all edges would be established stereoscopically and the rest of the surface would be reconstructed by SSD.

Most limitations for SSD result from many possible faults of the directional signal detection, headed by the shadowing effect. The limitation results from the fact that initial velocities of the emitted electrons can be tangent to the sample surface at the most ($\gamma < 90^\circ$). That means that c/d is the maximum value of $tg\phi_p$, at which a point detector ($\Delta\phi_A \rightarrow 0$) is still over the plane tangent to the sample surface in the impingement point and is able to collect secondary electrons. Apart from this elementary kind of shadowing that may be called the shadowing by the tangent plane, also elements of the surface topography can shadow the detector. Shadowing errors can be essentially reduced when the detector pairs are arranged so that their geometrical coefficients $a = c/d$, attain maximum values. According to diagrams in Fig.3, it implies zenith position and small size of the detectors, which is ransomed with a reduced efficiency of the detection.

Really essential problems concerning the directional detection of secondary electrons are caused by electric charges induced by e-beam on dielectric surfaces. Electric fields generated by them deflect electrons, disturbing their flow to detectors. Elimination of the low energy electrons that are most sensitive to electric disturbances, leads to their decreasing share with respect to back scattered electrons, with all the disadvantages as a weak signal with inaccurately defined distribution and a poor spatial resolution. There are some possibilities of compensation of the surface charges, created by the low voltage SEM or the variable pressure SEM. In the first case positive surface charges can be partly neutralised by secondary electrons attracted by them and in the second case negative charges can be compensated by similar attraction of positive ions. However, the both solutions imply some electric fields to make charged particles flow thus the SE directional detection may still be disturbed to some extend.

In spite of so many doubts, the "shape from signal distribution" method may be effective for quantitative evaluation of the surface topography in many applications

References

- [1] J. Russ, *Computer assisted microscopy*, Plenum Press (1990)
- [2] H. Tanaka et al., *Trans ASME*, **114**, 274 (1992)
- [3] J. Lebieczik, *Scanning*, **2**, 230 (1979)
- [4] L. Reimer, R. Bongler and V. Desai, *Scan Microsc*, **1/3**, 963 (1987)
- [5] K. Murata, *Phys Status Solidi*, **A 36**, 197 (1976)
- [6] T. Czepkowski, W. Slowko, *Scanning*, **18**, 433 (1996)
- [7] W. Slowko, *IX Conf El Microsc Solids*, *Zakopane*, 97 (1996)

Our research were supported by the Committee for Scientific Research (KBN). grant No.8T11B 01011

ON THE THEORETICAL UNDERSTANDING OF THE WIEN FILTER IN AN ELECTRON BIPRISM INTERFEROMETER

Peter Sonnentag, Harald Kiesel, and Franz Hasselbach
Institut für Angewandte Physik der Universität Tübingen
Auf der Morgenstelle 10, D-72076 Tübingen, Germany

In recent years, A. A. Michelson's visibility spectroscopy [1] has been realized successfully with electron waves instead of light waves [2]. For this, an electron biprism is used, and as a counterpart of the different path lengths of the interfering beams in light interferometry, a Wien filter in its compensated state is employed (see Fig. 1). A Wien filter consists of a crossed electric and magnetic field, both being perpendicular to the optical axis. It is said to be in its compensated or matched state if the electric and magnetic force for the main energy component of the electron beam cancel each other. From the decrease in fringe contrast with increasing excitation of the Wien filter, the energy width of the source can be determined, and even the form of the energy distribution can be obtained in case that it is symmetrical to its centre.

If the initial state of the electron is a *pure* state, i.e. all electrons form identical wave packets, then the action of the Wien filter is to introduce a longitudinal shift between the two partial wave packets coming from opposite sides of the biprism filament. Reduction of contrast of the interference fringes can then be explained by the lack of overlap between the two packets. The longitudinal shift is caused by the different group velocities inside the Wien filter being due to a different electric potential. If, on the contrary, the electron beam is made up of a statistical ensemble of electrons being in different energy eigenstates, then – at least for *narrow* energy distributions – the loss of contrast is the same as for a pure state with the same energy spread, but in this case it is caused by the displacement of the incoherently superimposed interference patterns relative to each other. This comes from the fact that for electrons with an energy differing from the one for which the matching condition is fulfilled there *is* a resultant force and therefore also a phase shift. But in reality, we have neither a pure state of the electrons nor a mixed state which is diagonal with respect to the energy eigenstates, so that both mechanisms of the reduction of contrast will be involved.

Whereas the Aharonov-Bohm effects yield phase shifts without affecting the centres of the wave packets, and the Sagnac effect or a homogeneous electric *or* magnetic field in an electron interferometer lead to both a shift of the fringes *and* of their contrast, the Wien filter in its compensated state produces a wave packet shift *without* a phase shift so that in the middle of the fringe pattern there is always a maximum – and this is also a difference to Fourier spectroscopy with *light*. Because of this special feature of the Wien filter it seemed worthwhile to do the calculation of the biprism interferometer with Wien filter for the case of a *wave packet* explicitly. This was done by using a form of the semiclassical approximation of the Feynman path integral for strongly localized wave packets [3].

For *monochromatic* waves – and consequently also for *incoherently* superimposed monochromatic waves – the electron-optical biprism can be replaced by two virtual sources

[4]. For wave packets, however, this model demands some modifications and care. Firstly, of course, the distance of the virtual sources from the optical axis is different for each energy component. Secondly, an additional energy-dependent phase φ_{virt} has to be added to $\frac{1}{\hbar} \int p_{\text{kin}} ds$ to get the correct wave function. Thirdly, for an interferometer with other optical elements following the biprism, the term $-\frac{\varepsilon}{\hbar}(t - t_{\text{source}})$ in the phase caused by the biprism does no longer cancel with the time evolution of the source, $-\frac{\varepsilon}{\hbar}(t_{\text{source}} - t_0)$, up to a common phase factor which can be omitted, as there will in general be different times t when the electron enters the next element. Fourthly, the time of flight - which is used to determine the energy components interfering with each other at a certain instant, which enters in $-\frac{\varepsilon}{\hbar}(t - t_{\text{source}})$, and which one could use to determine the wave packet shift - cannot be calculated using the virtual sources; this is an immediate consequence of the fact that for matter waves phase and time of flight are not proportional to each other. But it should be noticed that if the determination of the longitudinal shift of the wave packets relative to each other is made by first calculating the wave function and then searching for the maxima, the additional phase φ_{virt} needn't be taken into account as φ_{virt} does - to a good approximation - not depend on the position perpendicular to the optical axis or on the side of passage of the biprism, and therefore both wave packets get the *same* incorrect shift.

When dealing with Fourier spectroscopy, a complication arises as the fringe spacing s becomes narrower with increasing excitation of the filter, according to $s \approx s_0 - s_2 E^2$, where E is the electric field strength. This is due to the well-known focusing action of the Wien filter arising from the fact that rays which travel through the filter aside of the optical axis have velocities which do not fulfill the matching condition exactly, and the waves are deflected towards the axis.

The Fourier-spectroscopic measurement is carried out as follows [2]: At first, the electric and magnetic fields are zero. In a first step, the electric field only is increased by ΔE . Consequently, the interference fringes are deflected by, say, ΔN fringe widths. Then, by increasing the magnetic field until the zeroth order fringe is in the middle again, the Wien filter is put back into its compensated state, and the fringe pattern is recorded. These steps are repeated until contrast disappears.

The total number of fringes N by which the zeroth order fringe has been shifted to one side during this procedure is the sum of the ΔN . Each ΔN is given by the deflection induced by ΔE , divided by the fringe spacing s . Taking into account that the deflection is - to a very good approximation - proportional to ΔE and replacing the summation over the ΔN by an integration, we get $N \propto \int_0^E \frac{dE}{s} \approx \frac{1}{s_0} E + \frac{1}{3} \frac{s_2}{s_0^2} E^3$. On the other hand, the longitudinal shift of the wave packets relative to each other in units of the wavelength, N_{wp} , is approximately proportional to the strength of the electric field E and to the lateral separation of the paths in the filter. The latter is nearly proportional to the angle of convergence β (Fig. 1b) which is inversely proportional to the fringe spacing, so that $N_{\text{wp}} \propto \frac{E}{s} \approx \frac{1}{s_0} E + \frac{s_2}{s_0^2} E^3$.

Notice that the third order terms of N and N_{wp} differ by a factor of $\frac{1}{3}$ (a more accurate calculation [5] yields about the same factor). The wave packet shift N_{wp} is, taking into account these higher order corrections, larger than the shift given by the number of fringes N . This arises from the fact that for the determination of N a succession of different paths in the Wien filter is used which are all closer to the optical axis than the current path which determines N_{wp} .

For very narrow energy distributions and the Wien filter in its compensated state,

the phase difference $\Delta\varphi(k)$ of the two interfering parts of an energy component may be approximated by the first order term in the deviation δk of the wave number from its main value k_0 . Then, the phase shift caused by the Wien filter is equivalent to a difference in the geometrical path length in vacuum, so that $\frac{\Delta\varphi(k_0+\delta k)}{\delta k}$ is proportional to N_{wp} .

Fourier-transform spectroscopy demands a variable proportional to $\frac{\Delta\varphi(k_0+\delta k)}{\delta k}$. Therefore, neither E nor N – which has been used so far [2] – is suitable if the high precision of visibility spectroscopy shall be fully exploited. Because N_{wp} cannot be measured directly, we propose to use $\frac{E}{s}$ as the transformation variable, where s is taken from the recorded fringe patterns.

For the case of a *wave packet*, the decrease in fringe contrast with increasing excitation of the Wien filter can also be interpreted as being due to the increasing (*possibility* of getting) “welcher Weg” (which-path) information available from the difference in arrival time between the two packets. Another way how complementarity, in particular wave-particle duality, may be enforced in “welcher Weg” experiments is entanglement with orthogonal states – either with the environment (e.g., measurement device) or with an internal degree of freedom (e.g., spin). The effect of the Wien filter can, loosely speaking, as well be seen as a kind of entanglement: If we write the ordinary state space of the particle as a tensor product of the state space of positions on the detection screen and of the state space \mathcal{Z} of positions orthogonal to that screen (i.e., along the optical axis z), then because of the longitudinal distance Δz of the positions of the maxima of the partial wave packets we have entanglement with respect to the space \mathcal{Z} .

Helpful discussions with Richard Neutze and Tomáš Tyc are thankfully acknowledged.

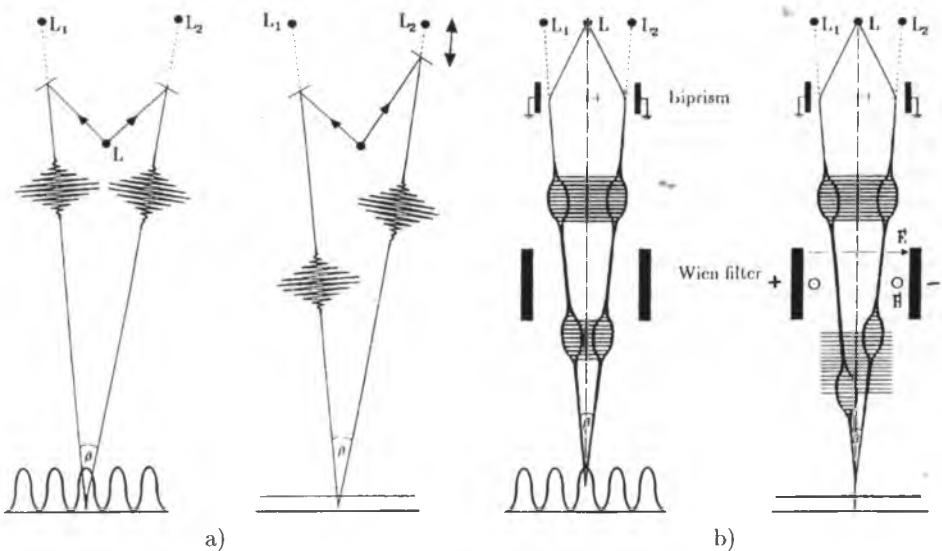


Fig. 1

References

- [1] Albert A. Michelson. On the Application of Interference-Methods to Spectroscopic Measurements.-I. *Philosophical Magazine*, **31**: 338-346. 1891.
- [2] F. Hasselbach, A. Schäfer, and H. Wachendorfer. Interferometric measurement of charged particle spectra (Fourier-spectroscopy). *Nuclear Instruments and Methods in Physics Research A*, **363**: 232-238. 1995.
- [3] S. Olariu and I. Iovitzu Popescu. The quantum effects of electromagnetic fluxes. *Reviews of Modern Physics*, **57**: 339-436. 1985.
- [4] J. Komrska and B. Vlachová. Justification of the model for electron interference produced by an electrostatic biprism. *Optica Acta*, **20**: 207-215. 1973.
- [5] Peter Sonnentag. Theoretische Untersuchungen zum Wien-Filter in einem Elektronen-Biprisma-Interferometer. Diplomarbeit, Institut für Angewandte Physik der Universität Tübingen, 1997.

VARIABLE AXIS LENS WITH AN EXTREMELY LARGE SCANNING AREA IN ONE DIRECTION

R. Spehr

Institute of Applied Physics, Technical University Darmstadt, Hochschulstraße 6, D-64289 Darmstadt, Germany

In order to obtain a large writing area on a single line, we have developed an electron lens design [1] quite different to that of usual variable axis lenses based on a round lens. The electrodes and the polepieces are formed by three parallel slits which in the x-direction are extending infinitely, at least in principle. Thus the geometry of the lens is translation invariant with respect to the x-axis as it is customary for a cylinder lens. For stigmatic focussing we combine two different fields, both fields being consistent with this geometry. Using a negative (or a positive) potential on the middle slit, we get a retarding (or an accelerating) electrostatic cylinder lens focussing in the yz-section [2]. In addition we superimpose a magnetic quadrupole field, which is oriented in such a way that focussing in the xz-section is achieved. This field is produced by fabricating the three slits out of magnetic material ($\mu_r \approx 10^5$) and by placing windings on both halves of the middle slit, which carry constant current density. In this three-dimensional arrangement the magnetic scalar potential is given by

$$U_{mag} = Q \times F(y, z). \quad (1)$$

The function $F(y, z)$ depends on the geometry of the slit in the yz-section and can be calculated by a suitable charge simulation procedure, which only needs to be two-dimensional. From eq.(1) we see that the form of the magnetic potential does not change when moving into the x-direction, while its value increases linearly. In practice the slits must have a final length. Then the magnetic material should enclose the opening of the slit and we need two additional coils situated at both ends of the middle slit which carry the opposite Ampere windings as the polepieces do.

The magnetic quadrupole field focusses in the xz-section, but defocusses in the yz-section. To obtain stigmatic focussing, the electrostatic cylinder lens needs twice the refractive power as the quadrupole. When the axis of the quadrupole field lies within the xz-section, this axis coincides with the lens axis of the whole arrangement. The axis of the quadrupole field can be shifted over the whole length of the slit into the x-direction simply by transferring some current from the coil at one end of the slit to the coil at the other end. Thus our lens acts as a variable axis lens. In principle the displacement of the axis with respect to the x-direction can be infinite without changing the imaging properties of the lens.

Like a round lens this lens does not show any aberrations lower than of third order due to its high symmetry. Furthermore there is no need for a separate stigmator as stigmatic focussing is achieved by balancing its cylinder lens field against its quadrupole field. Different to round lenses we have to distinguish between the x- and the y-direction when looking at its aberration coefficients. For instance the spherical aberration is given by three coefficients $C_{\alpha\alpha\alpha}$, $C_{\beta\beta\beta}$ and $C_{\alpha\beta\beta} = C_{\alpha\alpha\beta}$, where α and β are the angles of convergence with respect to the xz- and the yz-section respectively.

For the geometry of the lens we have built in Darmstadt [3] and for stigmatic focussing on the plane $z = 100\text{mm}$ we calculate

$$C_{\alpha\alpha\alpha} = 0,051\text{m} ; C_{\beta\beta\beta} = 18\text{m} ; C_{\alpha\beta\beta} = 0,47\text{m}. \quad (2)$$

The resulting trajectories in both sections can be seen in fig.1. From these trajectories we can also obtain the shift $\Delta z |_{H_x}$ and $\Delta z |_{H_y}$ of the principle lines relatively to the middle plane of the lens.

$$\Delta z |_{H_x} = -9.10\text{mm} \text{ and } \Delta z |_{H_y} = +4.29\text{mm}. \quad (3)$$

Using an additional weak magnetic octupole field superimposed to the quadrupole field, it is possible to correct for $C_{\alpha\alpha\alpha} = 0$ without changing $C_{\beta\beta\beta}$ and $C_{\alpha\beta\beta}$ significantly. This octupole field has to be shifted simultaneously with the quadrupole field when the lens axis is moving. (A moving octupole field can be obtained from a sextupole field of variable strength together with a constant octupole field.)

Fig.1 shows electron trajectories parallel to the optic axis being focussed by the lens. In the xz -section the trajectories are smoothly bent toward the axis by the action of the magnetic quadrupole. In the yz -section the retarding field of the electrostatic cylinder lens results in v-like trajectories. With the same focal point in both sections the principal lines in both sections differ and so the focal length does.

Writing speed depends on the usable solid angle of the beam. Due to the large value of $C_{\beta\beta\beta}$ the illumination angle in the yz -section has to be small, however the corresponding angle in the xz -section might be quite large as $C_{\alpha\alpha\alpha} = 0$ can be achieved.

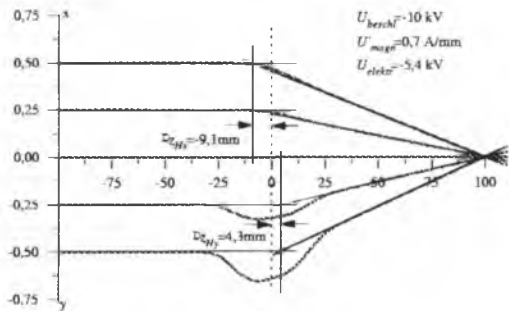


Figure 1: Electron trajectories within the xz - and the yz -section.

References

- [1] R. Spehr, Patent DE 196 34 456.5
- [2] H. Rose, Optik **36**,19 (1972)
- [3] G. Kerkhoff, diploma thesis, Technische Hochschule Darmstadt, march 1997.

DISTRIBUTED MONTE CARLO: SMART WAY FOR COMPUTING COMPLEX PROBLEM

R. Steklý, L. Frank and I. Müllerová

Institute of Scientific Instruments AS CR, Královopolská 147, 612 64 Brno, Czech Republic

The aim of this work was to create an engine for the distribution of an computation task in the TCT/IP network, to verify its operation and to achieve a low-cost great-volume computation power for simulations of electron scattering using the Monte Carlo method [1-3].

The available PC's have a sufficiently high computation output not only for office work but also for simpler scientific computations. The computation output of the best PC's is comparable with that of the cheaper series of the RISC workstation but their purchase cost is half that or less. Modern offices are being equipped with PC's with the operating system Win95 connected to the LAN network, which is often connected to the Internet.

At interactive work, the processor is operated noncontinuously and there are long inactive periods. Typical examples are text and graphic editors, table calculators and Internet browsers. On average, for a sufficiently long period, the processor is never used 100%. Therefore it has been decided to write a program that will make use of the time-outs for its own activity, will receive simple tasks via the network, make computation and send back the results [4]. Operating systems with pre-emptive multitasking can effectively work with priorities of processes and they are mostly equipped with the mechanism that allows the action of programs during the inactive period of the computer. The chosen platform Win95/NT implements this mechanism relatively well. The only problem is the back compatibility when the 16-bit programs (DOS, Win3.11) are being started using the computer emulator with the given operating system that causes the mechanism to stop because W95/NT are not capable of determining the state of the application with no implemented mechanism of communication with the given operating system.

The written computation program has very low demands on the operating memory, typically 2.7MB compared with the 30MB text editor, is easy to control, provides maximum information about its state, and works automatically without any intervention of the user. After starting, the program becomes connected to the computer that distributes the task, receives the data and starts computation. After finishing the computer work, the user makes the shutdown of the operating system, the program becomes logout from the computation process, sends the computed part of the task and becomes ended. The program is used as resident but the user can end it manually. The task distribution is carried out from one computer, which is determined in advance. This computer serves for data collection and recording of the current state of computation.

The operation of the engine was tested in the internal network of the Institute of Scientific Instruments. The test task was a simple computation of electron scattering in Au specimen at electron energy of 1 keV. The entire task is divided into subtasks. The maximum number of trajectories is limited so that all computers end the whole task at the same time. The computation process was running on the background, the test was made during the normal working time, the users were asked not to change their working habits.

The following formulas were used for statistically processing the operation:

$$\begin{array}{ll} \text{mean value} & \bar{x} = \frac{\Sigma \text{trajectories}}{\Sigma \text{time}}, \quad \text{variance} & D = \frac{\Sigma(x - \bar{x})^2}{n}, \\ \text{standard deviation} & \delta = \sqrt{D}, \quad \text{variation factor} & v = \frac{\delta}{\bar{x}} \end{array}$$

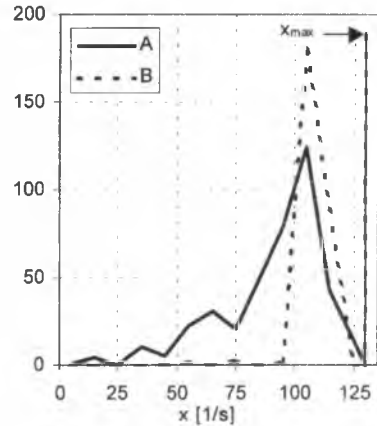
where x is the number of trajectories simulated for the unit of time during one subtask, and \bar{x} is the number of trajectories simulated for the unit of time during all the task.

The quantitative results are as follows: If the user of the computer on whose background the computation was running was working with programs MS Word, Excel, Corel Draw and PhotoPaint or was programming in DELPHI and was continuously checking E-mail or grabbing WWW pages, then the average computation output as regards the process run on the background amounted to 62% of the total computation output of the computer (Fig. 1A). In the case of work in MS Word, when E-mail was continuously checked, it amounted to 83% (Fig. 1B).

Table 1: Quantitative results

Computer	A	B
Task time [s]	50052	25516
Trajectories	4040000	2760000
Trajectories per task	10000	10000
$x_{max}[s^{-1}]$	130	130
$\bar{x}[s^{-1}]$	81	108
dispersion	1172,61	40,55
variation factor [%]	42,42	5,89

Fig. 1. Rate of occurrence of x values.



Two approximately identical computers A and B in configuration CPU Cyrix PR200, RAM 32MB EDO, PCI mainboard, IDE controller, for two working days were used for the test. In our application, packets were distributed every 120 seconds on average, which is an average data flow with the highest priority corresponding to 14,7 Bps. The size of the subtask-defining packet was 226 byte. Packets containing the evaluated data were sent back asynchronously with a lower priority so that they could not affect the flow of the communication data, and they have an average size less than 64 kbyte.

It can be stated that the computation carried out on the office computer in the above described way is a very interesting method for extensive computations that are not made often, and the purchase of a separate computation server is not profitable. The disadvantage of this method is a large disproportion between the data transmission of the LAN network and the computation output of the computer connected to it, which means a considerable restriction of types of tasks which can be distributed this way.

References

- [1] Z.-J. Ding, R. Shimizu, Scanning 18 (1996), 93.
- [2] S. Luo, D. C. Joy, Scanning Microsc. 2 (1988), 1901.
- [3] L. Reimer, Monte Carlo Simulation of Electron Diffusion, Introduction and Manual to the Software Package MOCASIM, 1996.
- [4] distributed.net, <http://www.distributed.net/>

AN E+B+E BEAM SEPARATOR FOR DETECTING SECONDARY ELECTRONS IN LOW VOLTAGE SEM

Katsu Tsuno, Nobuo Handa and Sunao Matsumoto

JEOL Ltd., 1-2, Musashino 3-chome, Akishima, Tokyo 196-8558, Japan tsuno@jeol.co.jp

1. INTRODUCTION

Among various proposals of the objective lens for high resolution low voltage scanning electron microscope (LVSEM), an immersion magnetic lens called Snorkel lens [1,2] and a combined electric and magnetic field lens[3] are now widely used. We classified various objective lenses for LVSEM and compared their electron optical performances [4-6]. For designing the optical system of SEM, not only spherical and chromatic aberration coefficients of the objective lens for the incident beam but also efficiency of collecting secondary electrons are important. In the strong magnetic field region just above the specimen, secondary electrons are spiral up into the bore of the objective lens when the Snorkel lens is used. However, once the electrons come up inside the bore, secondary electrons spread out and hit the wall of the lens, because there are no magnetic field. It is useful to apply a magnetic field along the optical axis to bring up those electrons to the top of the objective lens. A weak electro-static field is effective to pull up the electrons emitted with high angles.

In this investigation, we further show electron trajectories from the top of the objective lens to the detector. We use an usual Everhart-Thornley detector, which is inserted from the side of the optical column. High voltage 10 kV is applied to the detector. In the in-lens SEM with accelerating voltage of 20-50 kV, high voltage applied to the detector captures the secondary electrons without influencing the primary beam. However, in LVSEM, the detector must be set far behind the optical axis of the primary beam. In such the case, it is necessary to introduce a beam separator to deflect secondary electrons towards the direction of the detector. Sato[1] used the Wien filter as the beam separator. In this investigation, we propose a new beam separator, which is similar but not the same as the Wien filter. Recently, Philips announced a new beam separator with 3 stage electrode system[7].

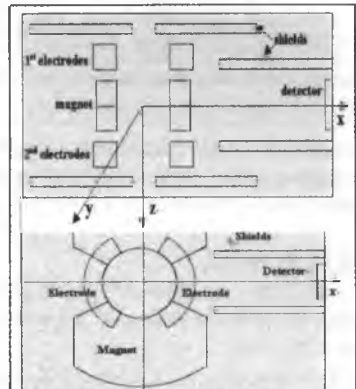


Fig. 1. Mesh layout of the E+B+E beam separator and the detector. (a) xz-plane (b) xy-plane.

2. ELECTRON TRAJECTORY CALCULATION IN THE SEPARATOR

As shown in Fig. 1, the new beam separator consists of the first electrodes, the magnet and the second electrodes. The length of the magnet is equal to the sum of the length of two electrodes. The electro-static and magnetic fields are calculated using EO3D and MO3D and the electron trajectories are calculated using CO3D[8].

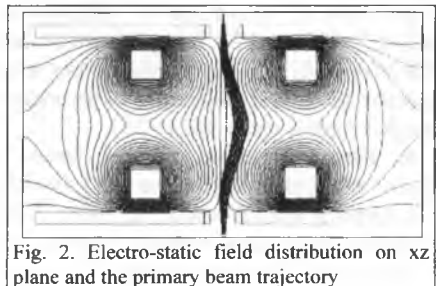


Fig. 2. Electro-static field distribution on xz plane and the primary beam trajectory

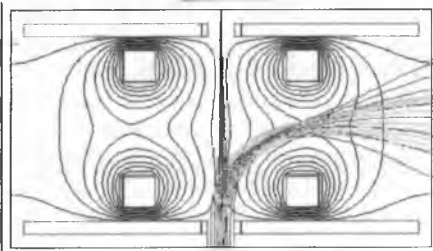


Fig. 3. Secondary electron trajectories in the E+B+E beam separator, which starts from the bottom, together with the primary beam trajectory, which starts from the top of the figure. We assumed that secondary electrons are accelerated to 100 eV before entering into the separator.

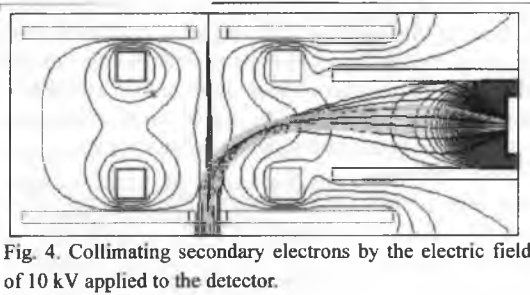


Fig. 4. Collimating secondary electrons by the electric field of 10 kV applied to the detector.

The primary beam from the gun is deflected by the first electrodes, deflected again but in the opposite direction by the magnetic field, and then deflected to the first direction by the second electrodes as shown in Fig. 2. The path of the electrons are similar to the omega filter and the final optical axis is the same as the input beam. The trajectories shown here are drawn under the field strength 13 times stronger than the following conditions to magnify the deflection of electrons.

Figure 3 shows the secondary electron trajectories together with the primary beam trajectory. Because the excitations of the separator are largely reduced from Fig. 2, the primary beam trajectory is nearly straight. Secondary electrons coming up from the bottom parallel to the optical axis have a focus above the second electrode and then diverge.

Figure 4 shows the secondary electron trajectories together with the primary beam trajectory in the same separator as in Fig. 3. Diverged electrons exit from the separator can be captured by the detector. The high

voltage of 10 kV contributes to converge these electrons. Therefore, we need no mind the diverging effect at the latter half in the separator. The trajectory is spread out in the electrostatic field of the detector for the off-axis beams.

REFERENCES

1. M. Sato, H. Todokoro and K. Kageyama, "A Snorkel type conical objective lens with E cross B field for detecting secondary electrons", SPIE vol. 2114 Charged Particle Optics, pp17-23, 1993.
2. S. Miyokawa, H. Kazumori, S. Nakagawa and C. NicholSEN, "Ultra-high resolution semi-in-lens type FE-SEM, JSM-6320F with strong magnetic field lens with built-in secondary electron detector", Proc. MSA pp484-485, 1995.
3. J. Frosien, E. Plies and K. Anger, "Compound magnetic and electro-static lenses for low-voltage applications", J. Vac. Sci. Technol. B7(11/12), pp1874-1877, 1989.
4. K. Tsuno, N. Handa and S. Matsumoto, "Immersion lenses for low voltage SEM and LEEM", SPIE vol. 2522 Charged particle optics, pp243-252, 1995.
5. K. Tsuno, N. Handa, S. Matsumoto and A. Mogami, "Optical properties of immersion objective lenses and collimation of secondary electrons in low voltage SEM", SPIE vol. 2858 Charged particle optics pp243-252.
6. K. Tsuno, "Electron magnetic lenses for electron microscopy" in "Charged Particle Optics" ed J. Orloff, CRC Press 1997, Boca Raton pp143-175.
7. A. Henstra, K.Z. Troost, K.v.d. Mast, P. Kruit, M.P.C.M. Krijn, R. Marx, J. Chmelik, CPO5 (Fifth Int. Cong. Charged Particle Optics) Abstract, p.94 (1998), Delft Univ. Tech.
8. J. Rouse EO3D Manual. Munro's Electron Beam Software Ltd. Tel/Fax: +44-71-581-4479

ANTIBUNCHING OF ELECTRONS AS A CONSEQUENCE OF THE
INDISTINGUISHABLENESS OF FERMIONS

Tomáš Tyc

*Dept. of Theor. Physics and Astrophysics
Kollářská 2, 611 37 Brno
Czech Republic*

The principal indistinguishableness of identical particles has a fundamental significance in quantum mechanics. One of its most important consequences for fermions is the Pauli principle. Another consequence of the quantum indistinguishableness is the difference of the statistics of arrival times of coherent particles emitted from a thermal source to a detector, with respect to the statistics of classical particles. This phenomenon is called *bunching* in the case of bosons due to the fact that bosons come more likely in groups of two, three etc. ("bunches") than alone. In the case of fermions we deal with *antibunching* because the fermions avoid each other, i.e., do not come to a detector even in pairs.

Bunching of bosons was predicted theoretically [1] and proved experimentally [2] with photons already over 40 years ago. The theory describing this phenomenon is richly developed (e.g. [3]). On the contrary, the theory of antibunching (e.g. [4, 5]) is quite incomplete and there are still many problems to be solved. Moreover, the antibunching of fermions has not been experimentally proved until now.

In the talk will be given a brief introduction to the theory of antibunching for electrons and its application to an interesting case of an electrostatic biprism interferometer.

[1] E. Purcell, *Nature* **178** (1956), 1449

[2] R. Hanbury Brown, R. Q. Twiss, *Proc. Roy. Soc. London* **242** (1957), 300

[3] L. Mandel, E. Wolf: *Optical Coherence and Quantum Optics*, Cambridge University Press, 1995

[4] M. P. Silverman, *Il Nuovo Cimento* **97B** (1987), 200

[5] S. Saito, J. Endo, T. Kodama, A. Tonomura, A. Fukuhara, K. Ohbayashi, *Phys. Lett. A* **162** (1992), 442 - 448

MEASUREMENTS OF THE SECONDARY AND BACKSCATTERED ELECTRON COEFFICIENTS IN THE VERY LOW ENERGY RANGE

M. Zdražil* and M. El-Gomati

Department of Electronics, University of York, York YO1 5DD, UK

*Permanent address: Institute of Scientific Instr., AS CR, Královopolská 147, 612 64 Brno, CZ

Low voltage scanning electron microscopy (LVSEM), in which the incident electron energy is less than 5 keV is an advantageous mode of electron microscopy operation for several reasons. These include: a high secondary electron yield for the low energy electrons [1], a reduced electron solid-interaction volume that makes the technique more surface sensitive, the possibility of inspecting insulating materials with the careful choice of the incident beam energy [2], a reduction (or minimisation) of topographical edge artefacts, and the possibility of detecting low material concentrations [3]. While these are all desired properties of LVSEM, the technique has so far been qualitative in nature. This is due to insufficient measurements of the secondary (δ) and backscattered (η) coefficients for low energy electrons as well as a varied specimen environment in the SEM. The work reported here is a study of δ and η under well-characterised specimen conditions and is aimed towards the quantification of LVSEM.

The backscattering (η) and secondary electron (δ) coefficients have been measured in the energy range 250 eV to 5 keV for these samples of 99.999 purity: C, Al, Si, Ti, V, Cr, Fe, Ni, Cu, Zn, Ge, Zr, Nb, Mo, Ag, Cd, Sn, Gd, Hf, Ta, W, Pt, Au and Pb. Measurements were carried out under vacuum conditions in the order of 10^{-9} mbar, and from sample surfaces that were cleaned by energetic ions (2 keV Ar ions of 10^{-4} Acm⁻²) to remove surface contaminants. Used detector is schematically depicted in Fig.1, which is a modified version of that reported earlier [3]. It differs from an earlier design in that the present detector has two grid electrodes instead of only one grid. We have found that in addition to reducing field penetrations for such a compact design, it also acts to reduce the collection of secondary electrons that can alter the value of the measured η . Fig. 2, is a plot of the η coefficient versus the incident electron energy E_p for four elements. Data from the as-inserted surfaces (dotted lines) and those that have been in-situ subjected to energetic argon ions (solid lines) are given. These show differences of up to 10%, with the exception of Cu which may have a thin oxide film on its surface that lowered its η values at low energies.

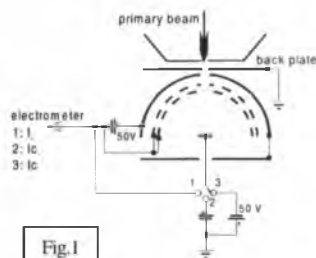


Fig.1

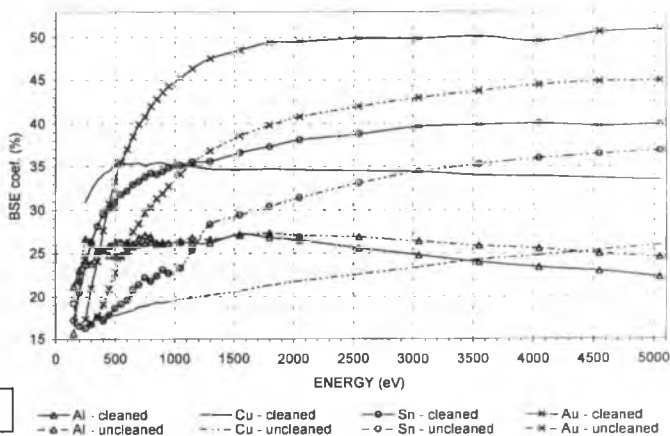


Fig.2

References:

- [1] D. C. Joy, *J. Microscopy*, vol. 147, 51-64, (1987)
- [2] L. Frank, M. Zdražil and I. Müllerová, *Mikrochimica Acta*, [Suppl.], 13, 289 (1996)
- [3] M. El-Gomati and A. Asaad, *Mikrochimica Acta*, (1998), In Press

IMAGING OF NON-CONDUCTING SPECIMENS BY NONCHARGING SCANNING ELECTRON MICROSCOPY WITH METHOD FOR AUTOMATICALLY ADJUSTED CRITICAL ENERGIES

M. Zadražil, L. Frank, J. Norris

Institute of Scientific Instruments AS CR, Královopolská 147, 612 64 Brno, Czech Republic

The total emitted electron current in the SEM is normally lower than the primary beam current so that some negative charge is dissipated into the specimen. In the case of a non-conductive specimen, the charge stays localised at the surface. It creates a unipolar electric field which deflects the primary beam and influences the trajectories of the signal electrons before their detection, and can also cause discharges, etc. Thus, non-conductors cannot be observed at normal energies. Between the critical primary energies at, say, 0.5 to 4 keV, the total electron yield exceeds the unity level and the positive surface charge attracts back a part of slow secondaries so that a balance is established with a potential of a few volts only.

The non-charging microscopy method [2,3] consequentially utilises the critical energies to avoid any charge dissipation. The difficult task to determine a critical energy at absolute minimum surface charge-up (see [4]), is solved by quick acquisition of the signal development in time after a pixel is illuminated for the first time. The method was realised in a cathode lens equipped SEM which enables one to adjust easily the electron landing energy and even to roughly align the SEM at a different energy. The drawback is that the cathode lens extracts the secondaries off the surface so that also the positive charging-up fully develops. The final step in the method development consisted in closing an automated loop formed by the following steps :

- 1: measurement of the signal vs. time curve in series of pixels not illuminated before;
- 2: smoothing of the curves by using the polynomial rms fitting method;
- 3: curve integration with respect to its asymptotic level;
- 4: stepwise discarding of the curves most differing from the average;
- 5: determination of the average integral as the total charge measure;
- 6: determination of the next suitable value of the cathode lens excitation, i.e. the electron landing energy;
- 7: adjustment of the specimen bias by the electronically controlled HV supply and approximate automatic refocusing based on tabulated data (this step is not ready yet, such that partly manual control is necessary).

The loop is preceded by definitions of pixels prescribed for the critical energy measurements and determination of the working distance, it is closed when a total charge measure falls below a pre-selected limit, and finally, a single-shoot picture at the critical energy is taken from the unused part of the view field.

The method was tested on two different ceramics materials. For both of them, signal vs. time curves were taken, and the curve integral was calculated. The sample (a) embodies only one critical energy (see Fig.1), which means that the sample is compact of materials with close values of critical energies. There was no problem in observing this sample with the SEM's landing energy set to the calculated value (1.6keV). On the contrary, we found two mutually distant critical energies on the sample (b) (Fig. 1). Under the latter circumstances, the method presented here cannot produce truly noncharged micrographs: a specimen of this kind of heterogeneity consists of domains, parts of which charge-up at any electron energy selected.

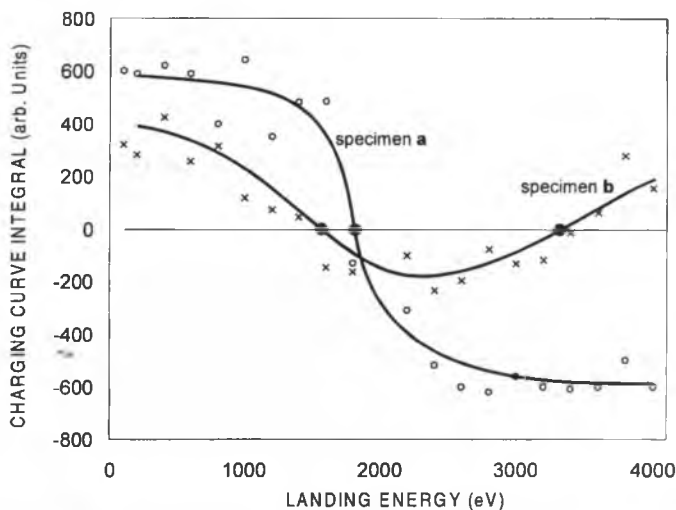


Fig. 1 – charging-up curve integrals above the asymptotic level, in the dependence on the energy for two examined specimens.



Fig. 2 - micrographs of the surface of two different samples of ceramic materials taken at electron landing energies 1.6 KeV (a) and 2.4 KeV (b), respectively. The difference in the images is a result of compositional complexities in sample (b) which do not exist in (a). For this reason, a distinct landing energy was not able to be calculated for (b) as it was for (a).

References:

- [1] J. Cazaux, *J. Appl. Phys.*, 59 (1986) 1418
- [2] L. Frank and I. Müllerová, *Proc 13th Int. Congr. El. Microsc.* Paris Vol.1, (1994) 139.
- [3] L. Frank, M. Zdražil, I. M. Müllerová, *Microchim. Acta [Suppl]*, 13 (1996) 289.
- [4] L. Reimer et al., *Optik*, 92 (1992) 14.
- [5] M. Zdražil, L. Frank., *5th Eur. Workshop EMAS, Book of Abstracts.* Torquay, EMAS (1997) 373.